Passive Low Frequency RFID for Detection and Monitoring of Corrosion under Paint and Insulation

A thesis submitted for the degree of Doctor of Philosophy

Mohammed Alamin

School of Electrical and Electronic Engineering,
Newcastle University

December 2013

Contents

List of Tables and Figures

List of Publications

M. Alamin, G. Y. Tian, A. Andrews, and P. Jackson, "Principal Component Analysis of Pulsed Eddy Current Response From Corrosion in Mild Steel," *Sensors Journal, IEEE,*vol. 12, pp. 2548-2553, 2012.

M. Alamin, G. Y. Tian, A. Andrews, and P. Jackson, "Corrosion detection using low frequency RFID technology," *Insight - Non-Destructive Testing and Condition Monitoring,* vol. 54, pp. 72-75, 2012.

M. Alamin, G. Y. Tian, A. Andrews, and P. Jackson, "Measurement and monitoring of corrosion under insulation using passive LF RFID," NDT 2013, Telford, UK, 2013.

Abbreviations

AM	Amplitude Modulation
ASTM	American Society for Testing and Materials
CSCC	Chloride Stress Corrosion Cracking
CUI	Corrosion Under Insulation
EC	Eddy Current
EIS	Electrochemical Impedance Spectroscopy
EMAT	Electromagnetic Acoustic Transducer
EMF	Electromotive Force
EPSRC	Engineering and Physical Sciences Research Council
FET	Field Effect Transistor
FFT	Fast Fourier Transform
FSM	Field Signature Method
GMR	Giant Magneto Resistance
HF	High Frequency
LF	Low Frequency
LO	Liftoff
MFL	Magnetic Flux Leakage
NDT	Non-destructive Testing
NDT&E	Non-destructive Testing and Evaluation
PC	Protective Coating
PCA	Principal Component Analysis
PEC	Pulsed Eddy Current
PMFL	Pulsed Magnetic Flux Leakage
PV	Peak Voltage
RF	Radio Frequency
RFEC	Remote Field Eddy Current
RFID	Radio Frequency Identification
SCC	Stress Corrosion Cracking
SHM	Structural Health Monitoring
SSPC	Steel Structures Painting Council
UHF	Ultra High Frequency
UT	Ultrasonic Testing
UWB	Ultra Wide Band

Acknowledgements

I wish to express my gratitude to the people without whom this work would not have been possible.

A special thanks to my supervisors, Prof. Gui Yun Tian, Dr. Paul Jackson and Jeff Neasham for supporting me throughout this project with their time, patience and knowledge.

I have been very lucky to have worked alongside a wonderful group of people. My colleagues, John Wilson, Maxim Morozov, Ilham Abidin, Anthony Simm, Stuart Crichton, Liang Cheng, Omar Bouzid, Abdul Qubaa, Hong Zhang, Ibukun Adewale, Waleed Amer and everyone at the Sensor Technology research group have provided many interesting and valuable discussions. I am also grateful to Trevor Wills and others at International Paint for their time and effort preparing samples. It has been a privilege working with you all.

Thanks to the Engineering and Physical Sciences Research Council (EPSRC) and International Paint for funding this project and providing material support.

I am also very grateful to Maede Besharati and Mr. Peukipine for their patience, support and encouragement. I would not have finished this thesis on time without them.

Finally, my deepest thanks go to my family for their love and support throughout all my endeavours.

Abstract

Despite decades of research, corrosion under insulation (CUI) still presents significant challenges for non-destructive testing and evaluation (NDT&E). One of the biggest challenges posed by CUI is the inaccessibility due to the large standoff distance introduced by thick insulation. The hidden nature of CUI may result in it going unnoticed for long periods of time leading to potentially catastrophic failures. Electromagnetic NDT&E techniques, which are widely employed in the pipeline industries in various forms, have large decrease in sensitivity primarily due to the insulation layer. Methods to overcome this typically involve either the removal of insulation or the use of high powered and expensive equipment. Limitations of existing NDT&E techniques create opportunities for novel approaches to tackle the challenges posed by CUI.

This research project, funded by the Engineering and Physical Sciences Research Council (EPSRC) CASE studentship in collaboration with International Paint®, proposes the use of passive low frequency (LF) RFID hardware for the detection and monitoring of corrosion on insulated pipes. The battery-free, low cost nature of RFID makes it attractive for long term condition monitoring. Experimental studies have been conducted using carefully designed samples to demonstrate the detection capabilities of the proposed system. The contribution of the research can be summarised as follows: (1) experimental feasibility study demonstrating the detection capabilities at large standoff distances; (2) demonstration of the increased sensitivity of the proposed system compared to tradition eddy current (EC) method; (3) use of multivariate statistical analysis to identify the most dominant features and relate them to time-domain features of the RFID waveform; (4) application of principal component analysis (PCA) to overcome the dependence of the aforementioned features on the position of the reader coil; and (5) performed accelerated CUI testing to demonstrate the potential of the RFID system in a realistic test scenario.

This work concludes that passive LF RFID hardware can be used to detect corrosion on steel under thick insulation. In comparison to traditional EC method, the RFID based method shows greater sensitivity at large standoff distances. However, significant challenges, particularly the high temperature survivability of RFID tags, limit the real-world applicability.

Chapter 1. Introduction

This chapter provides a brief introduction to non-destructive testing related to corrosion under insulation (CUI) and an overview of the work undertaken in the project. A synopsis of the objectives of the research is provided and the scope of the work discussed. Major research achievements are listed and finally the structure of the thesis is laid out.

1.1 Research Background

Corrosion under insulation is a major problem faced by many industries, primarily the chemical and petrochemical industry. The cost to industry runs into billions of pounds every year with estimates that up to 60% of all maintenance work is related to CUI. Pipes or other structures such as vessels that operate at high temperatures are typically covered with thermal insulation, tens of mm thick, to maintain process temperatures or for health and safety reasons. The pipes, usually made of carbon steel or steel alloys, are used to transport a wide variety of chemicals are operated at temperatures of 150 ºC or more.

CUI is caused by the ingress of water into the insulation material. Water can enter the insulation from the outside e.g. rainwater, if the waterproofing is insufficient and poorly applied or if there is damage to the protective casing surrounding the insulation. Flanges and joints are particular weak points where it is more difficult to waterproof. Water can also appear due to atmospheric condensation. Pipes that operate at a range of temperatures, can have repeated cycles of condensation and re-evaporation resulting in more aggressive forms of corrosion. The insulation itself acts as a sponge, holding and storing moisture for long periods of time. The presence of insulation can in many cases increase the rate of corrosion as moisture that would normally evaporate gets stored in the insulation.

The effect of CUI can be very severe. It can lead to sudden and catastrophic failure, especially in systems that operate at high pressure. Localised pitting corrosion can cause leaks, potentially releasing hazardous chemicals into the environment. What makes CUI a more severe form of corrosion is its hidden nature. Corrosion can progress undetected for long periods. The cost of CUI is not simply from replacing pipes but also possible clean up and down time that may result from it.

Currently the most effective method of inspecting for CUI requires the removal of thermal insulation. Instead of removing entire sections of insulation, often-small inspection holes are cut to gain access to the pipe surface. Removal of insulation is an expensive process that may require the shutting down of operations. Once there is access to the coated metal surface, various techniques such as visual inspection or electrochemical impedance spectroscopy (EIS) can be used to determine the condition of the metal and the level/severity of any corrosion that may be present.

What makes CUI particularly challenging for NDT is, along with the usual challenge of accurately detecting and quantifying corrosion, the task is made more difficult due to the large distance between the sensor and the metal surface introduced by the insulation layer, this distance is known as the standoff distance. The immediate effect of a large standoff distance is the reduction in spatial resolution and sensitivity to small changes in corrosion e.g. thickness of wall loss. This is particularly a problem for traditional electromagnetic NDT techniques, such as EC and MFL, which are typically surface or near surface inspection methods. Although there exists commercial eddy current based methods that can inspect through thick layers of thermal insulation, they require large currents and can be bulky. In addition, the thickness of the coating and insulation are not uniform, resulting in a variation of the standoff distance also known as lift-off variations. This variation can cause erroneous detection and measurement of corrosion.

To address the aforementioned problems, this work provides a study of how passive low frequency RFID hardware can be applied for the detection and monitoring of corrosion under insulation. RFID is a wireless tagging and identification system, which consists of two parts, the reader and the transponder or tag (used interchangeably). The advantage of RFID over tradition magnetic or electromagnetic NDT methods such as EC is illustrated in the figure below.

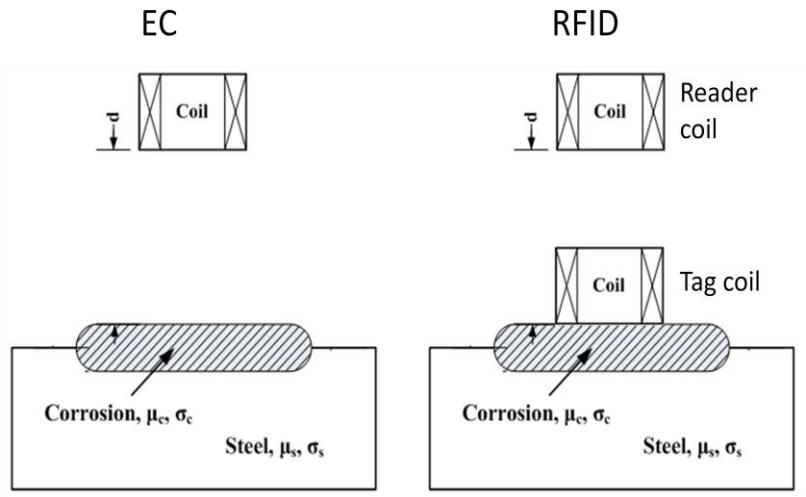

Figure 1.1. Illustration of the differences between traditional EC method and proposed RFID method. In the RFID setup, the large standoff distance is overcome by having the sensing element, the tag, directly on the target surface.

The tag, which is the sensing element, is placed upon the surface of the target metal and is then interrogated by the reader to obtain information about the condition of the metal. The other advantages of RFID are that it is cheap and the hardware is available off-the-shelf.

1.2 Research Objectives

The objectives of the research are summarised as follows:

- Investigate and implement a passive low frequency RFID based sensor for the monitoring of corrosion under insulation as an alternative to the traditional EC/PEC methods. The sub-objectives are listed below:
  - A thorough review of current electromagnetic ND&E methods for the detection of corrosion under insulation. Primarily focusing on the challenges associated with the large standoff distance due to the insulation layer and what effect that has on sensitivity. Additionally, a review of similar passive RFID based sensing system; particularly related to the area of NDT&E.
  - Experimental demonstration of the ability to detect and differentiate between different levels of corrosion and surface condition using RFID sensing system.
  - Experimental demonstration of improved sensitivity of RFID system compared to equivalent EC system.

- Identification of most dominant time/frequency domain features. That is, features which have the largest variance with respect to changes in corrosion/ surface condition.
- Development of method that enables measurement of corrosion change that is independent of reader coil position with respect to tag.

1.3 Scope of the Work

An experimental approach is taken to the assessment of the RFID sensing system, with carefully selected samples with certain known properties and using signal processing and feature extraction techniques to determine the repeatable performance of the RFID system.

Samples are designed such that they closely represent real world conditions. Corrosion is induced on mild steel samples via exposure to the atmosphere for varying periods. These samples are thus closer to real world corrosion than samples which model corrosion as simple metal loss.

Initially, feasibility tests are undertaken with carefully prepared samples with different surface conditions and corrosion levels in order to determine whether it is possible to detect and differentiate between several qualitatively graded mild steel samples. Samples are chosen and the experiment conducted in a manner such that a monotonic response is expected. Reader coil position relative to transponder is kept fixed in order not to distort the results.

Following the feasibility tests, experiments with and without a transponder present are carried out to demonstrate that the RIFD sensing method is sufficiently different from a traditional eddy current method where the excitation coil is also the sensing coil. More importantly, demonstration of the improvement in sensitivity of RFID over traditional EC method by measuring the output magnitude change for a given change in sample condition.

A PEC system is used, due to higher SNR at low standoff distances, in conjunction with PCA to identify, from a multitude of features, the most dominant feature. This feature is then used in analysis of all subsequent RFID measurement data.

Accelerated CUI tests were performed using two sections of mild steel pipes. Transponders were attached using adhesive to the surface of the coated pipes before being

encased in calcium silicate thermal insulation. The pipes were then thermally cycled and salt water was poured into the insulation layer in order to induce and accelerate corrosion development. The purpose of this and other experiments was to simulate realistic scenarios.

1.4 Main Achievements

- A thorough review of magnetic and electromagnetic NDE&E techniques for the detection and monitoring of corrosion under insulation (CUI) has been undertaken. Followed by a review of the literature on passive RFID based sensing. Following the literature review, passive low frequency RFID system for corrosion monitoring was proposed.
- It was found that commercially available LF RFID reader unit's maximum read distance was severely reduced when tag is placed on metal. Typically, it was not possible to obtain a reading beyond 15-20 mm. Therefore, a custom reader unit was designed, which allowed for measurements from up to 50mm with mild steel samples.
- Experimental validation of the proposed system, demonstrating the ability to detect and differentiate between different surface conditions and corrosion levels on mild steel samples.
- An important feature of the proposed system; improved sensitivity over comparable eddy current system has been experimentally demonstrated. It was found that the amplitude change in the reader coil due to a change in the sample was greater when a tag was present.
- Application of principal component analysis to identify the most dominant features by relating the principal components to time-domain features. These features account for the greatest variance in the measured data.
- By applying PCA to two features of the RFID data, position-independent measurements of corrosion progression has been experimentally demonstrated. Upon analysis using synthetic RFID data, it was found that the method works best when the two features are strongly collinear with respect to reader coil position and weakly collinear with respect to corrosion change, i.e. when the change in the carrier signal amplitude, due to a change in the corrosion condition, is much smaller than change in the tag signal amplitude. The method can also be applied to remove temperature variation effects.

- Publication of research in peer reviewed journal [1] and presentation of work to conference [2, 3].

1.5 Thesis Layout

Chapter 1 gives the outline of the thesis, which includes research background, aims and objectives, scope of work and general achievements related to the work.

Chapter 2 presents the literature survey of corrosion processes, specifically focusing on corrosion on coated and lagged pipelines. Next, analysis of the most common and widespread primarily electromagnetic inspection methods and their suitability for corrosion under insulation. The advantages and weaknesses of each are discussed. Finally, the use of RFID hardware for sensing applications is also reviewed.

Chapter 3 presents the theoretical background of passive low frequency RFID, followed by description of the operation of the transponder as a corrosion-sensing element. Behaviour of the RFID system near metals is discussed. The research methodology for the thesis is set out in the remainder of the chapter.

Chapter 4 elaborates the experimental case studies. Starting with an introduction to the samples used and how they were prepared, followed by an initial feasibility study. Subsequent experiments investigate detection of corrosion progression samples. The samples represent different stages of corrosion. Effect of liftoff on the transponder is investigated, demonstrating the possibility to detect changes of at least 100 microns. Using a simple experimental setup it has been shown that the presence of a tag improves the sensitivity in comparison to an equivalent eddy current setup.

Chapter 5 provides an introduction to the problem of repositioning and its effects on corrosion measurements. Existing methods to mitigate the effects of repositioning are discussed. A simplified model of the RFID output signal is given followed by proposed solution involving PCA. Experimental results of the proposed solution are provided. Application of the PCA method for the mitigation of varying temperature on measurements is also discussed.

Chapter 6 details the accelerated CUI experiment. The effects of high temperature on the tags are discussed. The limitations of the RFID system are also discussed

Chapter 7 summarises the research work so far, derives conclusions and outlines further work, which is based on the current investigation.

1.6 Chapter Summary

This chapter presents a brief introduction to the research work. The achievements and problems existing in previous research are generalised and depicted as the background to ongoing study, which is followed by the aims and objectives of the research. The contributions of the current work are presented. Following that, the layout of this thesis and content in each chapter are summarised.

Chapter 2. Literature Survey

Following on from a general introduction to the thesis provided in the previous chapter, the results of literature survey are presented in this chapter. First, corrosion under insulation; its causes and the problems and challenges associated with it are discussed. Next, the most common NDT&E methods applicable for detection and monitoring of corrosion are analysed in with regards to their strengths and weaknesses. A table summarising the strengths and weaknesses of the techniques reviewed is provided at the end of section 2.2. Next, a look into the literature regarding passive RFID sensing in general followed by the specific case of passive RFID corrosion sensing. Finally the problem summary is presented, outlining the need for a new, cheaper passive RFID based sensor for the long term monitoring of corrosion under insulation.

2.1 Corrosion under Insulation

Corrosion under insulation is a major problem faced by many industries, primarily the chemical and petrochemical industry. The cost to industry runs into billions of pounds every year with estimates that up 60% of all maintenance work is related to CUI [4, 5].

Pipes or other structures such as vessels that operate at high temperatures are typically covered with thermal insulation to maintain process temperatures or for health and safety reasons [6]. The pipes, usually made of carbon steel or steel alloys, are used to transport a wide variety of chemicals are operated at temperatures of 150 $°C$ or more [7]. The insulating materials can be generally divided into two groups depending on the operating temperatures. For low temperature applications, zero degrees Celsius or below, materials such as polyurethanes and phenolics are common. Whereas, calcium silicate, mineral wool, rockwool and fibrous glass are more common where the temperatures can reach hundreds of degrees Celsius [8]. As an extra layer of protection, the thermal insulation is then covered by a thin metal jacket made of either steel or aluminium.

Figure 2.1 shows the typical structure of an insulated pipe. The first layer shown (1) is the coating layer, applied to the surface of the steel pipe, which can be up to several hundred micrometres thick depending on type and method of application; layer (2) is the thermal insulation layer with thicknesses of tens of millimetres or more; the final layer is the metallic casing which can be either stainless steel or aluminium and is typically coated itself. Its thickness depends on the application and can be several millimetres thick.

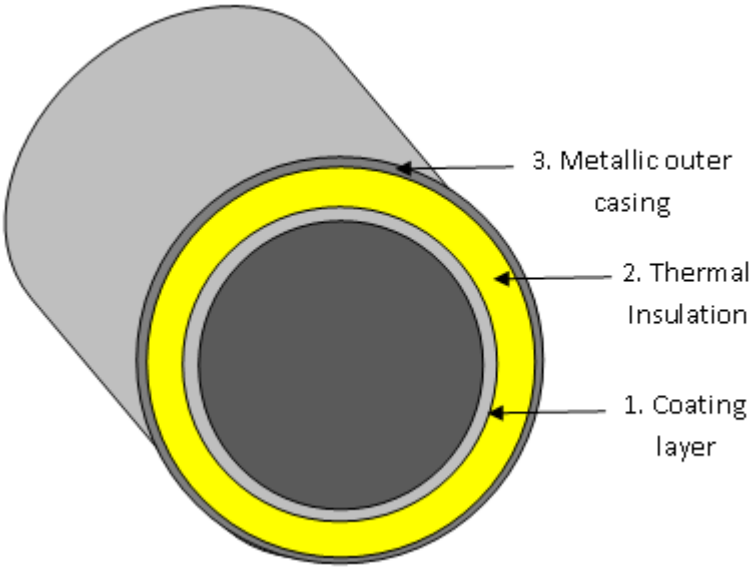

Figure 2.1: Layered structure of an insulated pipe.

Corrosion under insulation is caused by the ingress of water into the insulation material. Water can enter the insulation from the outside e.g. rainwater, if the waterproofing is insufficient and poorly applied or if there is damage to the protective casing surrounding the insulation. Flanges and joints are particular weak points where it is more difficult to waterproof. Water can also appear due to atmospheric condensation. Pipes which operate at a range of temperatures can have repeated cycles of condensation and re-evaporation resulting in more aggressive forms of corrosion. The insulation itself acts as a sponge, holding and storing moisture for long periods of time. At ambient temperature, calcium silicate can store up to 400% of its weight in water [7-9]. The presence of insulation can in many cases increase the rate of corrosion as moisture that would normally evaporate gets stored in the insulation [6]. Takemoto [10] suggests more absorptive insulation materials are more likely to be associated with corrosion problems. The iron in the pipes reacts with water and oxygen causing corrosion.

$$Fe \rightarrow Fe^{2+}$$

Electron

$$O_2 + H_2O \rightarrow OH^-$$

The top reaction leads to a positive anode. It can cause metal loss in the form of pitting. Pitting corrosion can, over time, lead to general wall loss, where large areas of metal are covered in an almost uniform rust layer. The second reaction creates a cathode. The re-

sult is a high pH substance (~14) that can cause loss of adhesion between the surface and any paint or coating applied. Chlorides and other chemicals in the water and in some insulation materials also contribute to and accelerate corrosion [7]. With austenitic steels and aluminium alloys, the chloride can cause stress corrosion cracking (SCC) where the metal can suddenly fail without showing significant visible signs of damage. In marine and coastal environments, salts can mix with water exacerbating the problem further. Figure 2.2 shows visible signs of external corrosion and damage to insulation.

Figure 2.2: (Left) Pipe with visible corrosion, (right) pipe with damaged insulation [11].

Corrosion under insulation can be categorised into the following three types; galvanic corrosion, alkaline or acidic corrosion and chloride corrosion [12].

Galvanic corrosion occurs when there are two different metals joined together. The difference between the two metal types creates a potential difference. The more noble metal acts as the cathode while the more active one acts as an anode. The presence of moisture creates a conduction path for electron flow. This leads to corrosion occurring between the joint [13].

Acidic corrosion occurs when there is low pH water with high concentration of hydrogen ions. Mixture of carbon dioxide and water forms a weak carbonic acid. The reaction between iron, water and oxygen can create a high pH alkaline solution. Aluminium and steels jackets are particularly susceptible to this form of corrosion which attacks through pitting and etching [12].

Chloride pitting occurs when insulations such as fire-retarded polyurethanes leach chlorides on the surface of metals. Grade 300 series of austenitic stainless steels, which are known to have good corrosion resistance, are particularly vulnerable to corrosion due to chlorides. If a metal is under tensile stress while suffering from chloride based corrosion

the result is a form of corrosion called chloride stress cracking corrosion CSCC. CSCC is a form of intergranular corrosion where the cracking develops along the grain boundary of the metal [12].

The effect of corrosion under insulation can be very severe. It can lead to sudden and catastrophic failure, especially in systems which operate at high pressure [8, 14]. Localised pitting corrosion can cause leaks, potentially releasing hazardous chemicals into the environment. Most carbon steel pipes fail due to general or local wall loss, while stainless steel pipes are susceptible to pitting and stress corrosion cracking failures [11]. Figure 2.3 shows how surface pitting can lead to hidden cracks developing within a structure. Chloride levels of less than 10 ppm are enough to cause SCC in stainless steel pipes operating above 60℃ [15]. What makes CUI a more severe form of corrosion is its hidden nature. Corrosion can progress undetected for long periods of time. The cost of CUI is not simply from replacing pipes but also possible clean-up and down time that may result from it.

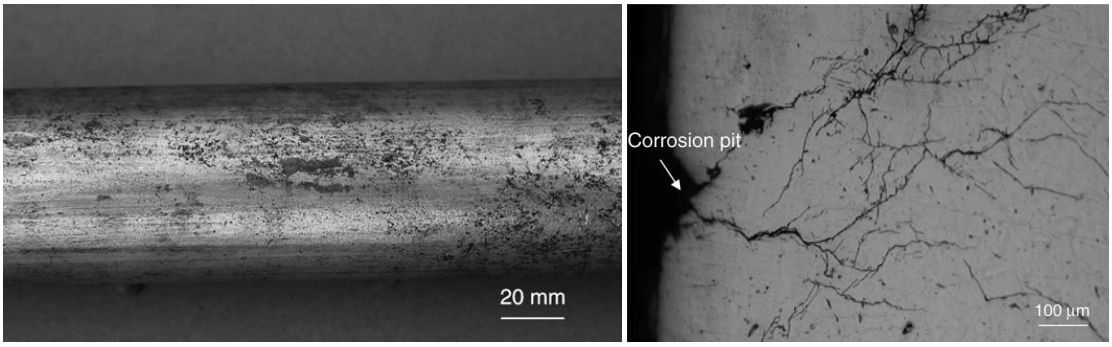

Figure 2.3: (Left) Pitting corrosion on external surface, (right) Cracks (intergranular and transgranular) emanating from corrosion pit on surface [16].

One of the most effective methods to slow down and in some cases prevent corrosion from occurring is to apply protective coatings (PC) onto metals. Protective coatings are paints specifically designed to have highly resilient anti-corrosive properties. The purpose of PCs is to act as a barrier preventing moisture (electrolyte) and other chemicals from interacting with the metal surface [11].

The type of coating used on a pipeline depends on the operating temperatures and environmental factors. Most common high temperature coating types are usually siloxane or epoxy based such as aluminium epoxy mastic which can operate up to 150℃ and epoxy phenolic with operating temperatures up to 230℃ [14]. For lower temperatures (up to ~100℃), inorganic polyurethane based coatings are used with zinc-rich primers [17].

For very high temperatures, up to ~500℃, pipes can be coated with a thin film of aluminium [14]. Other forms of coatings include silicone based acrylics [18]. All coatings require some level of surface preparation and cleaning for the coating to be effectively applied. Coatings are also chosen for their compatibility with the insulating materials. The thickness of coating can vary from tens of micrometres to hundreds of micrometres.

Although coatings provide a high level of protection against corrosion, they are also prone to damage and failure. Large temperature fluctuations, moisture evaporation/condensation cycles and abrasives such as salts contribute to coating failure. Changes in temperature cause the metal and coating to expand and contract [14]. The different contraction and expansion rate between the metal and coating causes reduction in adhesion between the two. The stresses that result may lead to the coating being compromised, allowing water to get in [7]. The flexibility of the coating is an important factor, repeated stress and low temperatures can cause some coatings to become brittle and less flexible. In certain environments, salts can be deposited on the surface of coatings acting as an abrasive agent. Coatings are also permeable to water and can have corrosion occurring beneath without any damage to the coating itself [12].

Currently the most effective method of inspecting for CUI requires the removal of thermal insulation [19, 20]. Instead of removing entire sections of insulation, often small inspection holes are cut to gain access to the pipe surface. Removal of insulation is an expensive process which may require the shutting down of operations. Once there is access to the coated metal surface, various techniques such as visual inspection or electrochemical impedance spectroscopy (EIS) can be used to determine the condition of the metal and the level/severity of any corrosion that may be present.

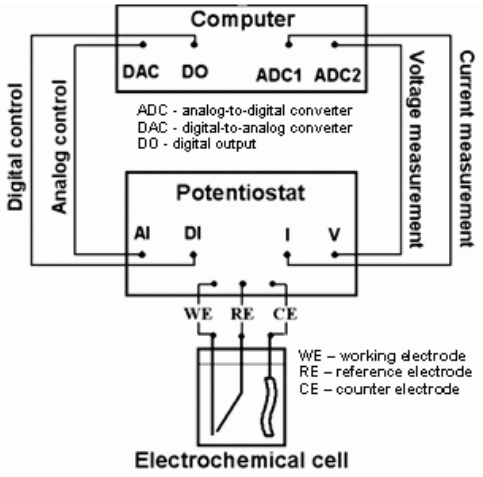

Figure 2.4: Electrochemical impedance spectroscopy system.

Electrochemical impedance spectroscopy is an inspection method used to characterise electrochemical processes such as corrosion. The method works by applying sinusoidal ac current of varying frequencies to a material and measuring its response [21, 22]. Analysis of the response is used to extract information about the interface, its structure and reactions taking place there [22]. Chemical reactions such as corrosion will tend to dominate at certain frequencies. The responses are then modelled as complex impedance circuits and analysed using Nyquist plots and Bode plots. The dielectric properties of the coating layer introduce a capacitance which along with resistive and inductive effects from the metallic surface can be used to characterise the materials and processes present. EIS is a highly sensitive technique which makes it a good reference for other NDT methods.

What makes CUI particularly challenging for NDT is, along with the usual challenge of accurately detecting and quantifying corrosion, the task is made more difficult due to the large distance between the sensor and the metal surface introduced by the insulation layer, this distance is known as the standoff distance. The immediate effect of a large standoff distance is the reduction in spatial resolution and sensitivity to small changes in corrosion e.g. thickness of wall loss. Also, the thickness of the coating and insulation are not uniform, resulting in a variation of the standoff distance also known as lift-off variations. This variation can cause erroneous detection and measurement of corrosion.

2.2 Survey of NDT Techniques for Corrosion Detection

This section provides an introduction to some of the most common NDT techniques used for corrosion detection and monitoring. The aim is to provide an overview of each technique; its advantages and disadvantages and what the current applications are. No single technique is suitable for all corrosion types and mechanisms. Often more than one inspection method is employed. A comparison between each technique is provided to assess their suitability to corrosion detection and evaluation in general as well as to corrosion under paint and insulation.

2.2.1 Magnetic flux leakage

In the magnetic flux leakage (MFL) technique, walls of a pipeline are magnetised to near saturation flux density. The presence of flaws or wall loss due to corrosion will cause changes in permeability. A reduction in permeability leads to an increase in reluctance, forcing flux to take different routes. Some of these routes will become saturated

and hence ‘leak’ flux into the air. This leakage can then be detected using magnetic sensors [23, 24]. The distribution of the leakage will be greatest near a defect. In fact, despite its name, flux leakage due to saturation is not required, since magnetising of carbon steel will result in remanent or residual magnetisation once the external magnetic field is removed. The strength of the residual field will depend on the geometry and magnetic permeability of the material.

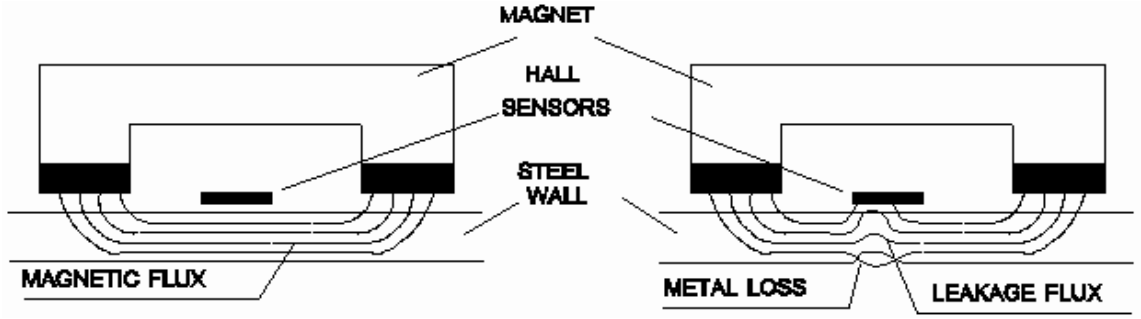

Figure 2.5: Illustration of the magnetic flux leakage method [25].

Traditional MFL techniques have had difficulty in sizing defects and discriminating between internal and external defects. Applying a pulsed magnetising field has been shown to overcome some of the weaknesses of MFL. Pulsed magnetic flux leakage (PMFL) is a recent extension to the MFL technique which uses a square wave excitation to the magnetising coils. The square wave contains multiple frequency components which along with transient signal analysis allows for better depth information as well as improved discrimination between internal and external defects [23].

MFL has been used for pipeline inspection for decades. It is a well established method widely used in the testing of ferrous materials such as steel pipes and storage tanks. Large areas, such as the entire circumference of a pipe, can be magnetised. The method is particularly suited for uniform wall loss and to a lesser extent, due to sizing complexities of traditional MFL, locating of pitting corrosion [26-28].

Another weakness of the MFL technique is that axially orientated cracks are not easily detected due to such defects not having large dimension in a direction orthogonal to the axially orientated excitation flux [29]. This effect is illustrated in Figure 2.6.

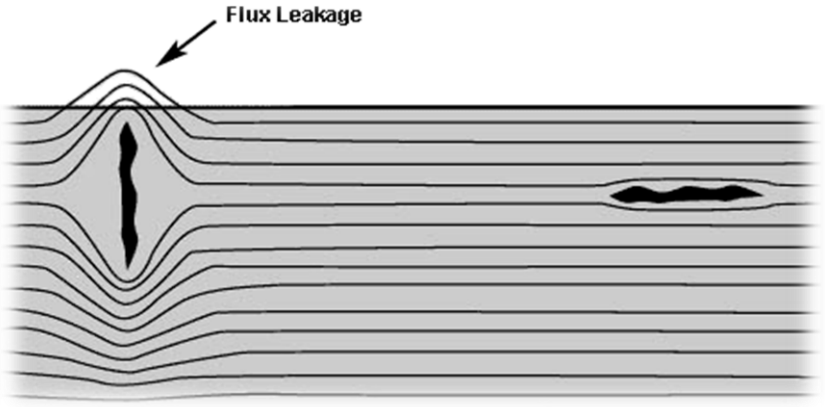

Figure 2.6: Effect of defect alignment on flux paths [30].

MFL is unsuitable for insulated pipes and is only intended for thinly coated pipes due to the small stand-off distance. However, a recent study in China [31] has demonstrated the potential of using PMFL to size corrosion defects on steel pipes with 20 mm insulation thickness. Although more work needs to be done to improve sensitivity, the result is a big improvement over traditional MFL.

2.2.2 Microwave

Microwaves are high frequency radio waves that have recently found application in NDT of corrosion. Microwaves occur in the region between 300 MHz – 30 GHz, frequencies of 30 GHz – 300GHz are known as millimetre waves [32]. Microwaves are transmitted towards an object using either coaxial cables or open-ended rectangular waveguides. The amplitude and phase of the reflected signal is used to determine condition of target object. The high frequencies of the microwaves make it useful for imaging of corrosion defects, the higher the frequency the better the spatial resolution. High spatial resolution enables sizing of smaller pitting corrosion for example. Recent trends in microwave NDT are moving towards millimetre waves [33, 34].

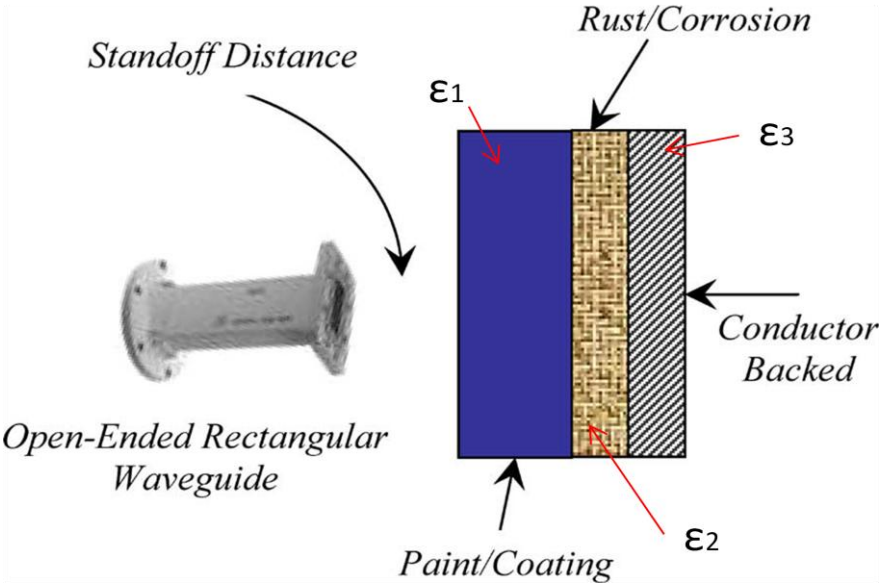

Figure 2.7: Typical microwave test setup showing an open-ended rectangular waveguide and a multilayered sample with different permittivity [33].

Microwaves are able to penetrate and interact with dielectric materials such as paint and non-conducting layered composites, showing potential for evaluating properties of the dielectric layer including thickness and detecting disbonds and delaminations [35]. The electrical impedance mismatch between different layers results in reflection of microwaves. In contrast to other electromagnetic NDT techniques, microwaves can be applied to non-metallic targets. The dielectric property of a material is a complex variable whose real part (relative permittivity) indicates the ability of the material to store microwave energy while the complex part (relative loss factor) indicates the ability to absorb microwave energy.

It has been demonstrated that microwaves can be used to detect small changes in the thickness of corrosion, with a 4 degree change in phase for every 10 micrometre change in the thickness reported in one study [36]. Work is being carried out at Imperial College London to use microwaves to detect moisture in the insulation, which is the precursor to corrosion. The pipe and the insulation has been shown to act as a coaxial waveguide which can be used to transmit microwaves along the pipe, the presence of moisture will attenuate the microwaves giving an indication to the likelihood of corrosion [37]. A direct measurement of corrosion using microwaves is limited to the surface of conducting materials due to the high frequency of the microwaves. Furthermore, microwave NDT requires expensive detection instrumentation such as network analysers which may be prohibitive for many applications.

2.2.3 Ultrasonic

Ultrasonic testing (UT) methods utilise high frequency sound waves (1-6 MHz) that can easily penetrate solids and liquids. The sound waves, which are also known as elastic waves in solids, are generated using devices such as piezoelectric transducers. A portion of the transmitted wave is reflected back from the surface of the target material while some of the wave will pass through it. An advantage of the ultrasonic method is its tolerance to different materials; it can be used on both conducting and non-conducting objects [38-40]. The way that sound propagates through a material is known as a mode, the most common modes used in ultrasonic NDT are longitudinal and shear/transverse waves. Longitudinal waves, also known as compression waves, travel in the same direction as the oscillations of the particles. Shear waves propagate perpendicularly to the direction of oscillation. The difference between longitudinal and shear waves are shown in Figure 2.8.

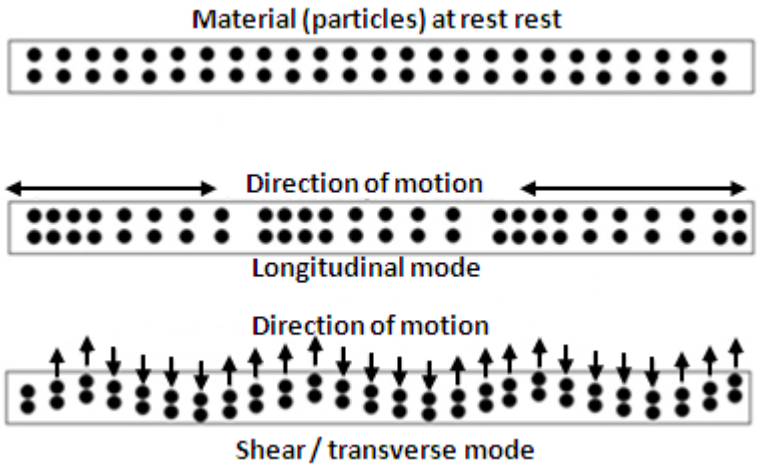

Figure 2.8: Longitudinal and shear/transverse modes of propagation of ultrasonic waves.

Ultrasonic inspection can also be divided into short and long range (see Figure 2.9). Short range ultrasonic inspection is mainly used to measure localised wall loss via time of flight thickness measurements. Transducer arrays are also employed for imaging purposes for which resolutions of 0.1 mm can be obtained [41]. Long range ultrasonic inspection, also known as guided waves or Lamb waves, involves transmitting an ultrasonic pulse along the pipe wall to be detected by a transducer at a distance down the pipe. Lamb waves travel along the surface of the pipe with very little spreading, depth of penetration into the pipe wall is limited to about 1 wavelength. This feature gives guided waves the advantage of being able to travel long distances of up to 20 m or more.

Unlike MFL, guided waves can detect both circumferentially and axially orientated defects [41, 42].

Both types of ultrasonic inspection methods require access to the pipe surface via inspection holes cut into the insulation. Furthermore, ultrasonic waves do not travel well through air and so require a coupling medium such as water to efficiently transfer the waves to the material surface. Another disadvantage of the ultrasonic technique, especially for short range, is the requirement for a clean and regular surface [43].

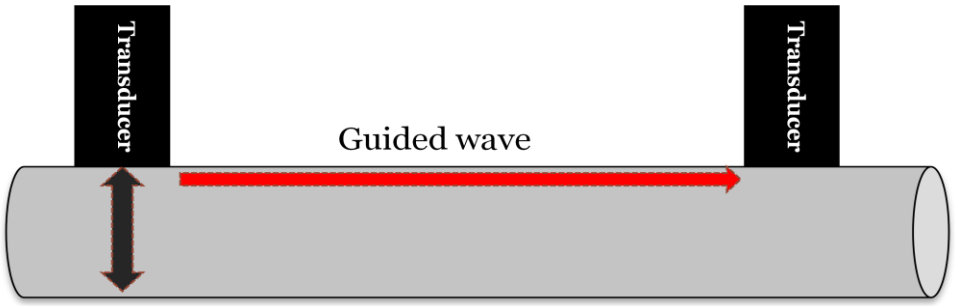

Figure 2.9: Diagram showing difference between short rand and long range ultrasonic testing.

To overcome the couplant requirement of conventional ultrasonic testing has led to the development of the electromagnetic acoustic transducer (EMAT). EMAT is non-contact method which generates ultrasound in a conducting material using eddy currents (see Figure 2.10). More recently, air coupled and laser induced ultrasonics have been introduced as another way to overcome to coupling issues [44-46]. However, the coupling efficiency and the signal-to-noise ratio are significantly reduced, raising further challenges for defect detection and quantification.

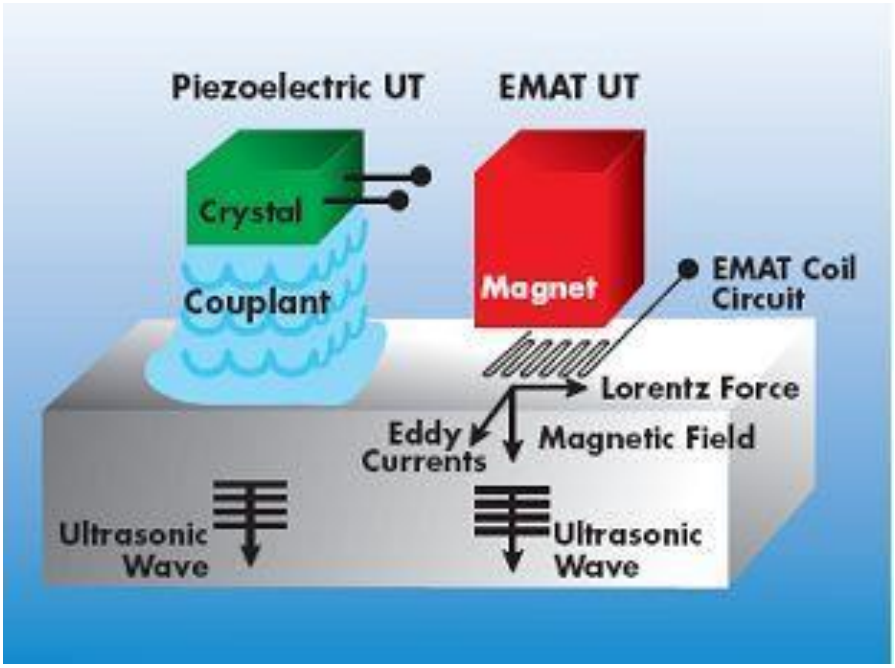

Figure 2.10: EMAT couplant free ultrasound transmission [47].

A coil with a high frequency ac current induces eddy currents on the surface of a conducting material. The presence of a magnetic field from a permanent magnet causes the surface electrons to experience a Lorentz force which results in the generation of elastic waves in the material i.e. ultrasound. EMAT can be used to generate guided waves but is limited to electrically conducting materials. A big disadvantage of EMAT is its low coupling efficiency [48], even with small liftoffs; coatings can result in significant drop in power transferred to metal. EMAT ultrasonic inspection has naturally been combined with the eddy current and pulsed eddy current techniques [48-50].

2.2.4 Field signature method

Field Signature Method (FSM™) is a patented NDT technique developed by CorrOcean ASA for the purpose of corrosion monitoring. The method relies on the measurement of changes in potential difference across the surface of a test material after a current has been passed through it. Several probes placed at various positions provide a profile of the electric field. The initial measurements are a unique signature of the material tested. Any subsequent changes in the material due to corrosion or other forms of damage will alter the resistance between the probes and hence the electric field pattern [51, 52].

Initial applications for FSM were in the offshore and pipeline industries, later the technique was developed for use in refineries [52]. FSM can distinguish the difference between localised pitting corrosion and general wall loss.

Relatively large areas can be monitored using multiple sensing probes, the typical distance between them being 2-3 times the wall thickness. Depending on the probe configurations, resolutions from 0.1% to 5% of wall thickness have been reported [53]. FSM can provide continuous monitoring. The disadvantages of FSM are that it requires access to the surface of the pipe and is limited by coatings [41].

2.2.5 Radiography

Radiography is the use of high energy, short wavelength electromagnetic radiation such as x-rays, gamma rays and also neutrons for non-destructive testing. A typical radiographic system consists of a radioactive source such as Iridium 192 and an array of digital radiation detectors. The high energy of the radiation allows it to penetrate thick objects both conducting and non-conducting. Radiography potentially offers the best resolution of all the techniques reviewed with reported detection of corrosion defects as small as 6mm in diameter and 1.2mm deep [41, 54]. It is used for both surface and subsurface defects including pitting and general corrosion. Although the technique offers more information about the condition of a pipe, there are some major drawbacks. Firstly, the use of ionising radiation poses health and safety risks and requires highly trained personnel to safely operate. The other disadvantage is the cost which is higher than other techniques and the equipment tend to be large and bulky.

2.2.6 Eddy current

Eddy current NDT relies on the principle that when a conducting surface comes into contact with a varying magnetic field electromotive forces (EMF) are generated around loops in the material. Due to the materials conductivity, currents loops are generated.

These current loops are known as eddy currents due to their resemblance to water currents. The induced voltage is proportional to the rate of change of the current. As the magnetic and electric fields are intrinsically linked, a change in the magnetic field will lead to a creation of an electric field as described by the Faraday equation [55]. Also, Ampere's law relates the magnetic field to its current source. To satisfy the conservation of energy, Lenz's law states that the induced current will circulate in such a way as to produce magnetic fields that oppose the field inducing the currents.

In traditional EC testing a sinusoidal signal is injected into the inducing coil. The ac signal, which is typically consists of one frequency component, creates a varying mag-

netic field that induces the eddy current in a conducting material. The resultant eddy current will produce its own magnetic field that can be detected by a sensor coil. The magnetic field is also detected using solid state devices such as Hall Effect and GMR sensors which are used in arrays for imaging purposes. The strength and phase of the eddy currents will affect the loading on the detection coil and hence its impedance [55, 56]. The presence of defects such as a surface cracks or other discontinuities will disturb the eddy current flow, reducing its strength and leading to an increase in the impedance of the coil [51, 55, 56]. The technique's ability to detect subsurface defects is largely determined by the skin effect phenomenon. Due to the skin effect, the majority of the current flow occurs on the surface of a conductor, exponentially decaying with increasing depth. The depth of penetration δ is defined as follows:

$$\delta \approx \frac{1}{\sqrt{\pi f \mu \sigma}}$$

The depth of penetration is dependent on the frequency *f*, the materials permeability μ and conductivity σ. The rate of change in magnetic flux is determined by the frequency of the ac current. The higher the frequency, the greater the rate of change and hence bigger voltages are induced in a conducting surface. It is analogous to increasing the velocity of a permanent magnet passing through a coil. However, with high frequencies the majority of the current in the conductor tends to flow in the surface. As the frequency increases so does the current density at the surface of the conductor. Since the region of the conductor that carries majority of the current decreases with frequency the resistance experience by the current increases substantially leading to greater losses. For non-ferrous materials the relative permeability μ_r is approximately equal to the free space value of one. These materials tend to have low resistivity and high conductivity e.g. aluminium and copper. However, for ferrous materials such as iron, the relative permeability can be very high, up to several hundred and thus have a significant impact on the formation of eddy currents. The eddy currents in materials with high μ_r have greater impedance and hence will result in weaker current densities. Eddy currents produce resistive losses in the form of heat. Therefore, eddy current flows are stronger in good conductors.

Development in eddy current NDT technology has led to pulsed eddy current (PEC) and remote field eddy current (RFEC) techniques. Both are a natural evolution of the EC

method and have been developed to improve penetration depth and tolerance to high permeability metals.

With conventional EC NDT, a fixed frequency sinusoidal current is used to generate eddy currents on the surface of a conductor. Whereas in PEC, the shape of the excitation current is a square pulse or step function. If we look at the Fourier transform of a step function, we will see that it contains a continuum of frequency components compared to just one for sinusoidal EC. Since the depth of penetration is dependent on the frequency, the PEC response signal will contain information from multiple depths, equivalent to multiple single-frequency EC scans [57].

The depth of penetration is also dependent on the permeability of the metal; ferromagnetic materials such as carbon steel have high permeability and thus severely limit the penetration depth. Conventional eddy current techniques use the direct field or near field, which decays exponentially with depth. Remote field EC measurements rely on the fact that some of the magnetic fields will radiate out of the conducting pipe and into the air where they will experience less attenuation. The fields then re-enter the metal at a remote point and can be measured by placing a sensor there. In an RFEC system the exciter and receiver coils are placed inside pipes a certain distance apart. The technique is able to detect flaws both on the inside and outside of the pipe [58].

The eddy current techniques have a wide variety of applications including subsurface defect/corrosion detection on aircraft frames, weld inspection, metal loss and SCC in steel piping and coating thickness measurements [59]. PEC has a high in-service repeatability of 0.2% (0.02mm on a 10mm wall thickness) compared to 0.4mm for ultrasonic testing which means that PEC can establish corrosion rates much faster [60]. PEC has also been applied to CUI with insulation thickness of up to 200mm [26, 61]. At 50mm insulation thickness the popular commercial INCOTEST PEC scanner has a resolution of about 80mm [26]. The system also requires relatively large input power to be able to induce eddy currents strong enough to be detected above the noise threshold. Traditional EC and PEC suffer from sensitivity to protruding parts such as flanges and nozzles. It is also sensitive to lift-off variations, where the distance between the sensor and the metal surface changes during inspection which can lead to defects being masked or false positives. There are however several techniques than can be applied to minimise lift-off sensitivity [62-64].

2.2.7 Capacitive imaging

Capacitive imaging, sometimes known as electrostatic imaging, is a NDT method where an AC electric field generated by two planar electrodes is perturbed by the presence of and change in samples directly beneath the electrodes. The electrodes and the sample form a capacitor (Figure 2.11). The electrodes can also be scanned across a surface to produce 2D images [65].

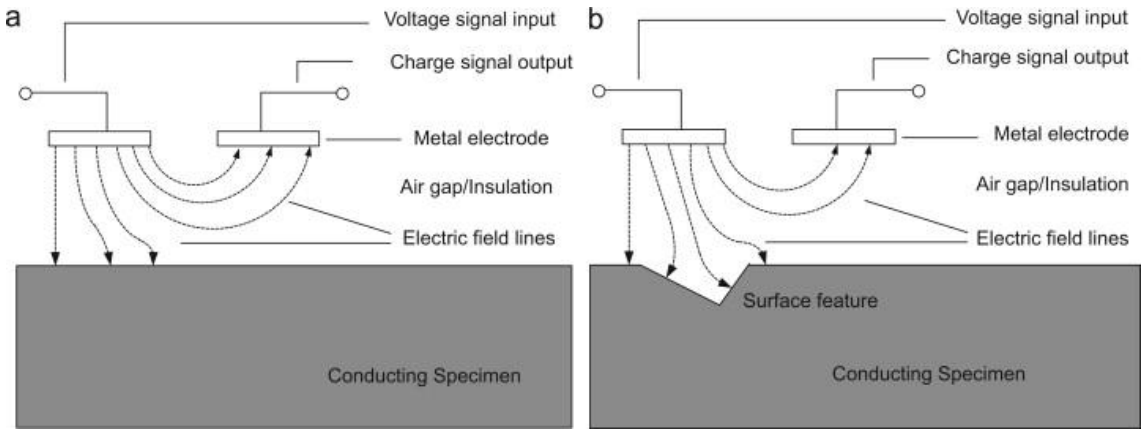

Figure 2.11: An electric formed by two planer conductors is disturbed by changes in sample [66].

Unlike eddy current based methods, non-conductive materials such as plastics [67, 68], concrete [69] and wood [70] can be inspected as their dielectric properties will determine the capacitance. Furthermore, due to the use of electrodes and not coils, the electric field is maximised as opposed to the magnetic field for eddy current based methods. Therefore, eddy current generation is discouraged. However, like EC/PEC methods, for high conductivity samples such as metals, charges can move freely and will accumulate on the conducting surface. As a result, the electric field will cause an equipotential surface, and only the surface features of the conductor can be detected [66].

Yin et al. [66] have employed the capacitive technique to image surface defects as small as 2mm in depth on metals through an insulation layer 20mm thick. Authors found that floating conductors and lift-off variations between the plates and the sample can cause uncertainties in the detection and lower the image resolution. It has also been noted by the authors that previous studies have demonstrated the sensitivity of coplanar capacitive sensors to moisture and water in non-conductive specimens [69, 71, 72]. This raises the prospect of detecting water in insulation as a precursor to corrosion. However, vary-

ing moisture levels in the insulation layer also has the potential to obfuscate the measurements of corrosion change.

2.2.8 Summary of NDT techniques for corrosion detection

Table 2.1 provides a summary of the literature survey into NDT methods for corrosion detection in general but also their suitability to CUI.

The selection of NDT techniques requires consideration of more than the detection and sizing capabilities of each method. The application, portability of equipment, inspection schedule, size of inspection area, types of materials, accessibility, costs and expected defect types are just as important in the decision process. Some techniques which provide good quantitative information perform poorly when insulation is introduced. The ultimate aim of inspection is to provide timely and accurate information which can facilitate the repair/replacement in such a way as to minimise costs and risks.

No one technique can address all the challenges presented by CUI. And despite all the advances made in the area of NDT&E, CUI is still a big problem which requires further development and refining of existing techniques as well as new ideas and concepts.

Table 2.1: Summary of NDT techniques.

Technique	**Advantages**	**Disadvantages**	**Primary defects**	**Through coating?**	**Through insulation?**
Eddy Current	Inexpensive, multi-layer, coating thickness	Low throughput, lift-off sensitivity, sensitive to protruding parts	Surface and subsurface flaws	Yes	No
PEC	Deep penetration, discriminate between surface/subsurface defects	lift-off sensitivity, sensitive to protruding parts e.g. flanges	General wall loss, pitting	Yes	Yes
RFECT	Internal and external flaws	Miss pitting corrosion	Internal and external wall loss	Yes	No
Ultrasonic (short range)	Fast, good sensitivity and resolution	Requires couplant[1] and clean and regular surface, coating/rust removal	General wall loss, SCC, subsurface defects, pitting, delamination	No	No
Ultrasonic	Fast, inspect large	Requires	General wall	Yes	No

(long range, guided wave)	areas	couplant[1], no absolute measurements	loss, SCC		
MFL	Established pipeline inspection method	Limited penetration depth	General wall loss	Yes	No
PMFL	Better defect sizing, surface and subsurface defects	Large standoff distance limitations	General wall loss, pitting	Yes	Yes
Radiography	Good resolution imaging	Radiation safety, expensive	General wall loss, pitting	Yes	Yes
FSM	Continuous corrosion monitoring	Small area, expensive	Surface flaws	No	No
Microwave	Good resolution, inspect coating properties	Surface defects only due to limited penetration depth, complex wave interactions	General wall loss, pitting	Yes	Yes
Capacitive imaging	Volumetric inspection of non-conducive objects	Susceptible to interference, variations in permittivity of insulation layer due to moisture	Defects, corrosion, coating defects	Yes	Yes

[1] EMAT does not require coupling medium.

2.3 Passive RFID Sensors

Passive RFID tags in various forms have been used for a variety of applications such as temperature, humidity, strain, permittivity and chemical sensing [73-76]. They are attractive due to their low cost and battery free operation, allowing tags to be embedded for long term structural health monitoring (SHM). Passive sensors, those which operate via inductive coupling using LC resonant circuitry, in general have been under development since the 1950s [77]. In this section the literature on the use of passive RFID as sensors in general and later the more specific case of passive RFID sensors for corrosion detection is reviewed.

Marocco et al. [74] have presented a way to detect changes in permittivity of a target surface using ultra high frequency (UHF) RFID tags. The system consists of multiple RFID chips placed as a cluster of antennae or onto a single multi-port antenna. The

mismatching of the antenna's input impedance with respect to a change in the target material is the sensing mechanism. The system also overcomes problems related to unknown separation distance between reader and tag by using a cluster of tags and measuring multiple independent signals.

Loh et al. [78] have developed a carbon nanotube thin film based RFID sensor. The carbon nanotube-polyelectrolyte-based nanocomposite thin film is deposited onto planar coil antennas of RFID tags. By controlling the polyelectrolyte species deposited allows for different sensing mechanisms e.g. strain and corrosion/ph. Varying pH levels and applied strain to the thin film changes its resistance which can then be detected as a change in the bandwidth of the RFID system.

Jia et al. [79] developed a prototype humidity sensor using passive UHF RFID tags. A humidity sensitive polyimide film is incorporated onto the top surface of the RFID tag for humidity sensing. UHF RFID tags are very sensitive to water and other conductive media. Presence of which alters the resonance frequency of the tag antenna due to Ohmic losses. The polyimide film absorbs and holds moisture near the tag antenna thus changing the tags operating characteristics. The change in moisture can be detected as a shift in the power reflected by the tag's antenna. The study does not address the effect of varying temperatures or the effect of varying separation distance between reader and tag which can also affect the reflected power.

Potyrailo et al. [80] have done extensive work involving the use of 13.56 MHz RFID tags as chemical sensors. By coating the tags with a solid polymer electrolyte sensing film they have demonstrated the detection of ethanol, methanol, acetronitrile and water vapours with parts-per-billion vapour detection limit. Additionally, by applying multivariate statistical analysis to four parameters of the complex impedance plot, the authors were able to identify and quantify several different vapours in air. In a follow-up study [81] the authors tackled the challenge of varying reader coil position on detection. They found that application of principal component analysis to the four measured parameters allows for position independent measurements. Recently [82] they have also demonstrated that the same techniques used to obtain position independent measurements can also be applied to compensate against fluctuations in ambient temperature.

One common feature among the aforementioned works is the application of various thin films to RFID tags. As mention previously, the changes in the thin film due to interaction with the environment allows for the detection of various chemical and physical

properties. A drawback of such approaches, especially for SHM and corrosion detection applications, is that the changes in the thin films may not be an accurate indication of the changes occurring on the structure the tag is placed on. Additionally, such thin film based sensors also may not be suitable for very long term monitoring of structures due to saturation or exhaustion of the thin film material.

2.3.1 Passive RFID corrosion sensing

In this section focus is directed towards literature on the use of passive RFID tags for the detection and monitoring of corrosion.

Leon-Salas et al. [83] have presented details of a smart RFID-based corrosion sensor that can be embedded in concrete. The sensor is a custom designed tag built using a microcontroller. Linear polarisation measurements are performed on a corrosion cell using a potentiostat with a resolution of 10 bits. The sensor is also able to monitor temperature. The problem of varying reader position is mitigated by digitally modulating the measured data with the carrier signal.

Andringa et al. [84] also present a smart RFID-based corrosion sensor to detect the onset of corrosion in steel reinforced concrete. In this case the transducer is a loop of bare steel wire attached to a modified RFID tag (Figure 2.12). The steel wire is exposed to the concrete environment. As the wire begins to corrode, this increases its resistance; a shift on the resonance frequency of the tag can be detected. The breaking of the exposed wire after a certain level of corrosion acts as a trigger, warning that corrosion may be occurring in the concrete.

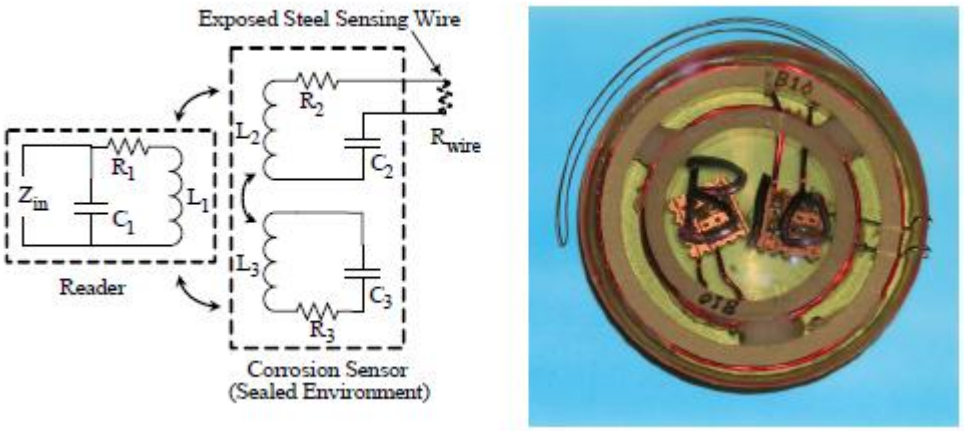

Figure 2.12: (Left) Circuit diagram of corrosion sensor showing the exposed steel wire. (Right) prototype corrosion sensor [84].

Friedersdorf et al. [85] presented the use of modified passive 13.56 MHz tags as corrosion sensors. Each sensing tag is modified by attaching a parasitic sacrificial metal element to the tag. This element is exposed to the atmosphere and thus corrodes over time. The amount of power the tag absorbs will depend on the corrosion state of the parasitic element.

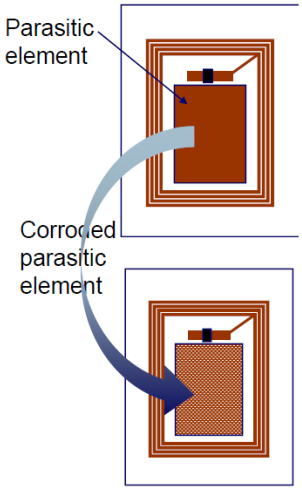

Figure 2.13: Sensor tag showing parasitic element which corrodes due to exposure to the atmosphere [85].

A particular limitation of some of the RFID corrosion sensors described above is the use of sacrificial elements. Just like the case with thin films, the sacrificial elements may not represent the actual corrosion condition of the metallic structure they are attached to. At best they may be used to detect the precursors to corrosion in an insulated pipe.

2.4 Summary and Problem Identification

One of the biggest challenges posed by CUI is the inaccessibility due to the large stand-off distance introduced by thick insulation. Moisture in the insulation and high temperatures create a microclimate which can accelerate the development of corrosion. The hidden nature of CUI may result in it going unnoticed for long periods of time leading to potentially catastrophic failures.

A review of the literature on the most common NDT techniques for corrosion detection showed that the majority of techniques are limited when it comes to online in-situ monitoring of CUI primarily due to the thick insulation layer. Solutions to overcome this problem typically involves either applying much higher input power using bulky, ex-

pensive equipment or the use of inspection holes in the insulation layer to send waves along the length of the pipe to another inspection hole.

The passive RFID sensors identified in the literature demonstrate the potential of cheap, battery free wireless sensing. RFID tags have been adapted to sense a wide range of diverse phenomena. Due to their battery-free operation, RFID tags have shown the potential to be embedded into structures such as concrete for long term condition monitoring. However, the sensing tags used in majority of the studies examined make use of either thin films or sacrificial elements added to the tag. The changes that occur to the thin films or the sacrificial elements may not represent the true condition of the structure on which the tag is embedded. Furthermore, long term monitoring using RFID tags is limited if the sensing elements of a tag degrades faster than the structure it's monitoring. Another challenge not addressed by existing studies is the resulting performance degradation when tags are placed onto metallic structures.

To tackle the particular problem of thick insulation, the use of passive LF RFID tags as corrosion sensors is proposed in this study. The developed system aims to address the following issues:

- Obtain corrosion measurements on steel through thick layers of insulation/ large standoff distances.
- Since the system is passive, a method needs to be developed to address the issue of varying displacement between the reader and the tag, i.e. obtain position independent corrosion measurements.
- The system much be very low cost, and use off-the-shelf components. To minimise costs further, the tag should be unmodified. The interaction between the tag coil and the metal being the sensing mechanism.
- Suitability for long term monitoring by not using any sacrificial elements.

In the next chapter the theoretical background of passive LF RFID is provided along with design and description of the hardware used in this study.

Chapter 3. Systematic Approach for the Development of an RFID Corrosion Sensing System

Following on from the challenges identified in chapter 2, chapter 3 presents the theoretical background of passive low frequency RFID, followed by description of the operation of the transponder as a corrosion-sensing element. Behaviour of the RFID system near metals is discussed.

3.1. Measurable Metal Properties Affecting Detection and Monitoring of CUI

As with all electromagnetic NDT methods, the primary detectable properties of the metal are changes to the electrical conductivity σ and the magnetic permeability μ.

3.1.1 Effect of corrosion on measurable properties

Traditionally, corrosion has been artificially simulated and modelled using rectangular regions of pure metal loss [86-88]. This approach has allowed links to be established between certain PEC features and the dimensions of the simulated corrosion. For example, there are relationships between the peak induction voltage and volume of corrosion and between the zero-crossing time and the depth of corrosion [86, 89]. However, real corrosion has chemical and physical changes, which, along with changes in the coating layer, have a more complex interaction with eddy currents. Gotoh and Hirano have found that corrosion leads to a large reduction in the electrical conductivity and magnetic permeability in steel and that corrosion product itself has a non-zero electrical conductivity and relative magnetic permeability greater than unity [90]. Furthermore, magnetic permeability reduces the skin depth of eddy currents which when combined with the surface changes due to corrosion results in greater influence of surface roughness on the flow of eddy current [91]. Surface roughness also increases the path length of eddy current, reducing the observed electrical conductivity [92]. Analytical solutions to eddy current inverse problems typically assume isotropic homogeneous conductivity [93, 94], however, the complex processes and material changes associated with real corrosion requires highly complex models.

3.2 Background to RFID

Radio frequency identification technology was originally created to identify friendly aircraft from enemy aircraft during the Second World War. It eventually found its way

into civilian applications ranging from door access control to livestock tracking. It is a wireless technology which is recently being used as a replacement for the traditional barcode system.

An RFID system consists of two hardware components: the reader and the tag/transponder. The reader itself typically consists of a microcontroller alongside RF circuitry such as envelope detectors and filters which are required to transmit and receive RF energy. The reader includes a coil or antenna which is used to transmit and receive. The functions of the reader include: (1) Transfer enough power to the tag to energise it; (2) receive the data stored in the tag's memory via response signal from the tag; (3) write data to tags memory. The hardware of the tag comprises a microchip with memory which stores the tags unique identification code. The RF portion of the tag is made up of a wound or printed coil connected to a capacitance to form a tuned LC circuit.

Tags can come in passive, active or semi-active forms. Passive tags, which have been used in this study, obtain all their energy from the RF field. Whereas, active tags contain a power supply such as a battery which makes them larger in size. Semi-passive are a combination of the two. The passive tags get all their power from the near field carrier signal generated by the reader via inductive coupling, illustrated in Figure 3.1. Due to the advantage of battery free operation, only passive RFID will be discussed from here on.

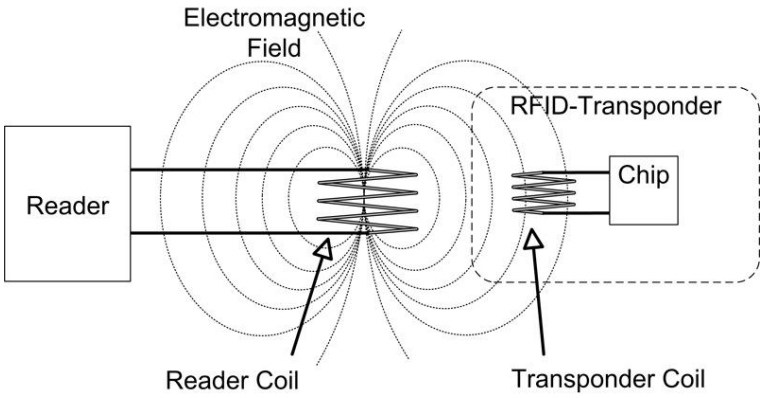

Figure 3.1: Principal of near field inductive coupling between readers coil and transponder coil.

Different RFID systems operate at a variety of frequencies which defines various factors such as cost, read distance and tolerance to certain environmental conditions e.g. near

metals or liquids. The table below lists some of the most common RFID operating frequencies.

RFID	Frequencies	Free Space Passive Read Distance
Low Frequency (LF)	125 kHz	10-20 cm
High Frequency (HF)	13.56 MHz	10-20 cm
Ultra-High Frequency (UHF)	868-928 MHz	3 m
Microwave	2.45 & 5.8 GHz	3 m

Table 13.1: Common RFID operating frequencies

For passive RFID, the frequency of operation also determines the mode of power transfer. Both LF and HF RFID operate in the near field and energy transfer is via inductive coupling. This limits the read distance of inductively coupled RFID. Whereas, for UHF and higher the communication and energy transfer is in the far field via the backscattering phenomena. Operating in the far field allows for much greater read distance in free space. However, in the presence of metals and other conductive objects, RFID systems operating at UHF or above suffer severe degradation in performance [95-97]. In many cases, UHF tags become completely unreadable when attached to metals. The common solution used to overcome this problem involves shielding the tag antenna from the metal [98]. Therefore, RFID systems operating at UHF and higher are not practical for passive corrosion sensing purposes. Whereas HF and LF RFID are more robust near conductive materials [96, 99]. An important factor in determining which frequency is most appropriate for sensing purposes is the skin depth (δ), which is defined as the depth below the conducting surface at which the current density falls to $\boldsymbol{e^{-1}}$ (about 37%). The skin depth for conducting materials is given by:

$$\boldsymbol{\delta = \frac{1}{\sqrt{f\pi\mu\sigma}}} \tag{3.1}$$

Where f is the frequency in Hz, μ is magnetic permeability (H/m) and σ is electrical conductivity. Applying the above equation it can be seen that moving from LF to HF the skin depth reduces by a factor of approximately 10. Smaller skin depth results in a

stronger eddy current field generated by the surface eddy currents. The eddy current field opposes the primary field from the reader resulting in less power being delivered to the tag. Considering the aforementioned factors, it was decided that LF RFID is the most suitable platform for passive corrosion sensing.

3.2.1 Passive LF RFID: theory of operation

Due to the close proximity of the tag and reader, the electromagnetic field can be regarded as an alternating magnetic field. The alternating magnetic field induces a voltage on the tag's antenna coil. The tag then rectifies this voltage and uses it to power the microchip. Once the tag has obtained enough energy to power the chip, it will start toggling a load resistance, drain-source resistance of an FET, on and off according to some binary code stored within it. Changing the resistance alters the antenna coil voltage. This results in amplitude modulation as shown in Figure 3.2. The passive tag does not technically transmit anything; instead it changes the load presented to the reader in a method known as reflective load modulation.

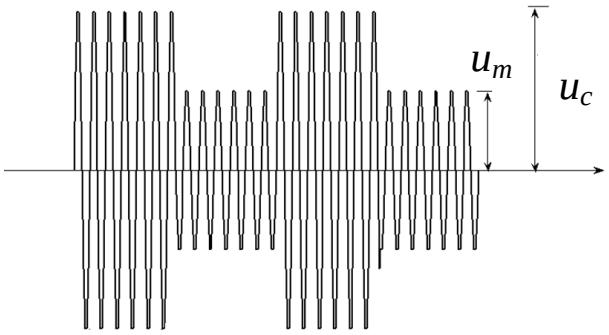

Figure 3.2: RFID amplitude modulation.

From Figure 3.2 the modulation index m_i is defined as:

$$m_i = \frac{u_c - u_m}{u_c + u_m} \tag{3.2}$$

Where u_c is due to the high impedance state of the FET and u_m is the result of the low impedance state.

The voltage induced in the tag inductor loop is governed by Faraday's law of induction which states that a changing magnetic flux Φ generates an electric field strength E_i. In its general form Faraday's law is written as:

$$u_1 = \oint E_i \cdot ds = -N\frac{d\Psi(t)}{dt} \tag{3.3}$$

Where u_1 is the induced voltage in the tag coil with N windings. Using the equivalent circuit of a magnetically coupled tag and reader coils, Figure 3.3, the induced voltage across the tag's coil can be deduced.

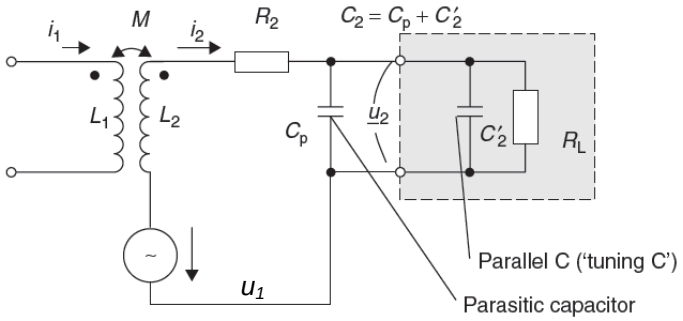

Figure 3.3: Equivalent circuit for magnetically coupled reader and tag coil [100].

A time variant current i_1 in the reader coil with inductance L_1 generates a time variant magnetic flux $d\Phi(i_1)/dt$ due to mutual inductance M. This subsequently induces a voltage in the tag coil with inductance L_2. The induced current in the tag is denoted by i_2. The flow of current creates a voltage drop across the tag's coil resistance R_2. The current through the load resistor R_L (microchip and memory) is calculated using u_1/R_L. Due to Lenz's law, the current flowing through L_2 generates an additional magnetic flux, which opposes the magnetic flux of the reader coil $\Psi_1(i_1)$. Ignoring capacitive effects, the above is summed up in the following equation:

$$u_1 = +\frac{d\Psi_2}{dt} = M\frac{di_1}{dt} - L_2\frac{di_2}{dt} - i_2R_2 \tag{3.4}$$

The mutual inductance M is given by:

$$M = \frac{\mu_0\pi N_1N_2(ab)^2}{2\sqrt{(a^2 + r^2)^3}} \tag{3.5}$$

Where:

μ_0= permeability of vacuum

N_1 and N_2 = the number of turns in the reader coil and tag coil respectively

a and *b* = radius of the reader coil and the tag coil respectively

r = distance between the two coils

The efficiency of the equivalent circuit in Figure 3.3 is greatly improved by the use of a capacitor C_2 connected in parallel to the tag coil L_2 to form a resonant circuit with a resonant frequency corresponding to the carrier frequency. The resonant frequency can be calculated using the Thomson equation:

$$f = \frac{1}{2\pi\sqrt{L_2 \cdot C_2}} \tag{3.6}$$

C_2 is a combination of the tuning capacitor C'_2 in parallel with a parasitic capacitance C_p. Taking resonance into account and we can thus calculate the voltage u_2 across the load resistor R_L using the following equation expressed in non-complex form [100]:

$$u_2 = \frac{\omega \cdot k \cdot \sqrt{L_1 L_2} \cdot i_1}{\sqrt{\left(\frac{\omega L_2}{R_L} + \omega R_2 C_2\right)^2 + \left(1 - \omega^2 L_2 C_2 + \frac{R_2}{R_L}\right)^2}} \tag{3.7}$$

Where *k* is the coupling coefficient:

$$k = \frac{M}{\sqrt{L_1 \cdot L_2}} \tag{3.8}$$

3.2.2. RFID corrosion sensor

To understand how the RFID system can operates as an eddy current based corrosion sensor we will look at the following two factors: 1) behaviour of the tag coil when placed above a ferromagnetic plate such as the mild steel samples used in this study and 2) the effect of tag modulation on reader coil which affects the reader sensitivity. Lateral and angular misalignment between the reader coil and tag is discussed in subsequent sections.The behaviour of a coil next to a conducting half space is described by the formulas of Cheng [101], Dodd and Deeds [102]. The difference in inductance, $\Delta L = L(\omega) - L_{air}(\omega)$, of a tag's coil when placed next to a uniform conducting half space

with inductance $L(\omega)$ and when it is in free space with inductance $L_{air}(\omega)$ can be obtained using modified formulas of Cheng, Dodd and Deeds [103]:

$$\Delta L = M \int \frac{P^2(\alpha)}{\alpha^5} A(\alpha)\phi(\alpha)d\alpha \tag{3.9}$$

Where

$$\phi(\alpha) \equiv \frac{\mu_r \alpha - \sqrt{\alpha^2 + j\omega\mu_0\mu_r\sigma}}{\mu_r \alpha + \sqrt{\alpha^2 + j\omega\mu_0\mu_r\sigma}} \tag{3.10}$$

The permeability of free space and relative permeability are denoted by $\boldsymbol{\mu_0}$ and $\boldsymbol{\mu_r}$ respectively. Conductivity is denoted by σ. The integration variable α is the transform of a Bessel function decomposition of the electric/magnetic field and represents spatial frequency. M is the mutual inductance between the tags coil and the conducting half-space and is given by:

$$M \equiv \frac{\pi\mu_0 N^2}{(l_2 - l_1)^2 (r_2 - r_1)^2} \tag{3.11}$$

Where N is the number of turns in the tags coil, r_1 and r_2 are the inner and outer radii of the coil and l_1 and l_2 denote the height of the bottom and top of the coil. The factor $P(\alpha)$ is defined as:

$$P(\alpha) \equiv \int_{\alpha r_1}^{\alpha r_2} x J_1(x) dx \tag{3.12}$$

Finally, $\boldsymbol{A(\alpha)}$ is defined as:

$$A(\alpha) = \left(e^{-\alpha l_1} - e^{-\alpha l_2}\right)^2 \tag{3.13}$$

Rose et al. have found that the change in inductance of an air-core coil near a uniform ferromagnetic half-space is well described by a two-parameter scaling relationship for a variety of coil types [103]. The scaling relationship is:

$$\Delta L(\omega) = \Delta L_0 L^*(\omega/\omega_0) \tag{3.14}$$

The overall strength of the inductance change is determined by the constant $\boldsymbol{\Delta L_0}$. The real part of a coil's inductance has been found to increase with the presence of a ferro-

magnetic half-space at sufficiently low frequencies due to magnetisation of the metal. Whereas, as the frequency increases, the real part of the inductance decreases and at a certain characteristic frequency $\boldsymbol{\omega_0}$, the change in the real part of the coils inductance is zero [103, 104]. The zero-crossing or scaling frequency is given by:

$$\omega_0 = \frac{\mu_r \alpha_0^2}{\sigma \mu_0} \tag{3.15}$$

The scaling function $\boldsymbol{L}^*$ is approximated by:

$$L^*\left(\frac{\omega}{\omega_0}\right) = \left(1 - \sqrt{\frac{j\omega}{\omega_0}}\right) \Big/ \left(1 + \sqrt{\frac{j\omega}{\omega_0}}\right) \tag{3.16}$$

The constant ΔL_0 depends only on the coil and is independent of conductivity and permeability. ΔL_0 is defined as:

$$\Delta L_0 \equiv M \int \frac{P^2(r_1, r_2) A(\alpha)}{\alpha^4} d\alpha \tag{3.17}$$

The decrease in real ΔL is due to eddy currents which become increasingly stronger as frequency increases. For angular frequencies above ω_0, eddy currents dominate and real ΔL becomes negative [104]. The above is however for the case of a single coil above a ferromagnetic plate, which is a far simpler condition than that of an RFID system where two coils are involved. Introducing the reader coil into the picture means taking into account the interaction of the reader with the tag and the ferromagnetic metal. Below we will analyse the effect of the tag on the reader due to mutual inductance.

When a tag is placed in the field of a reader coil, the mutual inductance between the two causes a change in the reader current i_1. The effect of the mutual inductance on the reader equivalent circuit can be modelled by including in series an imaginary impedance Z_T' which is the complex transformed tag impedance. $|\boldsymbol{Z_T}'|$ is zero when the tag is removed from the reader coils field.

At resonant frequency, the source voltage u_0 at the reader is given by:

$$u_0 = R_1 i_1 - j\omega M i_2 \tag{3.18}$$

Here, R_1 is the series impedance of the reader coil and M is the mutual inductance between the reader and tag coils. Replacing i_2 with tags parameters we obtain:

$$u_0 = R_1 i_1 + \frac{\omega^2 k^2 L_1 L_2}{R_2 + j\omega L_2 + Z_2} i_1 \tag{3.19}$$

Where Z_2 represents the parallel connection of C_2 and R_L. Dividing both sides by i_1 and replacing Z_2 with its constituents gives us the expression for $Z_T{}'$:

$$Z_T{}' = \frac{\omega^2 k^2 L_1 L_2}{R_2 + j\omega L_2 + \frac{R_L}{1 + j\omega R_L C_2}} \tag{3.20}$$

3.2.3 Effect of metals

The presence of metals near the tag and reader has two significant influences. The first is the distortion of the primary reader near the surface of the metal [105]. Applying appropriate boundary conditions on Maxwell's equations, it is obtained that only normal electric fields to the surface and tangential components of the magnetic field are allowed in the surface of a perfect conductor. A metal is not a perfect conductor, resulting in distortions of the magnetic field near the surface [99].

The second effect is the detuning of the tag. Detuning is caused by the eddy current field perpendicular to the metal surface. The eddy current field thus opposes the primary field as shown in Figure 3.4.

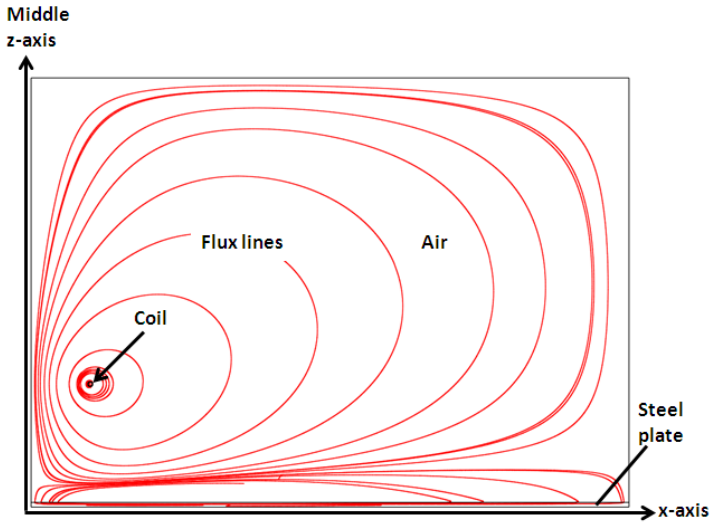

Figure 3.4: Axisymmetric FEM-flux line simulation of a coil above a steel plate. The eddy currents induced on the metal creates magnetic field opposing the primary field of the reader coil.

Metals near a tag can be modelled as an additional parallel inductance L_m on the circuit of the tag [106]. This parasitic inductance usually leads to a lower total inductance in the tags equivalent circuit [107]. A reduction in the tag coil inductance L_2 will not only shift the resonant frequency of the tag and hence lead to a reduction in the power absorbed but it will also result in a reduction in the transformed impedance Z_T' causing a reduction in the reader coils sensitivity.

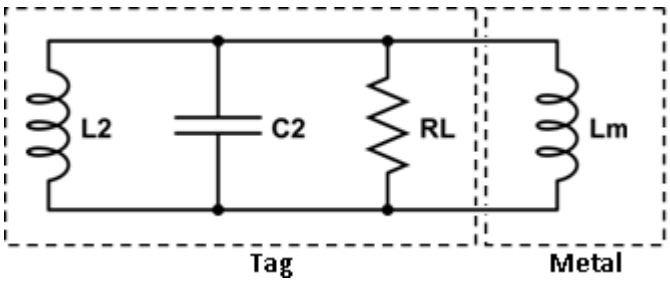

Figure 3.5: The effect of the metal on the tag modelled as a parallel inductance in the tag's circuit

When placed on a non-corroded metal surface, the tag's resonance frequency will shift significantly causing a large drop in the power absorbed by the tag. The resonant frequency on metal f_m will subsequently shift towards the free space resonant frequency f_0 as corrosion develops. Since the tag's inductor and capacitor form an LC tank circuit, even small changes in the resonance will result in detectable voltage changes at the reader coil. This is depicted in Figure 3.6.

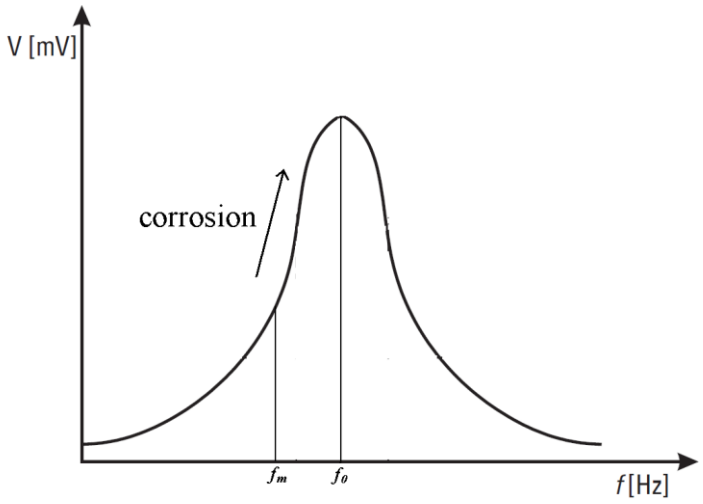

Figure 3.6: Depiction of a typical frequency response curve for resonant tank circuit. The metal causes a shift away from free space resonant frequency. Build-up of corrosion results in shift in frequency towards free space resonance.

More specifically, highly electrically conductive metals such as copper reduce the inductive reactance due to the opposing eddy current field and increase the resonant frequency of a coil compared to free space [108]. The resistance of the coil increases, leading to dampening of the coil's quality factor. When a coil is brought near a ferromagnetic metal such as mild steel, where the relative magnetic permeability is more prominent, the inductive reactance of the coil increases due to the magnetic permeability of the metal concentrating the coil's magnetic field. The effects on the coil from the magnetic permeability overshadow the effects from conductivity since they are so much stronger [109]. Development of corrosion on steel results in a decrease in the electrical conductivity and magnetic permeability, leading to a decrease in the inductive reactance and resistance of the coil towards free space/air values. This is true for both the reader and tag coils. However, since the tag coil is much closer to the metal surface than the reader coil, the change in the tag coil's properties is much greater. This will be demonstrated in section 4.1.5 and later utilised for position independent measurements in Chapter 5.

In terms of measurements, the effect of frequency shift due to metal causes a decrease in the amplitude of the tag's response signal (Figure 3.7).

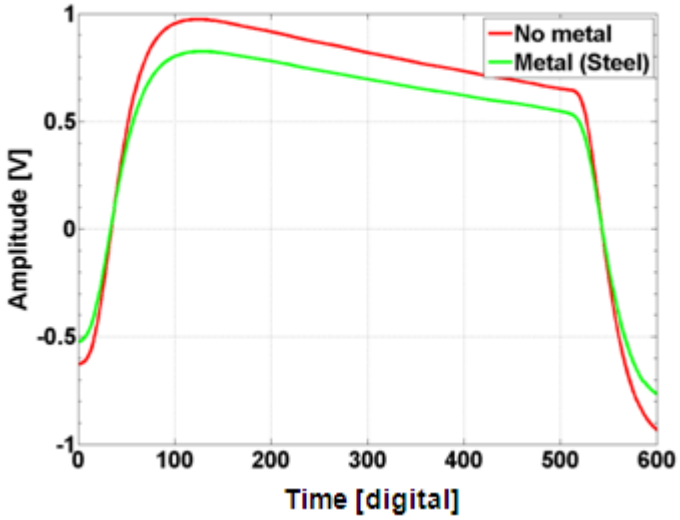

Figure 3.7: Experimental results demonstrating the decrease in amplitude due to the presence of the metal shifting the resonance frequency of tag. A single period is shown.

In the next section we will discuss the effect of changes in the reader coil position with respect to the tag and how that influences the measurement of corrosion.

3.2.4 Effect of reader coil position

Being a passive system, the amount of power received by the tag and the measured output signal amplitude is determined to a large extent by the position of the reader coil with respect to the tag.

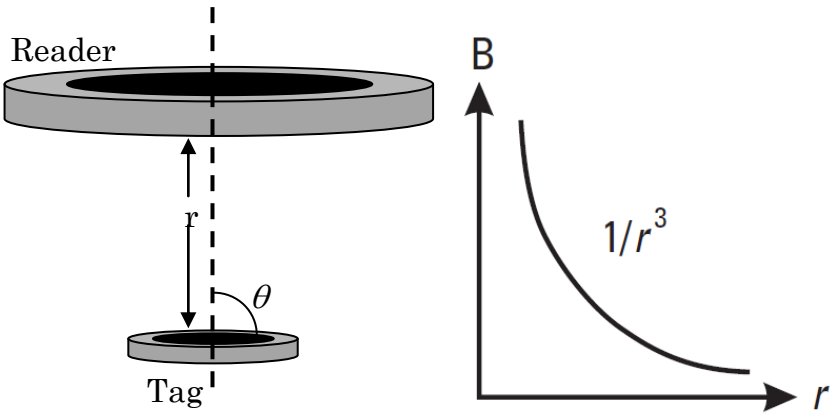

Figure 3.8: The magnetic field produced by the reader coil drops off by $1/r^3$.

The magnetic field of the reader coil rapidly decays ($1/r^3$) with distance r for values of r greater than the radius. The available RF power falls off even faster at $1/r^6$ [100, 110]. This is also the biggest factor limiting the range of near field inductively coupled RFID.

The available power is also determined by the reader coil- tag angular alignment (θ). The optimum value of θ being 90º. Any other value will result in non-optimal coupling and the induced voltage in the tag coil becoming a function of $sin(\theta)$.

Such drastic changes in power available to the tag due to r and θ can become a problem for corrosion detection and monitoring if the reader coil – tag position is not fixed for all measurements. Changes in the output signal amplitude due to corrosion can be masked by the influence of the reader coil – tag position on the output signal amplitude. This repositioning problem is tackled in chapter 5.

3.3 RFID System

3.3.1 RFID reader design

The reader unit used in this study is custom designed to allow easy access to the analogue signal from the coil and produce an intense field allowing reading of the tag on metal from distances up to 50mm which is critical for use under thick insulation. The block diagram of the reader is provided below. A detailed circuit schematic is provided below.

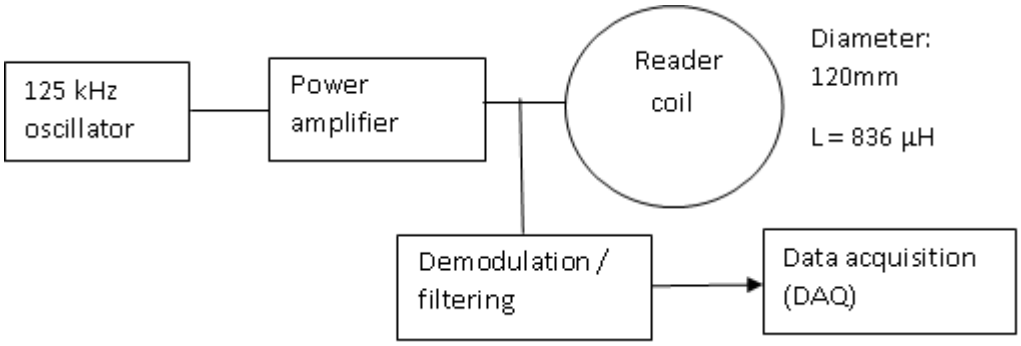

Figure 3.9: Custom RFID reader unit block diagram and reader coil properties.

The power amplification stage, Figure 3.10, consists of two IRF630 MOSFETS driven in anti-phase by a 5V 125 kHz square-wave signal.

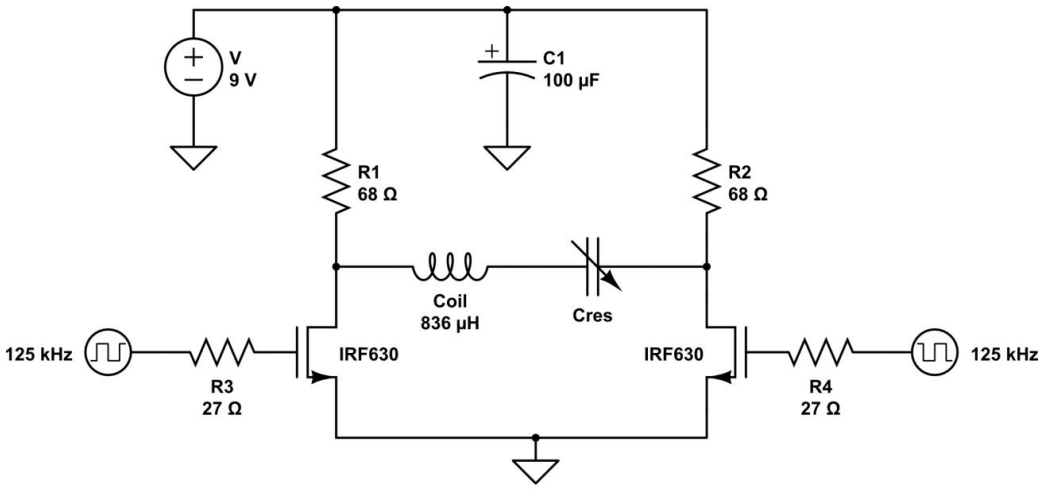

Figure 3.10: RFID reader amplification circuit.

When one MOSFET is turned on the other is turned off. This results in the two ends of the series LC being pulled alternatively high by *R1* or *R2* or pulled low by one of the MOSFETS. The coil and C_{res} are tuned to resonate at 125 kHz using the Thomson equation (3.6). The 68Ω resistors are a simplification of the bridge circuit. Ideally these would be replaced by high side MOSFETs to form a full bridge.

The 125 kHz square-wave signal is generated using a U2270B IC from ATMEL. The U2270B is a self contained RFID reader unit containing an oscillator, power amplifier and demodulation circuitry (Figure 3.11). The IC can be operated in differential mode by selecting the mode select (MS) pin, resulting in the outputs coil1 and coil2 being in anti-phase.

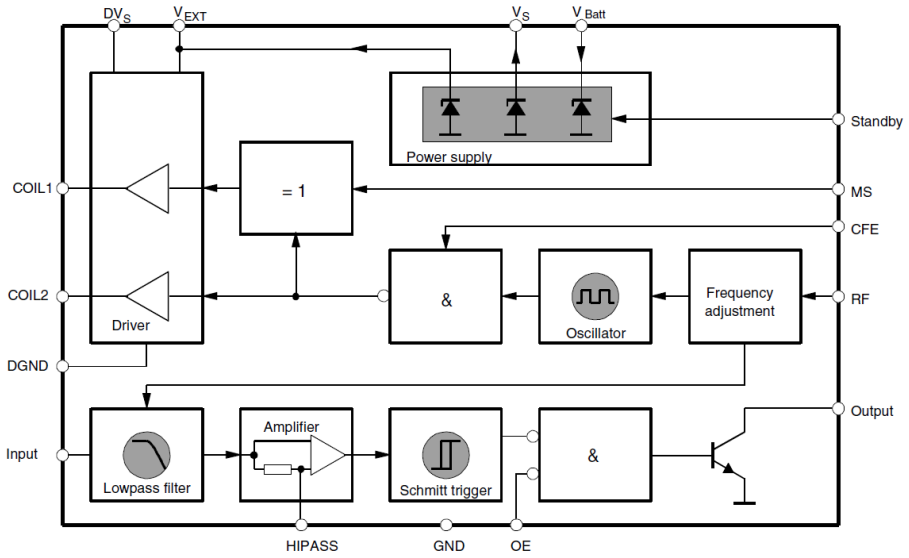

Figure 3.11: U2270B internal block diagram.

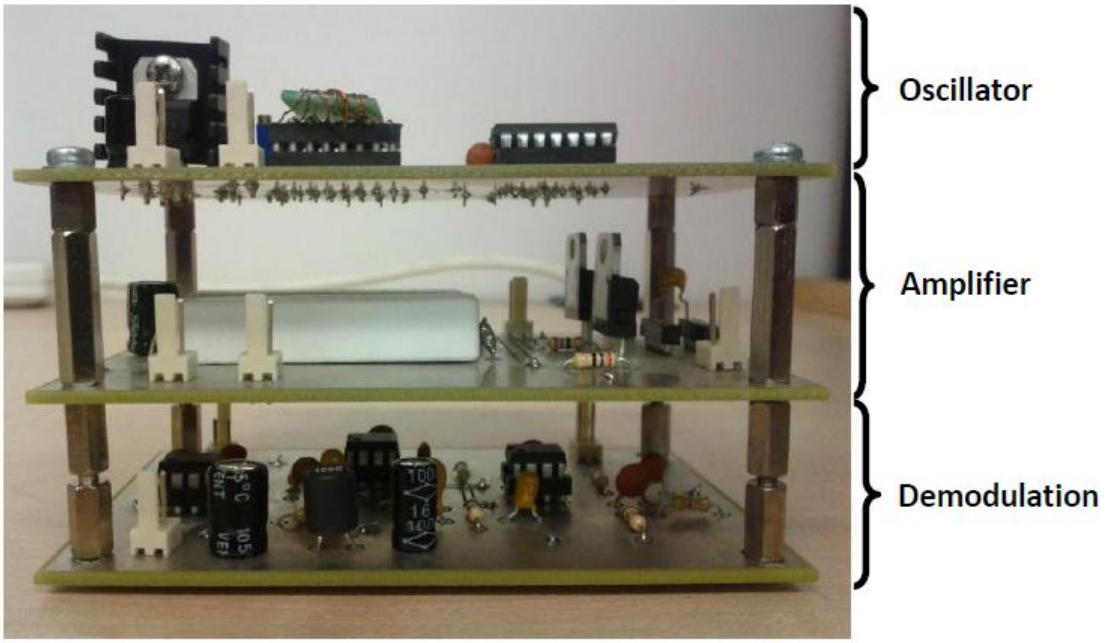

Figure 3.12: Side view of reader unit prototype.

Description of the demodulation stage is provided in chapter 4.

The design of this particular reader unit is not critical to this project. The only important factor is that it allows us to read the tag from distances equal to or greater than the typical thermal insulation thicknesses. There is scope to improve many aspects of this reader unit.

3.3.2 RFID transponders

Commercially available tags were employed as sensors in this project. The three tags used were the TK5551, ATA5567 card tag and the ATA5577 disk tag from Atmel Corporation [111, 112]. The three tags have a large difference in size in order to assess the performance of small and large coils. For the intended application of placing the tags on insulated pipe, the TK5551 tag is better suited due to its smaller dimensions allowing for easier attachment onto curved surfaces.

Figure 3.13: Three commercially available tags used in study and their dimensions.

The internal block diagram of the TK5551 tag is shown in Figure 3.14. The tag coil is attached to an analogue front end which converts from ac to dc in order to power the microchip. All tags have the same basic layout. All three tags used come in plastic packages.

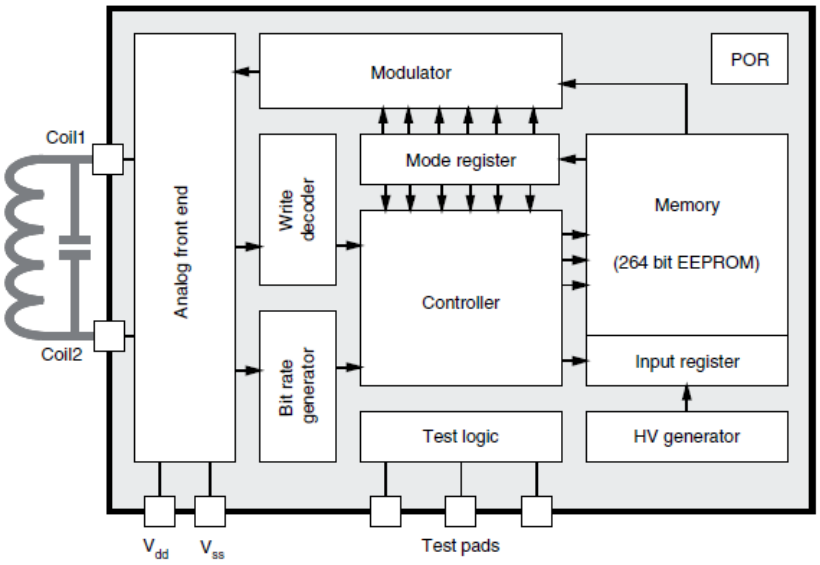

Figure 3.14: Internal block diagram of the TK5551 tag.

3.4 System Usage Scenario

It is envisioned that the ultimate use for the system considered in this study is for the monitoring of corrosion on insulated steel pipes or structures where the surface is inaccessible. Tags placed at various locations on an insulated pipe are interrogated periodically to monitor the pipe for corrosion development.

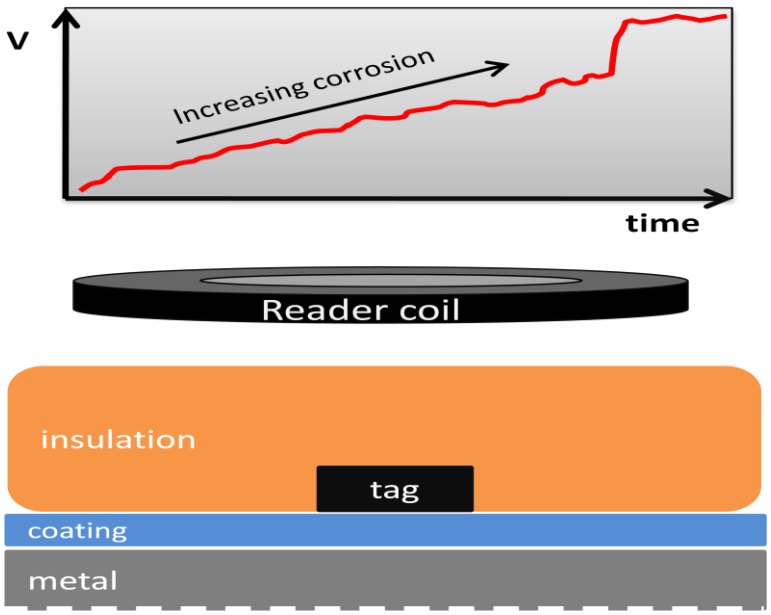

Figure 3.15: Depiction of intended usage scenario with tag embedded under insulation to monitor any corrosion development on the steel pipe.

The passive nature of the tags means that they can be implanted under the insulation for long periods of time without any battery depletion concerns.

3.6 Chapter Summary

In this chapter, introduction to and the theoretical basis of passive LF RFID corrosion sensing has been discussed. The reasons for selecting LF RFID over other frequencies are provided. The effect of metal on the tag and the influence of reader coil position on the output signal have been discussed. The reader unit and tags used in this project have been identified.

The rest of this thesis will report on the experimental studies carried out and the solutions developed to overcome problems identified. Critical analysis and discussion of the results is provided and identification of weaknesses of the approach is in the following chapters.

Chapter 4. Experimental Investigation of RFID Corrosion Sensor

In the previous chapter the underlying theory behind RFID corrosion sensing was outlined. In this section the research methodology followed by results from several experimental studies investigating the detection capabilities of the RFID system are outlined. First, the samples used in the experimental studies are described. Next, properties of the tags that play a crucial role in detection are discussed. This is followed by description of data acquisition, signal processing and feature extraction methods. The rest of this chapter consists of the results from 5 experimental studies. The first study demonstrates the RFID systems ability to differentiate not just between corroded and non-corroded steel but four different qualitative surface conditions that are of importance to the coatings industry. The second study investigates the tag's response to the addition of increasing displacement between the tag and metal. This has important implication for the detection of physical changes such as blistering and delaminations in the coating layer. Study 3 looked into what effect the tag's data bit rate or switching frequency has on detection. In study 4, using a set of naturally corroded steel plates, the RFID system's capability to differentiate between corrosion levels, defined by the exposure time of the steel to the atmosphere, has been investigated. Finally, study 5 discusses the differences between the RFID system and tradition eddy current testing. Using a simple experiment the increased sensitivity of the RFID system over an equivalent EC setup to changes in corrosion is demonstrated. The work in this chapter is based on [1, 2]

4.1 Research Methodology

This project involves the experimental investigations using carefully created samples to demonstrate the possibility of using passive LF RFID for the monitoring of corrosion on insulated pipes. An RFID reader is designed and constructed to allow reading of tags on steel at large standoff distances. Signal processing methods are developed to extract meaningful features. Experiments are conducted with special attention to the samples and how they change. Along with careful control of certain parameters, such as the reader coil position, the measured features are correlated with known qualitative properties of the samples to demonstrate detection capabilities. All the corrosion samples used in this study have been naturally corroded by exposing the steel to the atmosphere for various periods of time.

4.1.1 Study 1: Surface preparation grade samples

The first experimental study involved steel samples which were differed in terms of corrosion levels as well as surface roughness created by applying various surface preparation methods. The separation distance between the reader coil and tag is carefully controlled to avoid repositioning errors.

The major assessment criteria for the tests involving the surface preparation grade samples will be:

- Corrosion detection and differentiation; tests using steel samples with and without corrosion will be undertaken to demonstrate ability of the RFID system to reliably detect and differentiate between corroded and non-corroded steel.
- Detect and differentiate between surface conditions; four steel plates have been prepared in such a way as to have four qualitatively graded surfaces, based on surface roughness. The test is to determine what effect surface roughness, which is important for the bonding of coating to steel, has on the RFID tag signal amplitude. It is expected that a rougher surface will have lower amplitude due to shorter eddy current path lengths.

4.1.2 Study 2: Tag liftoff

Following on from study 1, study 2 aims to investigate the effects of physical displacement between the tag and metal. The displacement between the tag and metal was simulated using sheets of 100 micron thick paper placed beneath the tag. A total of ten sheets of paper are used to create a maximum 1mm displacement.

The major assessment criteria for the tag liftoff tests will be:

- Detection of minimum displacement; by incrementally increasing the displacement between the tag and metal the minimum detectable change will be determined. This test has important implications for the detection of coating related defects such as blisters and delaminations which may be a precursor to corrosion.

4.1.3 Study 3: Effect of tag's frequency

In study 3 the influence of the tag's data rate or switching frequency on measurements is investigated. The samples and experimental setup is the same as study 1, the variable being the tag's frequency.

4.1.4 Study 4: Corrosion progression samples

A new sample set is introduced to assess the RFID system's capability to differentiate between different stages of corrosion on steel. The samples vary in terms of the length of time they have been exposed to the atmosphere resulting in increasing corrosion levels with increasing exposure time. The test is arranged such that the samples exhibit a monotonic change in corrosion i.e. increasing exposure time, while keeping other parameters such as reader coil position fixed. The signal features can then be correlated with the change in the sample property.

4.1.5 Study 5: RFID vs. traditional eddy current NDT

An experiment was undertaken to demonstrate the benefit, in terms of sensitivity, of having a RFID tag on the metal as opposed to a setup consisting of just a reader coil over a metal akin to traditional eddy current NDT. Once again, the reader coil position for each measurement is kept constant. The variables in this experiment are the presence (or lack of) a tag and change in sample condition (corroded vs. non-corroded). The percentage change in the signal amplitude is obtained for both setups to evaluate the sensitivity.

4.1.6 Position independent corrosion measurement

The problem of the measured signal features dependence on the position of the reader coil is tackled in two complementary steps. First, synthetic RFID data is created to simulate measurements of different samples with the reader coil at varying heights above the samples. Statistical analysis is performed on the data to remove the effect of reader coil position. The synthetic data is also used to understand what parameters of the data are important for position independence. In step two, two experimental studies are undertaken. The first experiment involves measurements performed on three samples with the reader coil at increasing heights above the sample. Displacement is only in the vertical direction. The reader coil is mechanically fixed in order to prevent movements in the horizontal directions. The second experiment involves measurements of the

same three samples but with the reader coil at unknown positions both vertically and horizontally with respect to the tag. Statistical analysis is then performed on both experimental data and the results are compared to assess success of method to remove effect of reader coil position from measurements.

The same statistical method is then extended to tackle the problem of temperature variation. Three corrosion samples, arranged such that there is increasing severity of corrosion, are heated using hot plates at increasing temperatures with the tag placed on top. Measurements are then taken at each temperature step. Statistical analysis is then applied to the combined data from all three samples to decouple the influence of temperature and corrosion.

4.1.7 Accelerated corrosion under insulation testing

In the final experimental study, two steel pipes with tags attached at different locations are covered with 50 mm thick calcium silicate insulation. The pipes are then cyclically heated and salt water is added to the insulation to induce and accelerate corrosion development on the surface of the pipes. Measurements are then taken over a period of days. The experiment aims to create realistic environmental conditions that tags placed on real pipes may encounter.

4.2 Samples

To explore the detection capabilities of the RFID system, carefully designed samples have been prepared by International Paint. These samples present realistic surface conditions and corrosion levels to test whether the RFID sensor can detect and differentiate between them. All the samples used in this study are made from structural steel (S275) which is a low carbon mild steel.

The samples are grouped into two sets. The first set, called the *surface preparation grade* samples, are designed to test the capability of the RFID system to reliably differentiate between non-corroded and corroded steel. Furthermore, these samples allow us to test the system's ability to differentiate between four qualitatively graded steel surface conditions which are of importance to International Paint and the protective coatings industry as a whole.

The second set of samples, called the *corrosion progression* samples, has been created to investigate the RFID systems capability to differentiate between different levels of

corrosion. The samples are created by exposing the steel plates to outdoor conditions for different lengths of time. The result is natural corrosion for a more realistic experimental scenario.

4.2.1 Surface preparation grade samples

The long term effectiveness of anti-corrosive paint applied to steel is primarily dependent on the surface preparation carried out before applying the coating. Poor surface preparation can lead to the paint not adhering to the surface of the steel. Therefore, it is vital to be able to specify the condition of a surface which in turn will help in choosing the best preparation method required. The Steel Structures Painting Council (SSPC) in cooperation with the Swedish Corrosion Institute and the American Society for Testing and Materials (ASTM) have created a standard for qualitatively grading steel surfaces. The surface grades used in this study are described below.

Four 30 by 10 cm steel plates have been prepared. Three of the plates have been placed inside an environmental test chamber for 1 month to accelerate the build-up of corrosion. All the samples were then surface treated. From Table 4.1, rust grade A plate has been blasted (Sa2.5) using an abrasive agent primarily to ensure a surface free from corrosion/contaminants prior to applying a coating layer. Therefore, the grade A plate has no corrosion. Grade B or SP11 plate has had any surface corrosion power tooled down to bare metal. As can be seen in Table 4.1, the SP11 treated plates are much thinner than the rest. The power tooling also resulted in a smother surface as shown by the laser profilometry measurement of average surface roughness Ra. Next, we have the ST2 treated plate which has had any loose surface corrosion scraped away to leave a layer of rust with no significant pitting visible. Finally, we have the grade D sample, which has had no surface preparation. The result is a very rough surface with significant level of visible surface pitting and flaking rust. A photograph of the four samples is shown in Figure 4.1.

Table 4.1: List of samples along with average thickness measurements and laser profilometry measurements of average surface roughness Ra.

Sample	Surface grade/ preparation	Average plate thickness (mm)	Average surface roughness Ra [um]
UC1	A / blasted (Sa2.5)	4.077	18.3
UC2	B / SP11	3.898	16.1
UC3	C / ST2	4.142	29.1
UC4	D / unprepared	4.429	56.7

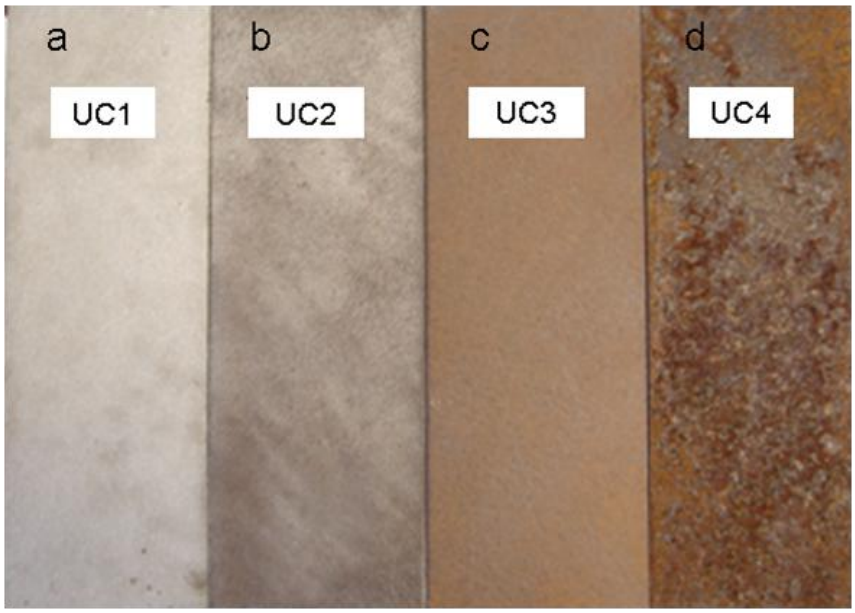

Figure 4.1: Photograph of all four surface preparation grade samples. The differences between the samples can be clearly seen.

4.2.2 Corrosion progression samples

The corrosion progression samples consist of ten 30 by 15 cm steel plates that have had a 3x3 cm section of the surface exposed to the atmosphere for 1, 3, 6, 10 and 12 months to allow rust to build up. The rest of the plate surface was covered by an adhesive tape to prevent any exposure to the atmosphere. After exposure, half the plates were spray painted with an epoxy phenolic based paint with a typical thickness of 100 microns. So for each exposure duration there is one uncoated and one coated plate. Images of the uncoated and one coated rust patch are shown in Figure 4.3.

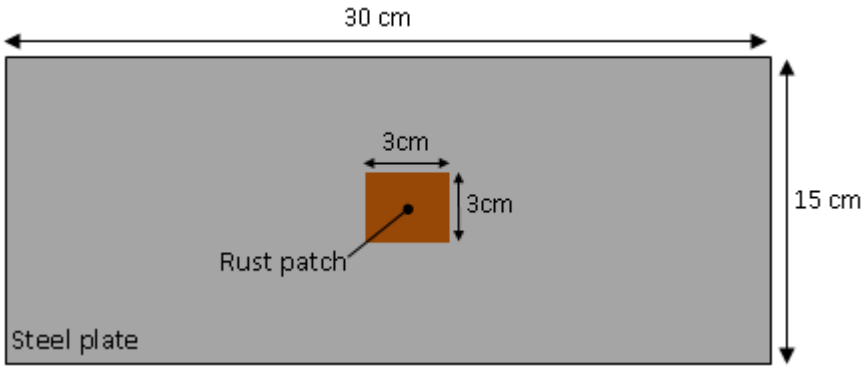

Figure 4.2: Dimensions of the sample and rust patch.

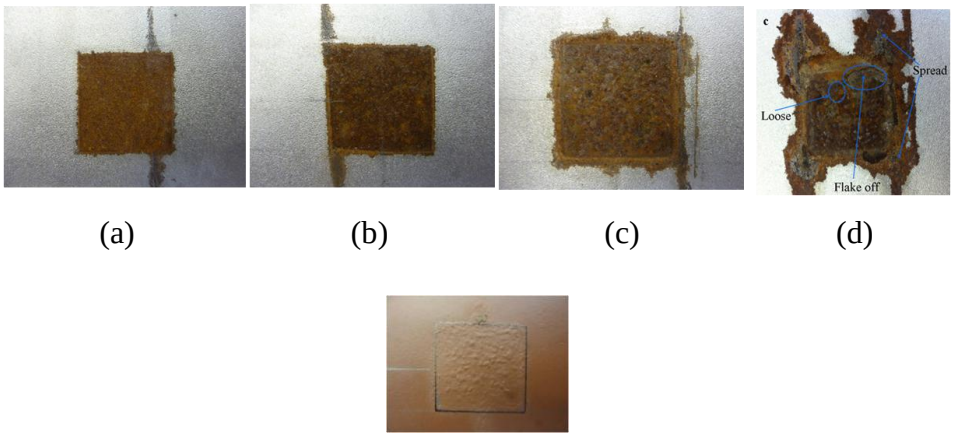

(a) (b) (c) (d)

(e)

Figure 4.3: Image of (a) 1 month, (b) 3 months, (c) 6 months, (d) 10 months and (e) coated 3 months exposure samples. The 6 month and 10 month samples show signs of the corrosion spreading into the surrounding metal.

The main purpose of these samples is to demonstrate The RFID system's capability to differentiate between corrosion at different stages in time.

4.3 RFID Tag Modulation Code

The modulation code stored in the memory of an RFID transponder is what gives it its unique ID. Most commercial tags including the ones used in this study allow the code to be modified by the user. The advantage of modifying the ID is that it allows us to create a uniform stream of 1's or 0's by filling the tag's data blocks with either '00000000' or 'FFFFFFFF' (see Figure 4.4) that are easier to process and extract features from as it allows for averaging over many cycles.

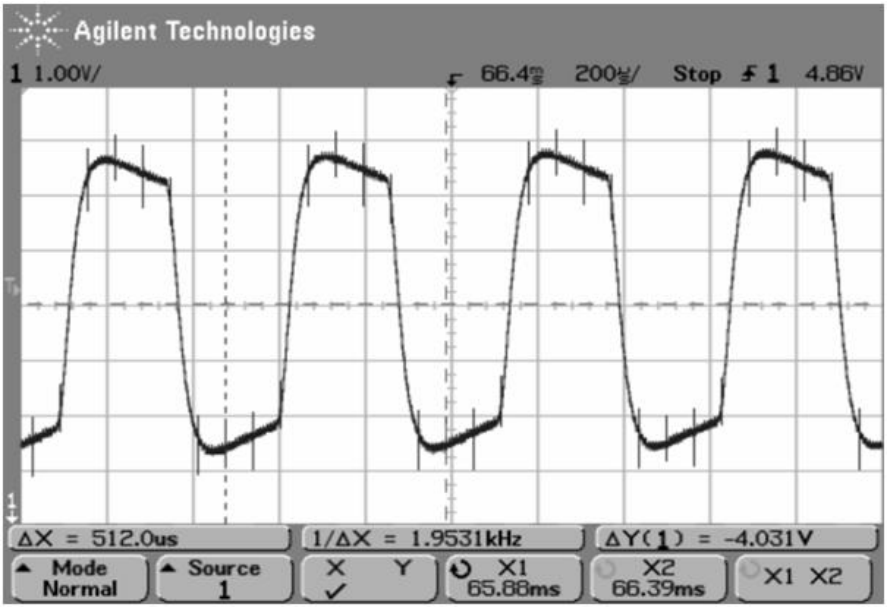

Figure 4.4: Section of the tag's ID showing the uniform code.

The tags used in this study were programmed using the ATA2270B-EK1 RFID reader kit from ATMEL Corporation (Figure 4.5) [113]. The kit provides a PC interface for easy programming of the tags. Additionally, the tool allows the tag's data rate or frequency to be set. The effect of tag frequency on detection is explored in Study 3 below.

(a) (b)

Figure 4.5: The ATA2270b-EK1 RFID reader kit from ATMEL used to program the memory content of the tags. The main board (a) and the RFID reader daughter board (b) are shown above.

All the tags used in this study such as the ATA5577 contain 7 32bit user rewritable memory blocks. The configuration window for the ATA5577 tag is shown below.

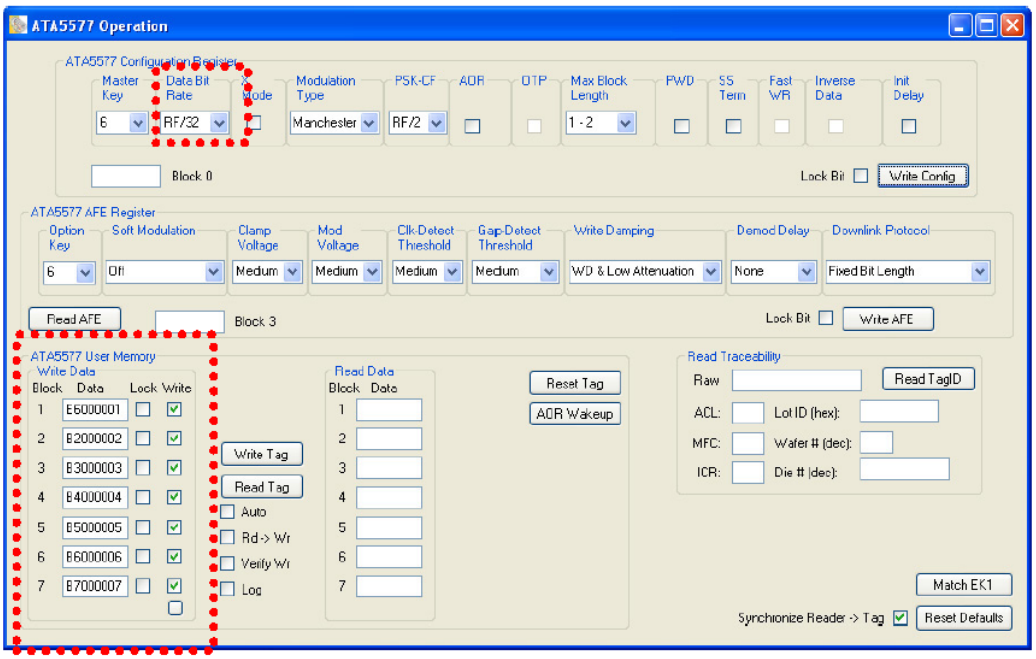

Figure 4.6: User interface to program ATA5577 tag. The writable memory blocks and the data bit rate portion of the configuration register are highlighted.

4.4 Data Acquisition, Signal Processing and Feature Extraction

The signal taken from directly across the reader coil is passed through demodulation circuitry, Figure 4.7, to remove the 125 kHz carrier and any unwanted noise. The circuit includes an envelope detector connected to an op-amp buffer. The signal is then fed into an op-amp bandpass filter with cut-offs at 160 Hz and 16 kHz. The gain of this stage is 10. The final stage of demodulation is a non-inverting buffer whose output is then connected to the data acquisition card. The circuit is supplied by a wall adapter that outputs 9V that is then converted to 5V using a voltage regulator. Although not shown in the circuit diagram, the supplies to the op-amps are decoupled to earth using capacitors to reduce noise.

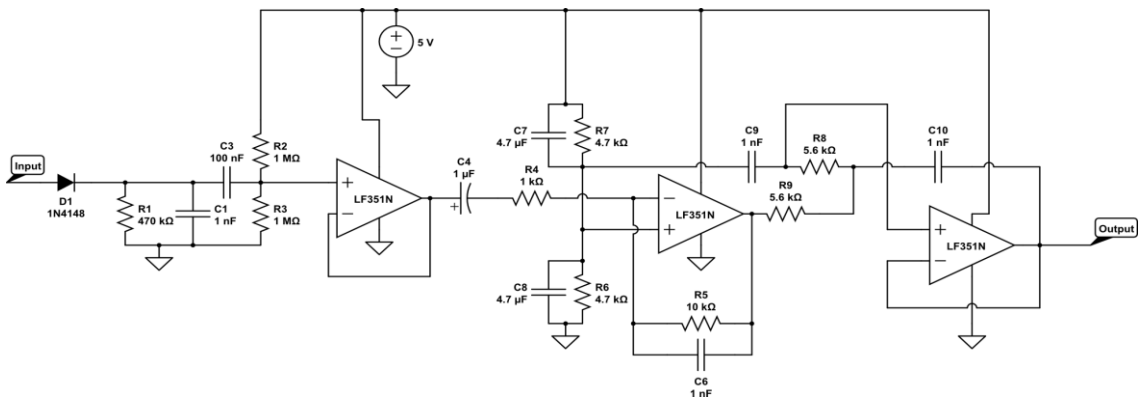

Figure 4.7: Demodulation subsection of the reader circuit.

The output signal of the demodulation circuit is sampled using a 14-bit Adlink 2010 data acquisition card. The card has the capability of acquiring data at a maximum rate of 2MS/s. The data acquisition is controlled in the PC using a LabVIEW program which allows the user to set the sample rate and the number of samples to be acquired.

The feature selected for analysis is the peak voltage (PV) value of the RFID tag signal. The amplitude change accounts for more than 99% of the variance and is therefore the best choice. Unlike PEC NDT, transient analysis of the tag pulses is not available since the eddy currents generated in the metal is by the 125 kHz sinusoidal excitation. The square pulses of the tag's signal are due to load modulation via the switching of a FET in the tag i.e. there is no magnetic field component at the data frequency. A simple peak detection algorithm in Matlab is used to find all the maxima points, see Figure 4.8, of a mean subtracted waveform containing n periods. An average value of the PV's is then obtained to minimise the effect of any noise that may be present in the waveform. This averaged PV is then the feature for each sample/ measurement.

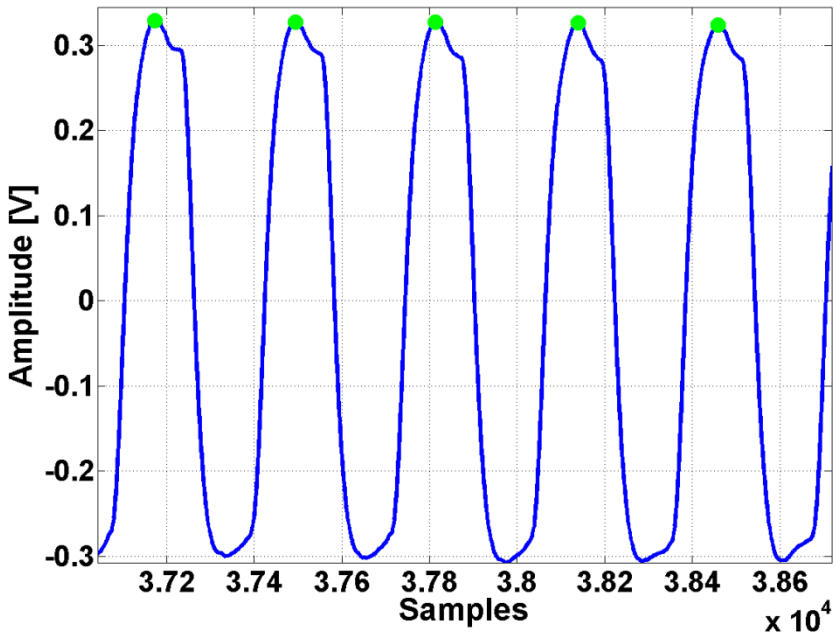

Figure 4.8: A section of the RFID tag waveform with the peak values indicated by a peak detection algorithm.

4.5 Study 1: Surface Preparation Grade Samples

The first experimental study involving the surface preparation grade samples was an attempt to provide a proof of concept. The experimental setup shown in Figure 4.9 was used. A card tag was placed at the centre of the steel plates with the reader coil me-

chanically fixed using nylon bolts 40mm directly above the tag. The tag-reader coil separation distance and alignment was carefully controlled in order to prevent any position dependent signal change as discussed in section 3.2.4. Five measurements per sample were performed. The output was sampled at 1 MHz with 100000 data points.

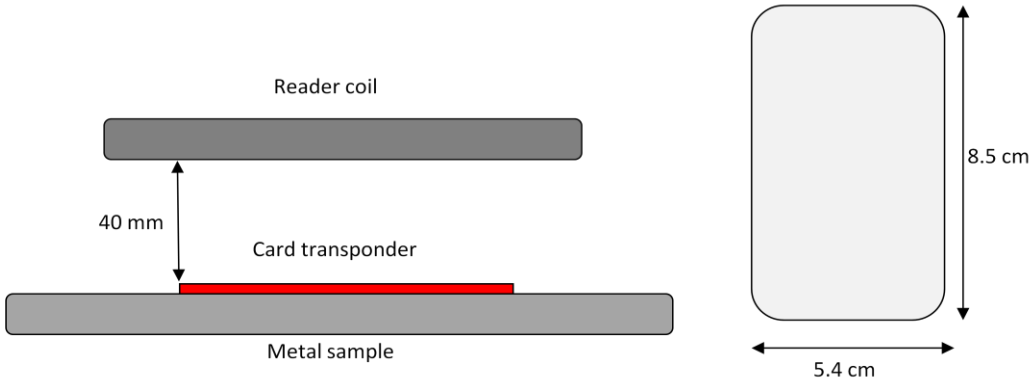

(a) (b)

Figure 4.9: (a) Experimental setup to test whether the four surface preparation samples can be distinguished. (b) Card tag dimensions.

The ATA5567 card tag was chosen for this experiment because of its large size. It was assumed that the tag's large coil diameter will result in an averaging of the rough surface of the samples. The card tag was programmed with 'FFFFFFFF' in all data blocks and a data bit rate of 125 kHz / 40 = 3125 Hz with 50% mark-space ratio.

The average PV for each sample is plotted in Figure 4.10. The first thing to note is that all the samples are distinguishable with very small deviation from the mean PV. With the exception of UC2, the trend seen in the results are in accordance with increasing corrosion and surface roughness. The corrosion in UC3 and UC4 reduce the conductivity σ and magnetic permeability μ 'seen' by the tag. With decreasing σ and μ, the tag's resonant frequency moves towards the free space resonant frequency resulting in the tag absorbing more power from the reader and hence an increase in the PV. Increasing surface roughness is expected to have an effect similar to decreasing conductivity as a rough surface increases the eddy current path length. This may also explain why sample UC2, which has the smallest measured surface roughness, has a smaller PV than UC1. Additionally, the application of power tooling to UC2 has resulted in greater inhomogeneities in magnetic permeability because with ferrous metals, the measured magnetic field can vary significantly due to the magnetization and magneto-resistive

effect. In contrast to magnetic permeability, the electrical conductivity variation across a non-ferrous conductor, due to metallurgical variations, does not exceed a few percent [114]. The reduced thickness of the UC2 plate is not expected to be a factor in the results since the skin depth for carbon steel at 125 kHz is expected to be much less than 1mm. Finally, the trend seen in Figure 4.10 correlates with the average surface roughness Ra values in Table 4.1.

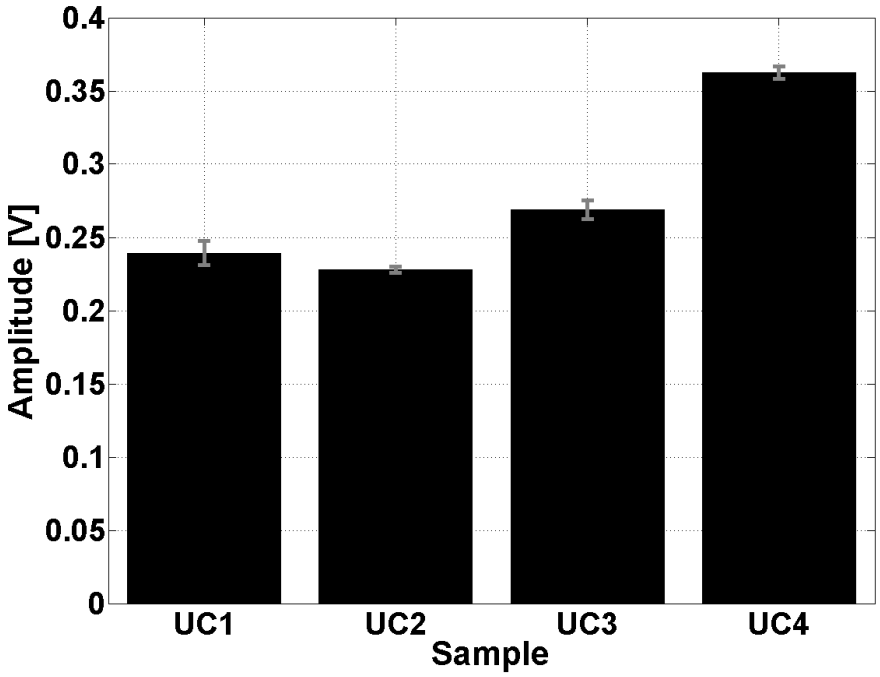

Figure 4.10: Average PV for each sample

4.6 Study 2: Tag Liftoff

Traditionally in NDT, liftoff (LO) is defined as the displacement between a sensing element and the material under test. LO is an important factor that needs to be taken into account in measurements and is used in eddy current based measurements of coating thickness. In this study the LO if defined as the distance between the tag and the surface of the metal. The purpose of this experimental study was to investigate the minimum change in displacement that can be measured using the RFID system. This has important implications for the detection of coating related defects such as blistering and delaminations.

It was difficult finding a method to introduce small liftoff steps. The xyz scanning table available in the lab has a minimum step size of 1 mm which is far too large in compari-

son to the typical coating thicknesses. A precision scissor jack was available that could be used to create very small increments in liftoff. However, it is made of metal which will severely disturb the magnetic field of the reader coil. Eventually, it was found that sheets of standard printer grade A4 paper have a very consistent thickness of approximately 100 microns. So the LO was created by adding sheets of paper between the tag and the metal. A total of 10 sheets were used with an average thickness of 108 microns measured using a Mitutoyo digital micrometer. The total liftoff was approximately 1 mm.

The experimental setup was almost the same as for the first study. The difference is the addition of sheets of paper between the tag and metal. Sample UC1 was used for all measurements. Just as the previous study, a card tag was placed at the centre of the sample with the reader coil fixed at 40mm above. Once again the displacement and alignment between the tag and reader was carefully controlled. Three measurements were taken for each liftoff height. The output was sampled at 1 MHz with 100000 data points. The tag's frequency was set at 3906 Hz. The PV change in response to increasing liftoff is plotted in Figure 4.12.

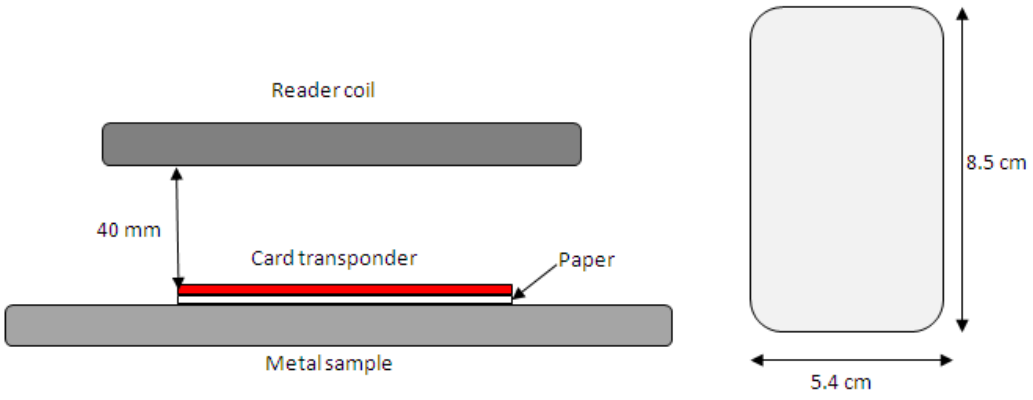

(a) (b)

Figure 4.11: Experimental setup for testing the effect of tag liftoff.

The results clearly show that the RIFD system can detect changes in liftoff of at least 100 microns. It is expected that smaller changes in liftoff may be detected, however, there was no way to increment LO by less than 100 microns. A near linear change in PV is observed for the range of liftoffs. It is predicted that the PV values will level off when the LO is very large as there will be negligible interaction between the tag and metal. Essentially becoming a free space measurement.

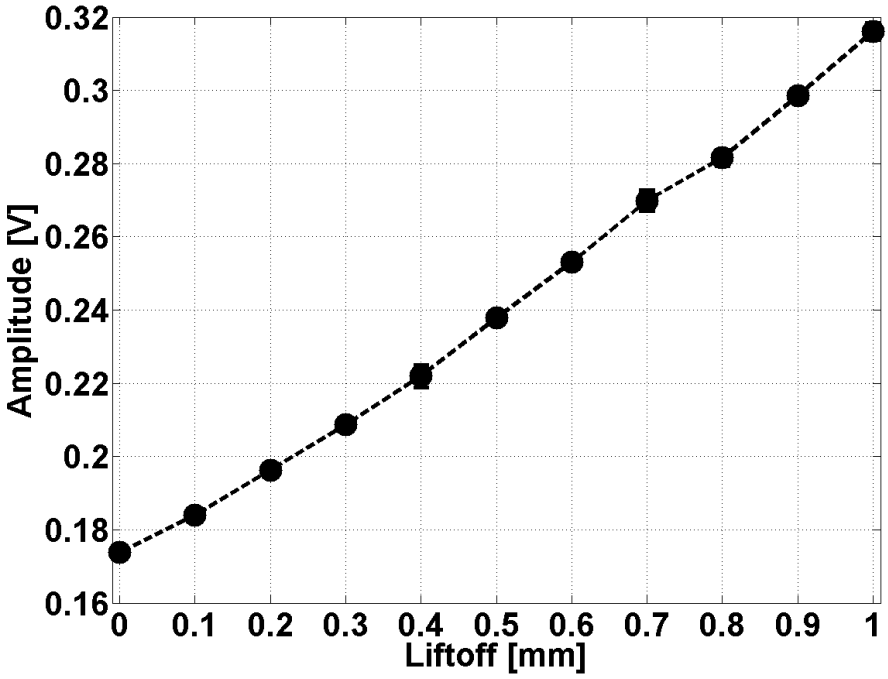

Figure 4.12: Plot showing changes in PV with increasing liftoff.

4.7 Study 3: Effect of Tag's Frequency

As mentioned in section 4.3, the tag's data rate or switching frequency can be modified by the user. In this section we investigate what effect different switching frequencies have on the detection capability. The experimental setup and samples are the same as described in section 4.5. The card tag was reprogrammed with 125 kHz / 128 = 976 Hz and 125 kHz / 32 = 3906 Hz switching frequencies. The results are plotted in Figure 4.13.

The results show that increasing the tag's switching frequency reduces the amplitude. This is most likely due to the load MOSFET switching characteristics (on/ off time).

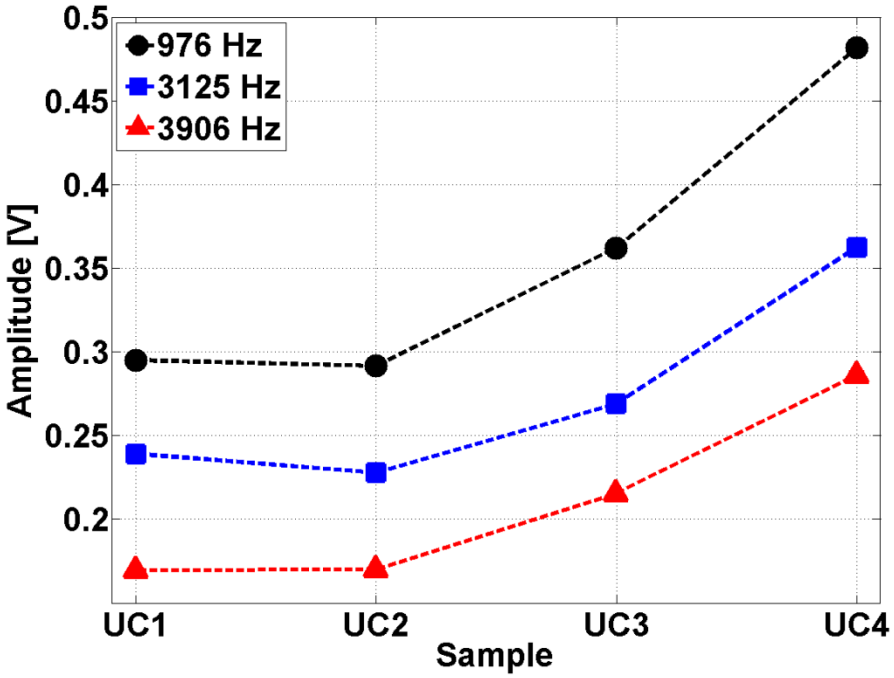

Figure 4.13: Plot showing the effect of tag switching frequency on detection. Lower switching rates results in higher PV.

4.8 Study 4: Corrosion Progression Samples

In this study we show the RFID systems capability to differentiate between 5 naturally corroded samples. As described in section 4.2.2, the samples have been created by exposing a small 3×3 cm section of the plates to the atmosphere for 1, 3, 6, 10 and 12 months.

Due to size of the corroded region the ATA5577 disk tag, which has a 3 cm diameter, has been chosen as the sensor. The tag is placed on the corroded region with the reader coil 45 mm above in fixed alignment (Figure 4.14). The tag's frequency has been set at 3125 Hz and 50% duty ratio.

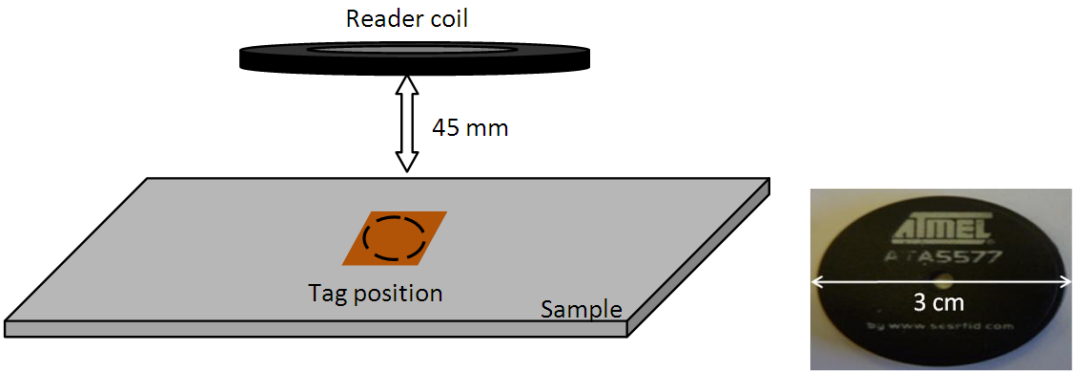

(a) (b)

Figure 4.14: (a) Experimental setup with tag placed on the corroded region. (b) Image and diameter of ATA5577 disk tag.

For each corrosion sample the measurements were repeated 10 times. The output was sampled at 1 MHz. The results for the coated and uncoated samples are shown in Figure 4.15(a) and Figure 4.15(b) respectively.

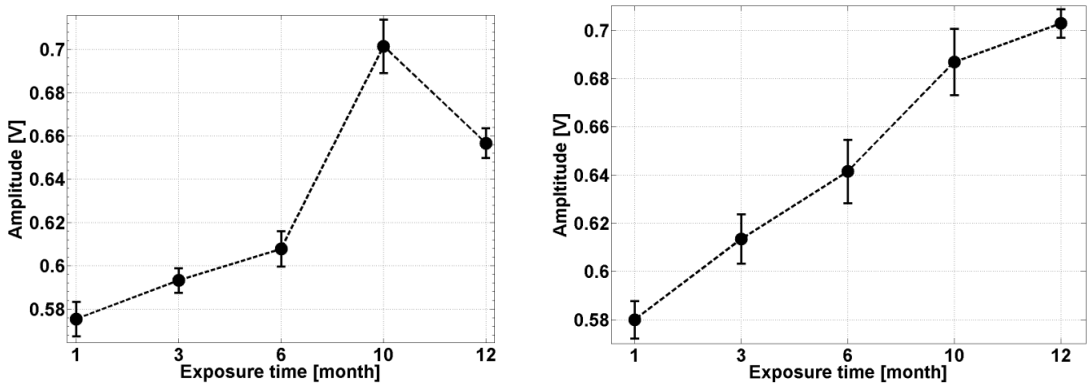

(a) (b)

Figure 4.15: Change in PV with increasing corrosion/ exposure time for (a) uncoated and (b) coated samples.

With the exception of the uncoated 12 month exposure sample, a monotonic increase in amplitude with increasing exposure time is observed for both the uncoated and coated samples. This once again can be explained by the corrosion build-up reducing the coupling between the tag and metal. The uncoated 12 month sample shows a drop in amplitude, which is not observed for the coated sample. This can be explained by the fact that after a certain exposure period the rust begins to flake and peel off over time. This ultimately reduces the thickness of the rust patch, bringing the tag closer to the metal and

hence lower tag's signal amplitude. The coating has prevented such flaking and loss of material.

The amplitude of the tag response from the coated samples is greater than the uncoated samples. This can be explained in two ways. Firstly, the coating layer increases the separation distance between the tag coil and the metal surface, reducing mutual coupling. The shift in the tag coil inductance is smaller and hence the resonant frequency of the tag is closer to the readers' frequency. In addition, eddy currents induced on the surface of the metal produce magnetic fields perpendicular to surface. These fields oppose the primary field of the reader coil, damping the magnetic flux and creating a 'dead zone' just above the metal surface [105]. The closer the tag is to the surface, the lower the flux linkage in the tags coil due to reduced coupling with the reader coil.

4.9 Study 5: RFID vs. Traditional Eddy Current NDT

It may be argued that the presence of the tag provides no benefit in terms of sensitivity and that the RFID setup is equivalent to a traditional eddy current setup without the tag. In this study we demonstrate that in fact the presence of the tag improves sensitivity compared to an equivalent eddy current setup. To demonstrate this, consider the experimental setup shown in Figure 4.16.

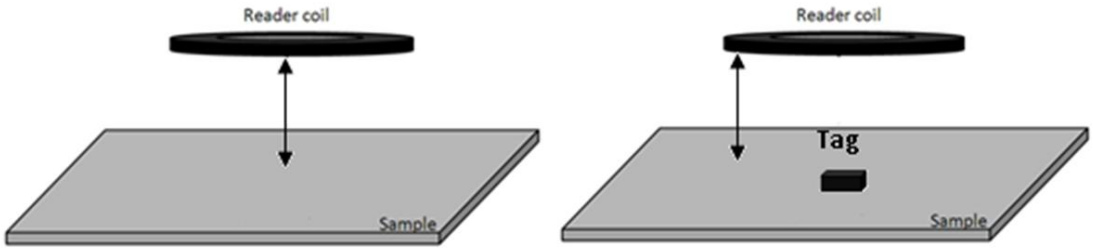

(a) (b)

Figure 4.16: Experimental setup (a) without tag and (b) with tag.

The experimental setup shows a reader coil at a height above a steel sample with and without a tag present on the sample. First, let us consider the setup without a tag. The reader coil, supplied with a sinusoidal excitation, will induce eddy currents in the metal. The power lost in the metal due to eddy currents with no tag is denoted as P_1. Any significant change in the sample e.g. due to corrosion will cause a change in the power lost in the metal ΔP_1. This change in power absorbed by the metal may be detected by a subsequent change in the impedance of the reader coil ΔZ_1.

Now considering the setup with the tag present we denote the power absorbed by the metal and the tag as P_2. Once again, a change in the sample condition will result in a change in power absorbed ΔP_2. Change in P_2 will cause a change in the reader coil impedance ΔZ_2. Now, for the claim of the increased sensitivity of the setup with the tag to be true, and assuming all other things being equal, ΔP_2 must be greater than ΔP_1 and hence ΔZ_2 must be greater than ΔZ_1. In both cases the power absorbed by the metal is approximately the same. Therefore, the change in power absorbed by the tag due to a change in the sample must be big enough for our claim to be true. This is a reasonable assumption since, as discussed in chapter 3, the tag is a tuned resonant system. Small shifts in the resonant frequency will result in relatively large shifts in power absorbed by the tag. Therefore, the tag is essentially amplifying the changes in the sample.

To demonstrate this experimentally, the setup in Figure 4.16 along with samples UC1 and UC3 were used. The reader coil was fixed 30 mm above the samples with measurements taken with and without the tag present. For each arrangement the measurements were repeated 5 times. The whole experiment was also repeated with the reader coil 40 mm above the sample. The output was sampled at 1 MHz with 100000 data points. The tag used for this study was the TK5551 with 2.5 kHz frequency.

In this study we used two features: the peak amplitude of the tag signal and the peak amplitude of the carrier signal when no tag is present. The demodulation circuit shown Figure 4.7 was bypassed since it removes the carrier signal and so the output was taken from the point directly after the diode. At this stage the signal contains both the 125 kHz carrier and the 2.5 kHz tag signal. Also, the voltage is low enough for the DAQ.

To extract the amplitudes of the tag and carrier waveforms it was more efficient to transform the data into the frequency domain using the Fast Fourier Transform (FFT) and obtain the amplitudes of the respective signals (see Figure 4.17). In the setup with no tag, only the carrier amplitude was obtained and in the setup with a tag, only the tag's signal amplitude was taken. The results are shown in Table 4.2.

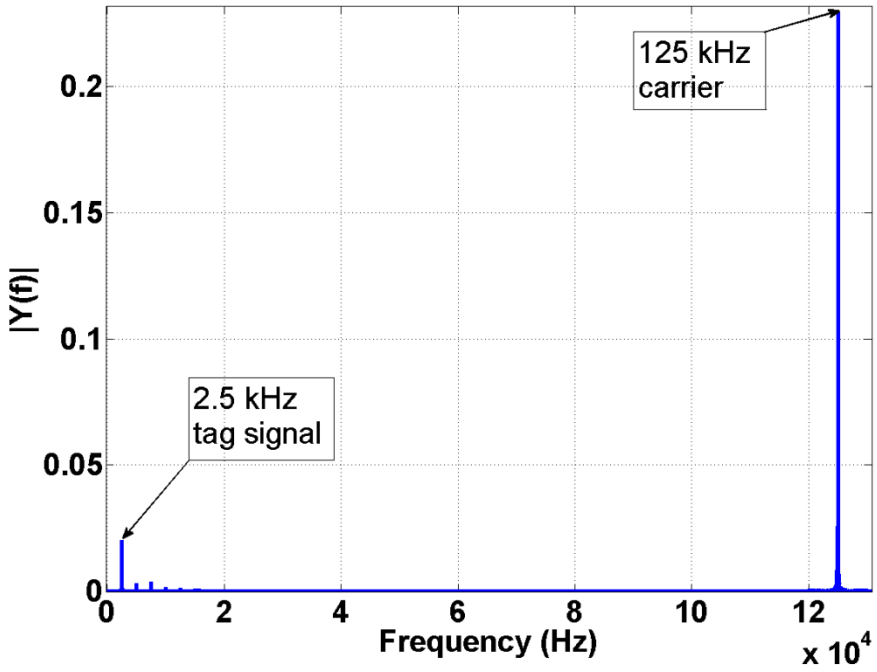

Figure 4.17: The tag and carrier components in the frequency domain.

Table 4.2: The change in tag and carrier signal amplitude with change in sample.

	Sample / Tag/carrier	UC1	UC3	Percentage change %
30 mm	**Tag amplitude [arb]**	**$0.0476 \pm 1.4\times10^{-4}$**	**$0.0505 \pm 5.4\times10^{-5}$**	**5.7**
	Carrier amplitude [arb]	**$0.2311 \pm 2.1\times10^{-4}$**	**$0.2300 \pm 1.9\times10^{-4}$**	**0.5**
40 mm	**Tag amplitude [arb]**	**$0.0193 \pm 2.1\times10^{-5}$**	**$0.0200 \pm 1.1\times10^{-4}$**	**3.5**
	Carrier amplitude [arb]	**$0.2333 \pm 2.1\times10^{-3}$**	**$0.2324 \pm 2.0\times10^{-4}$**	**0.4**

Results show that the percentage change in the tag's signal amplitude is approximately 10 times greater than the percentage change in the carrier signal amplitude for the same change in corrosion condition. Thus, we have demonstrated that the presence of an RFID tag improves sensitivity when large standoff distances are involved.

4.10 Chapter Summary

Several experimental studies have been performed to assess the detection capabilities of the RFID system. The samples used and the methods to process the data and extract features have been detailed.

An initial feasibility study has demonstrated the sensing capabilities of the RFID system. Four samples with different levels of corrosion and surface conditions were differentiated. The results show that the steel sample that had its surface power tooled had lower tag amplitude than the clean blasted steel sample. Power tooling appears to increase the conductivity and/or magnetic permeability experienced by the tag.

To test the tag's response to physical displacements between the tag and the steel surface, sheets of 100 micron thick paper was used. The results show that changes of at least 100 microns can be detected. Smaller increments weren't possible. This raises the prospect of employing the tags to detect some of the precursors of corrosion such as blisters and delaminations.

The tag's switching frequency or data bit rate has shown to affect detection. Lower frequencies have larger amplitude signals. This is likely due to the switching characteristics of the load MOSFET.

Two sets of steels plates with different levels of corrosion were created by exposing the plates to the atmosphere for different lengths of time. The experimental results show that using the RFID system it is possible to distinguish between the different stages of corrosion. The tag's signal amplitude increased with increasing exposure/ corrosion due to the reduction in electrical conductivity and magnetic permeability experienced by the tag. The tag's resonant frequency moves closer to the free space resonant frequency with increasing corrosion.

The final study in this chapter demonstrated the increased sensitivity of the RFID system over an equivalent eddy current system with no tag present. The resonant operation of the tag means that small changes in the surface condition of the steel is amplified by the tag resulting in almost 10 times greater amplitude change than the eddy current setup.

Chapter 5. Position Independent Corrosion Measurement

In the previous chapter the detection capabilities of the RFID system was experimentally demonstrated. To do this, however, required keeping the displacement between the reader coil and tag fixed for all subsequent measurements. Keeping the displacement fixed may not always be practical and so the applicability of the RFID corrosion sensor is limited. Even small changes in position can completely mask any useful information due to changes in corrosion in the RFID tag signal. Therefore, it is vital to the wider acceptance of the proposed RFID corrosion sensor to address the effect of repositioning. In this study, we demonstrate through the use of both synthetic and experimental RFID data how applying principal component analysis (PCA) to two RFID signal parameters can compensate for the repositioning effects, allowing us to detect corrosion independent of reader coil position.

5.1 Problem Background

As discussed in section 3.2.4, the amplitude of the tag's waveform is not only dependent on the condition of the steel but to a larger extent on the position of the reader coil with respect to the tag. This effect is shown in Figure 5.1 where the surface preparation grade samples are measured with the reader coil at three different heights above the tag.

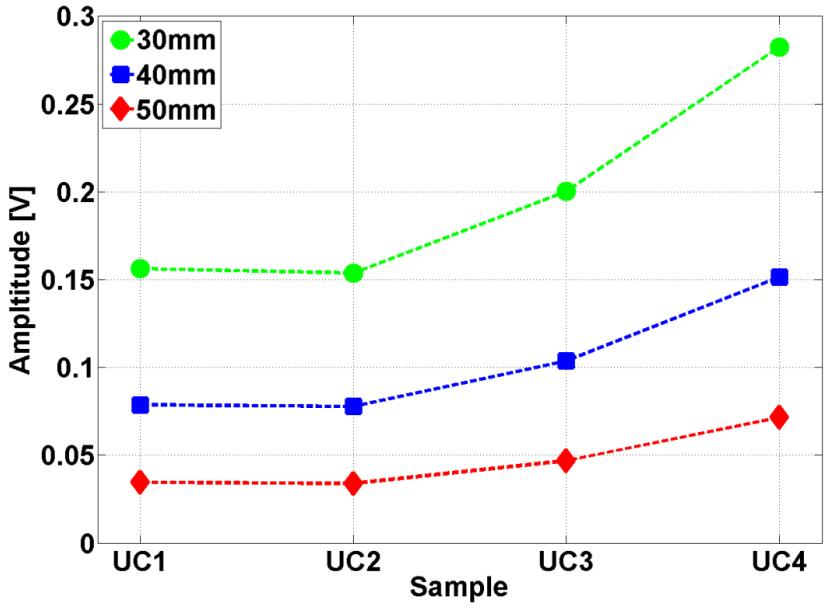

Figure 5.1: Plot showing the measurements from four samples with the reader coil at three different heights.

As can be seen from Figure 5.1 the changes in amplitude due to changes in reader coil position are much greater than the changes due to changes in sample.

To understand this problem further, a simple model of the tag's waveform has been created. The measured waveform of the tag (x) is modeled as:

$$\boldsymbol{x = A_R A_c A_T \, sin(\omega t)} \tag{5.1}$$

In equation (5.1) the tag's waveform is approximated as a sinusoidal signal. The variables in equation (5.1) are described in Table 5.1.

Table 5.1: Description of the variables in equation (5.1).

Variable	Description
A_R	Amplitude that is a function of reader-tag coupling/ displacement.
A_c	Amplitude that is a function of metal electrical properties (tag-metal coupling).
A_T	Amplitude which is a functions of tag's internal properties e.g. switching frequency.
ω	Tag data rate or switching frequency.

The repositioning problem arises due to the fact that changes in A_R are typically bigger than changes in A_c.

$$\boldsymbol{\Delta A_R > \Delta A_c} \tag{5.2}$$

The solution to this problem is based on work by Potyrailo et al. [115] who have successfully demonstrated position-independent analyte quantification by applying principal component analysis to four parameters of the RFID complex impedance. They observed that the second principal component (PC2) was position independent. The parameters of the complex impedance used are the frequency of the maximum of the real part of the complex impedance (F_p), the magnitude of the real part of the complex impedance (Z_p), resonant frequency of the imaginary part of the complex impedance (F_1), and anti-resonant frequency of the imaginary part of the complex impedance (F_2) [116].

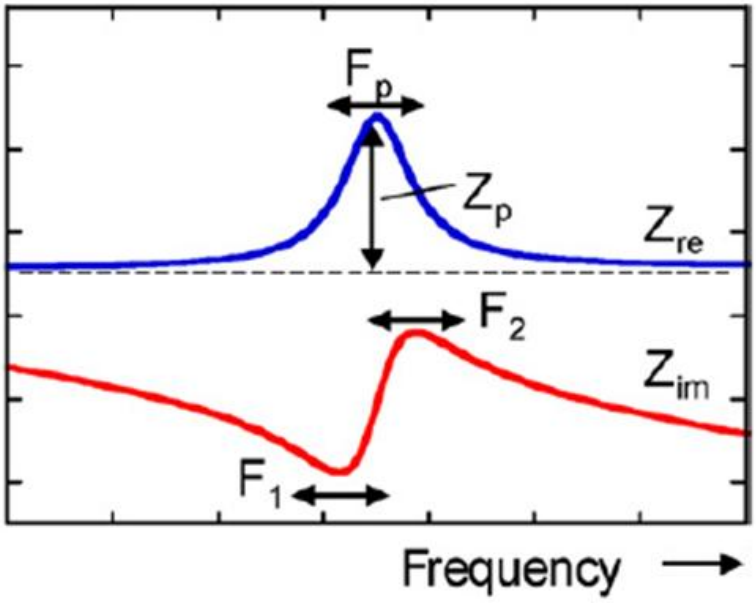

Figure 5.2: Features used by Potyrailo et al [115, 116].

In this study, we show that it is possible to attain position independence by applying PCA process on only two parameters of the RFID amplitude modulated waveform, namely the amplitude of the tag's signal and the amplitude of the 125 kHz carrier signal. Unlike [115], these two parameters do not require a network analyser and so are easier and cheaper to obtain. Furthermore, through the use of synthetic RFID data, we show how the properties of the two parameters influence the ability to compensate for position errors. The information learnt from the analysis of the synthetic data is then used to improve the position compensation for experimental results.

5.2 Feature Extraction

As previously described in sections 4.3 and 4.4 the analogue output signal of the RFID reader is the result of amplitude modulation (AM) of the tag switching frequency and the carrier frequency. The two features/ parameters of the AM signal used in this study are the amplitude of the tag's signal (t) and the amplitude of the carrier signal (c). These can be obtained either by filtering in the time domain or by extracting the amplitudes of the respective frequency components in the Fourier domain. The latter method has been used in this study.

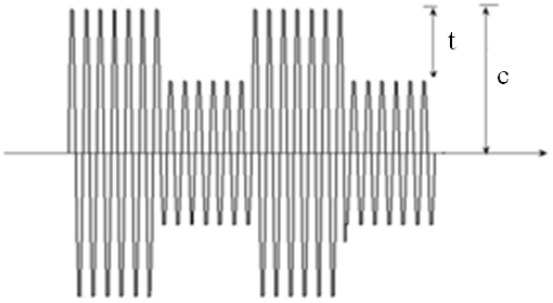

Figure 5.3: RFID amplitude modulation.

Values from multiple (n) measurements are then combined into an n×2 feature matrix **F** which contains the vectors ***t*** and ***c***:

$$\mathbf{F} = \begin{pmatrix} t_1 & c_1 \\ \vdots & \vdots \\ t_n & c_n \end{pmatrix} \tag{5.3}$$

PCA is then applied to **F**.

As previously discussed in section 3.2.3, any change in the metal's properties (σ, μ) will result in a bigger change in the tag coil's properties, as demonstrated in section 4.1.5, due to the fact that the tag coil is much closer to the metal than the reader coil. Furthermore, since the amplitude of sidebands (tag signal amplitude) of the carrier signal depends on the properties of the tag's coil, the change in t is greater than the change in c due to corrosion development. For the purposes of position independent corrosion measurement, it has been assumed that the vectors ***t*** and ***c*** are weakly collinear with respect to corrosion change and strongly collinear with respect to the position of the reader coil. This assumption, as will be subsequently demonstrated, is crucial to explaining the results obtained by PCA.

5.3 Principal Component Analysis

PCA is a multivariate statistical analysis method which transforms the RFID data into uncorrelated eigenvectors or principal components (PCs) corresponding to the maximum variability within the data [117]. The PCs are weighted sums of the original variables. The first PC accounts for the largest variation in the data. Subsequent PCs correspond to the remaining variability. PCA can extract the most dominant trends in data

and has been applied in the field of non-destructive testing to analyse data from pulsed eddy current (PEC) testing of corrosion [1, 118, 119].

The PCA method has been used in this work for following reasons: firstly, PCA has already been demonstrated by Potyrailo et al. [115] to produce position independent RFID sensor measurements. It is also mentioned in their paper that PCA removes collinearity which is ideal since, as discussed in section 5.2 above, it is assumed that the vectors ***t*** and ***c*** are strongly collinear with respect to the reader coil position and weakly collinear with respect to corrosion change. Therefore, applying PCA should remove this collinearity, producing position independent corrosion measurements.

The principal components can be obtained by the following procedure:

1. Remove the mean variable-wise (row-wise) from **F**.
2. Calculate the covariance matrix **C** of **F**:

$$\mathbf{C} = \sum_{i=1}^{n} [(t_i - \mu_t)(c_i - \mu_c)] \tag{5.4}$$

$$= \begin{pmatrix} \mathrm{var}(t) & \mathrm{cov}(t,c) \\ \mathrm{cov}(c,t) & \mathrm{var}(c) \end{pmatrix} \tag{5.5}$$

Where μ_t and μ_c are the expected values of the vectors t and c respectively.

3. Calculate eigenvectors (loadings) **W**, and eigenvalues of the covariance matrix. **W** is a 2x2 matrix which has been observed to be of the form (Hankel):

$$\mathbf{W} = \begin{pmatrix} -a & -b \\ -b & a \end{pmatrix} \tag{5.6}$$

Where *a* and *b* are the variance and covariance respectively.

4. Generate PCA component space (PCA scores) by multiplying **W** with the mean subtracted **F**:

$$\mathbf{PC} = \mathbf{W} \times \mathbf{F}^T \tag{5.7}$$

5. The output data matrix PC is expressed as a linear combination of orthogonal vectors along the directions of the principal components. The second principal component (**PC2**) has position independence:

$$\mathbf{PC} = \mathbf{W} \times \mathbf{F}^T$$

$$= \begin{pmatrix} -a & -b \\ -b & a \end{pmatrix} \times \begin{pmatrix} t_1 & \cdots & t_n \\ c_1 & \cdots & c_n \end{pmatrix}$$

$$\mathbf{PC1} = \begin{pmatrix} -b & a \end{pmatrix} \times \begin{pmatrix} t_1 & \cdots & t_n \\ c_1 & \cdots & c_n \end{pmatrix} \tag{5.8}$$

$$\mathbf{PC2} = \begin{pmatrix} -a & -b \end{pmatrix} \times \begin{pmatrix} t_1 & \cdots & t_n \\ c_1 & \cdots & c_n \end{pmatrix} \tag{5.9}$$

PC1 and PC2 are linear combinations of optimally-weighted observed variables. They are optimal in the sense that the components account for the maximal amount of variance in the data.

5.4 Synthetic RFID Data

The purpose of the synthetic RFID data is to help understand why PCA of the two real RFID features results in position independence and how changes in the properties of the two features affects the compensation process. The data is highly idealised and simplified representation of real RFID data.

The synthetic RFID data is created by assuming that the tag is placed upon three different corrosion samples with properties as shown in Table 5.2. These samples are the corrosion progression samples described in chapter 4.

For each sample, ‘measurements’ are taken with the reader coil at three heights in the vertical z direction (20mm, 30mm and 40mm) above the tag. There are 9 ‘measurements’ in total. The plots of the two vectors are shown in Figure 5.1. The values chosen for ***t*** and ***c*** are arbitrary – only the trend in vector ***t*** is based on experimental observations.

Table 5.2: Properties of the three corrosion samples.

Sample	Condition
S1	No corrosion, clean metal
S2	1 month corrosion
S3	6 months corrosion

For simplicity and to facilitate understanding of how the properties of the two RFID features affect **PC2**, the following assumptions were made:

1. No measurement errors or noise. In reality, external and internal noises create spread in the measurements.
2. Negligible effect of corrosion on the carrier wave features i.e. the amplitude for every sample at each height is the same. Experiments show that this is not strictly true. There is a small but noticeable effect due to change in corrosion on the carrier signal amplitude.
3. Displacement is only in the vertical (z) direction for simplicity.

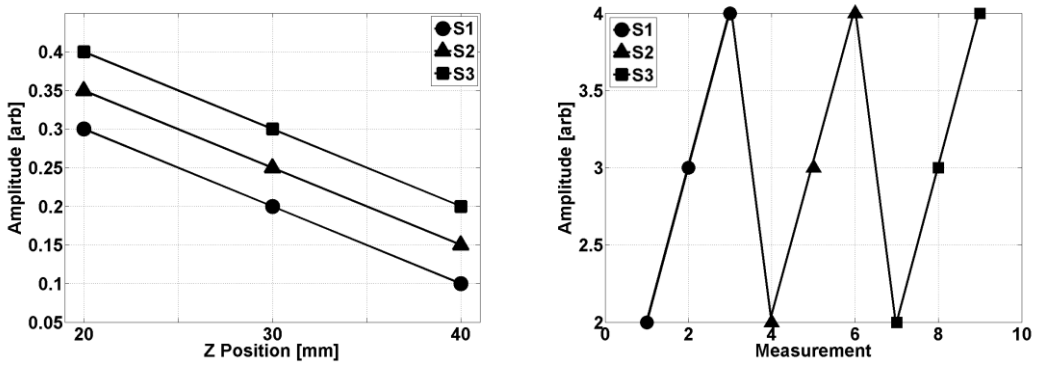

(a) (b)

Figure 5.4: Plots of vectors (a) t and (b) c.

Applying PCA, we obtain the following values for **W**:

$$\mathbf{W} = \begin{pmatrix} -0.995 & -0.0997 \\ -0.0997 & 0.995 \end{pmatrix} \tag{5.10}$$

As mentioned previously, **PC2** is position independent as shown in Figure 5.5. All nine measurements per sample are approximately the same amplitude and the three samples can be clearly distinguished. This is better illustrated if we average the nine measurements for each sample Figure 5.6.

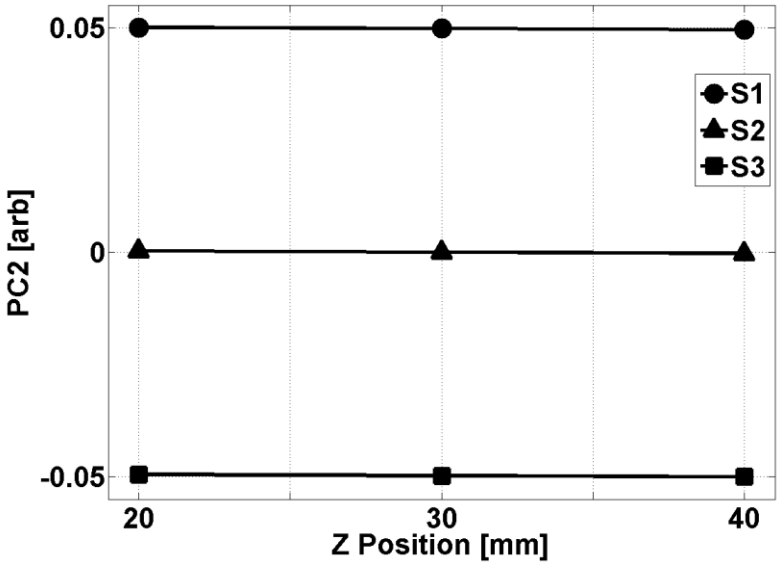

Figure 5.5: Plot of PC2 showing the amplitude independent of z position.

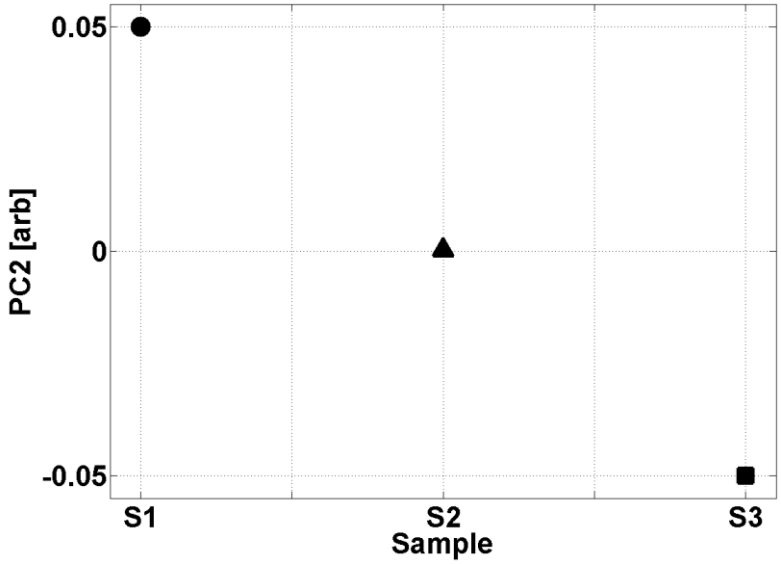

Figure 5.6: Plot of PC2 averaged over 9 measurements per sample.

5.5.1 Effect of scaling

The difference in magnitude between the vectors ***t*** and ***c*** determines how good the posi-

tion compensation will be. If the difference in magnitude is below a certain value, approximately 2 in this case, the position compensation is less effective. To demonstrate, vector ***c*** is divided by a scaling factor $s = 5$ before applying PCA.

The scaling leads to the separation of the different position measurements as seen in Figure 5.7. That is, the standard deviation (error) increases. The mean value for each corrosion sample get closer as the difference in magnitude between ***t*** and ***c*** becomes smaller. The effect on the matrix **W** is that the coefficient *a* slowly converges towards 0 while *b* rapidly converges to 1. The opposite is observed when the difference in magnitude increases. When assumption number 2 is true, position compensation works best when $a = 1$ and $b << 1$.

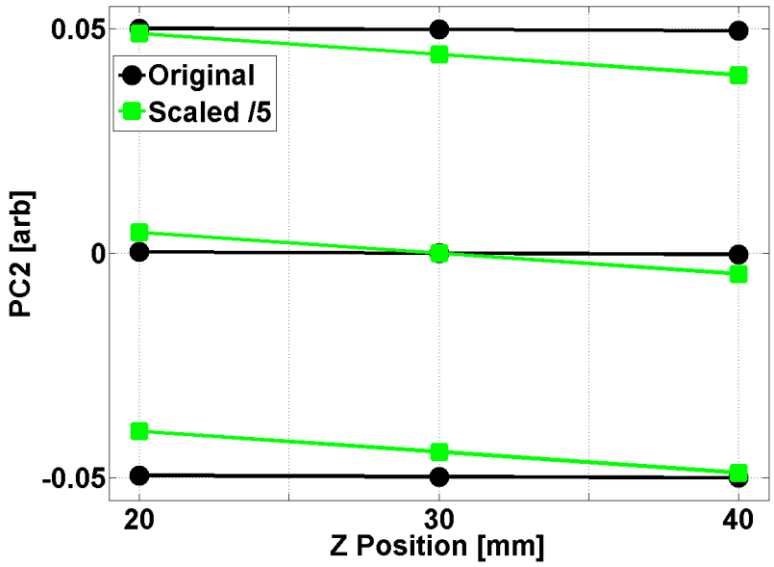

Figure 5.7: Effect of scaling on the second principal component (PC2).

There is an optimum value for *s* which can be found by observing the eigenvalues. Of the two eigenvalues, λ_1 and λ_2, of the covariance matrix ***C***, the smaller λ_2 converges at a certain scaling factor *s* (Figure 5.8). Since λ_2 converges, increasing *s* any further has no effect on **PC2**.

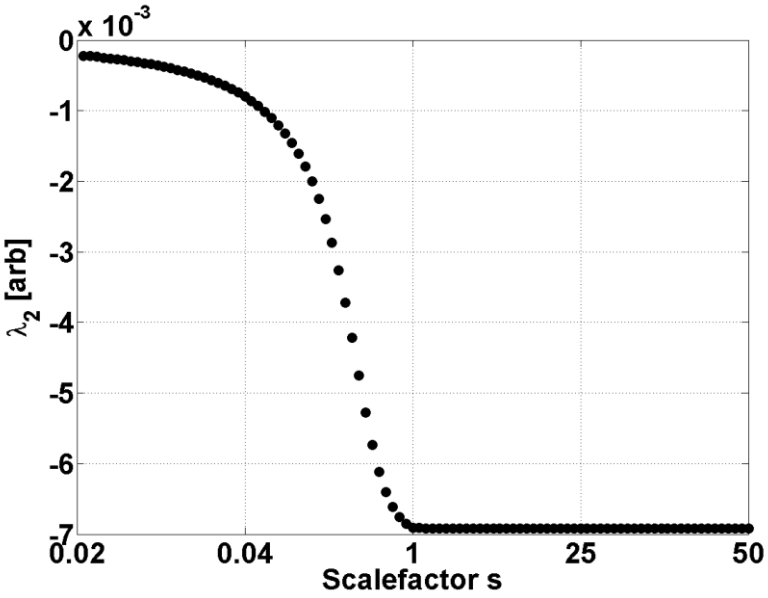

Figure 5.8: λ_2 converges with increasing s.

5.5.2 Effect of gradient on carrier signal

Previously we assumed there is no effect of corrosion on the carrier signal. Now we simulate the effect of corrosion on the carrier signal amplitude by adding a linear gradient or rotation to the vector **c**. As seen in Figure 5.9, the effect of the gradient is that the amplitude at the same height for subsequent samples is greater than the previous. This brings the synthetic data closer to experimental data.

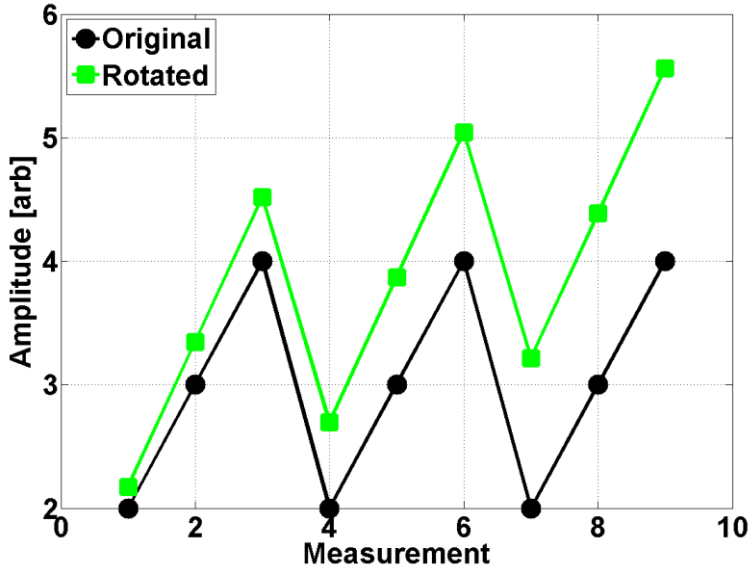

Figure 5.9: Vector ***c*** before and after applied gradient.

As in the case of scaling, the gradient leads to separation of the different position measurements as seen in Figure 5.10. Again, the standard deviation increases. With increasing standard deviation, there is a greater chance of overlapping between different corrosion samples.

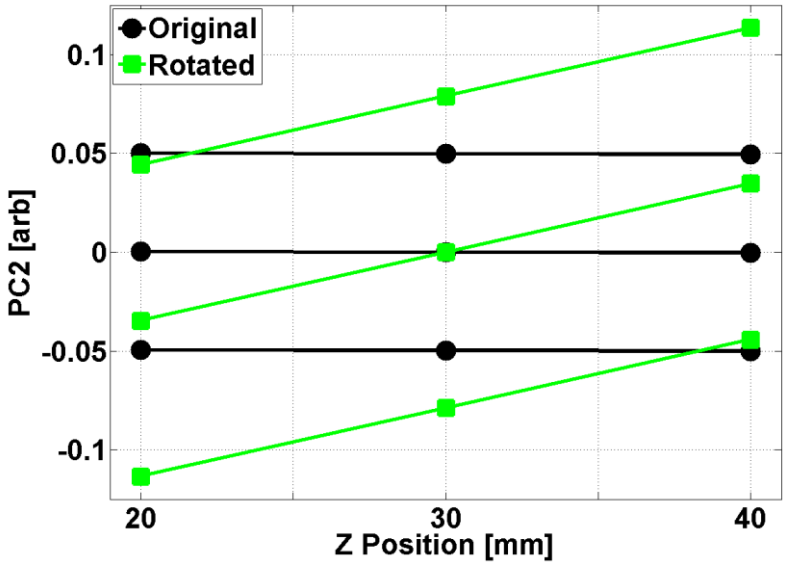

Figure 5.10: Effect of applied gradient on PC2.

In an ideal scenario, the effect of the gradient can be reversed by simply reducing or removing the linear gradient. However, given real data, it is difficult to estimate the gradient, which may not be linear, and to determine whether any apparent gradient observed is due to changes in corrosion or some other local features of the conductive surface. We can conclude that as the effect of corrosion change becomes more significant on **c,** PCA for position independence becomes less effective. This is due to greater correlation between **c** and **t** with respect to corrosion information. Therefore, the further the reader coil is from the metal surface the better the position-independence.

5.6 Experimental RFID Data

5.6.1 RFID system

The experimental study was performed using the ATA5577 circular disk tag (diameter 30mm, thickness 4mm).

5.6.2 Samples

The samples used in this study are from the set of corrosion progression samples described in section 4.1.2. One sample is completely free of corrosion. The other two samples have a 30mm x 30mm section of metal exposed to a corrosive environment for 1 month and 6 months respectively (Table 5.). All three samples were then coated with an epoxy phenolic based paint with a typical thickness of 100 microns. The difference between the 1 month and 6 month corrosion samples can be seen in the images of the uncoated rust patches (Figure 5.11).

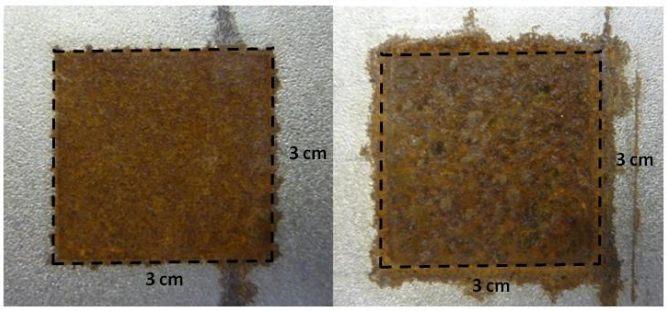

(a) (b)

Figure 5.11: Image of (a) 1 month and (b) 6 month corrosion. The 6 month corrosion appears to have rougher texture as well as greater spreading into the surrounding metal.

5.6.3 Test setup

To experimentally evaluate the effects of repositioning, the test setup is shown in Figure 5.12. The RFID tag is placed on the centre of the test sample. For samples S2 and S3 this is the location of the corrosion patch. The reader coil was then placed directly above the tag at varying heights z = 30, 35, 40 and 45 mm. As with the synthetic RFID data, the displacement is only in the z direction. Five measurements were performed for each z position.

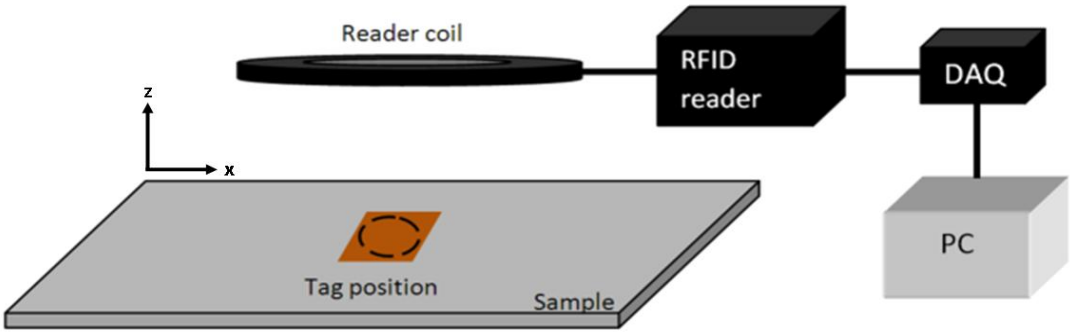

Figure 5.12: Schematic of the test system showing the sample and RFID system. The reader coil is mechanically fixed so as to prevent any displacement in the x direction.

The analogue amplitude modulated output of the reader was sampled at 1 MHz. Post-processing, including PCA, was carried out using Matlab.

5.6.4. Results and discussion

Figure 5.13 and Figure 5.14 show the measured tag and carrier amplitudes, respectively. As expected, the amplitude of tag signal decreases with increasing displacement between tag and reader coil. Whereas the amplitude increases with each subsequent sample at the same height i.e. the amplitude at 30mm for S3 > S2 > S1 at that height. Without compensation of repositioning effects, some measurements from S1 have larger amplitudes than measurements from S3. This can lead to the false conclusion that there is more corrosion in S1 than S3.

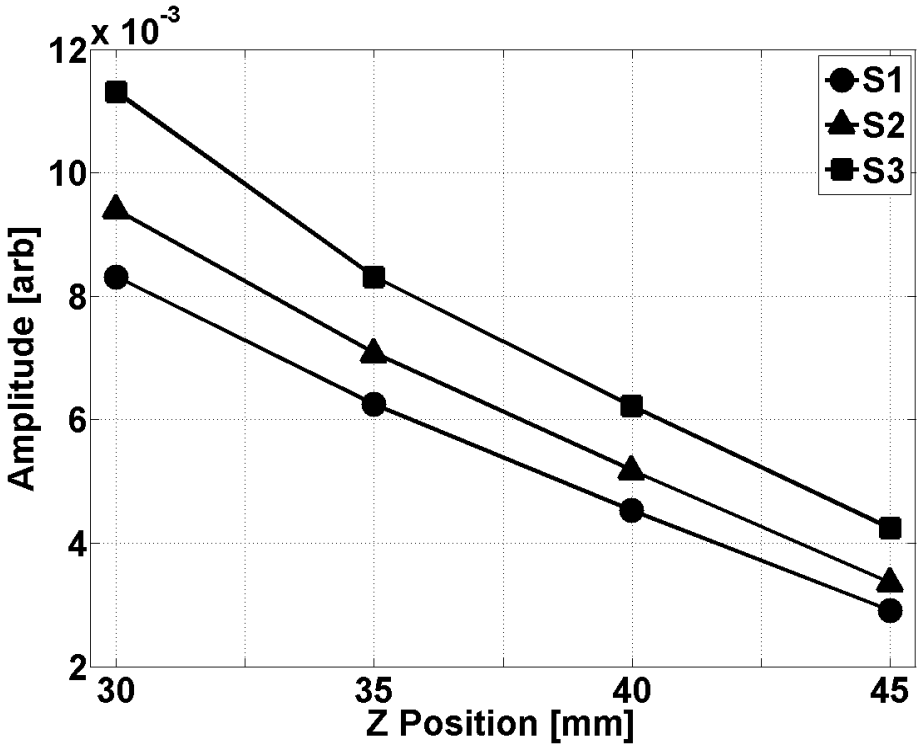

Figure 5.13: Plot of tag signal amplitude with increasing z position.

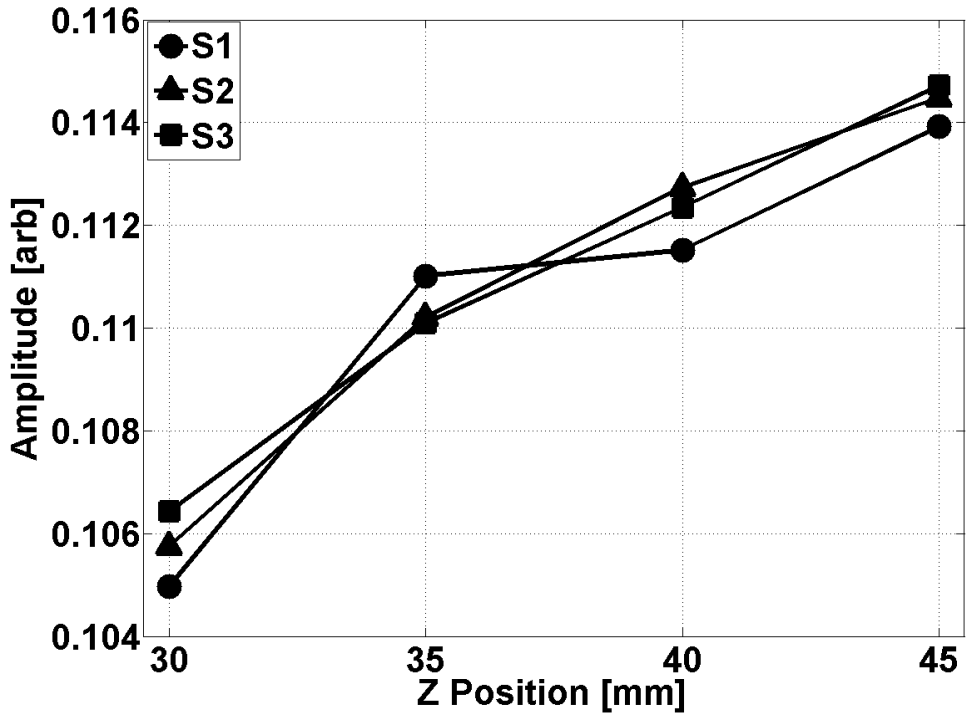

Figure 5.14: Measurements of carrier signal amplitude averaged over the 5 measurements per z position.

Applying PCA, we can observe in Figure 5.15 that it is possible to distinguish the three samples as the measurements from every height for each sample are closer together i.e. smaller standard deviation. This is clearer once all the measurements per sample are averaged (Figure 5.16).

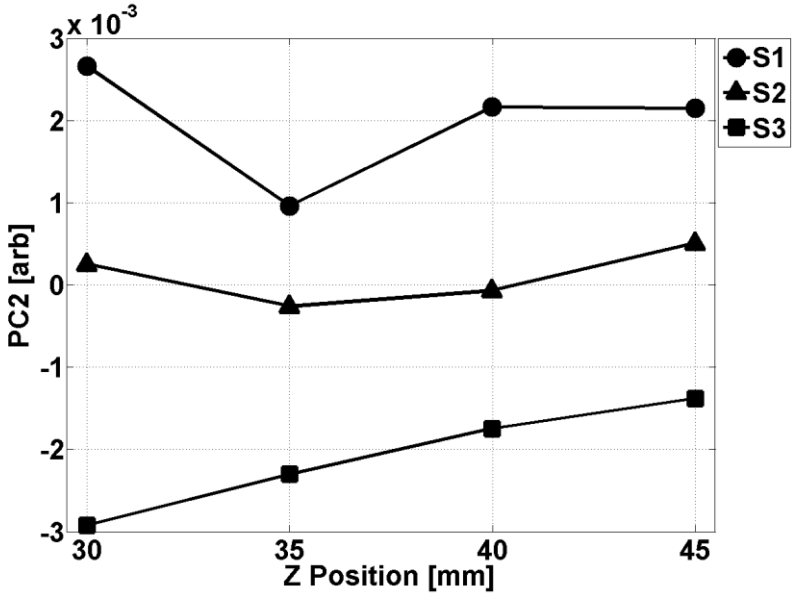

Figure 5.15: Plot of PC2 showing the three samples can be distinguished despite changes in z position.

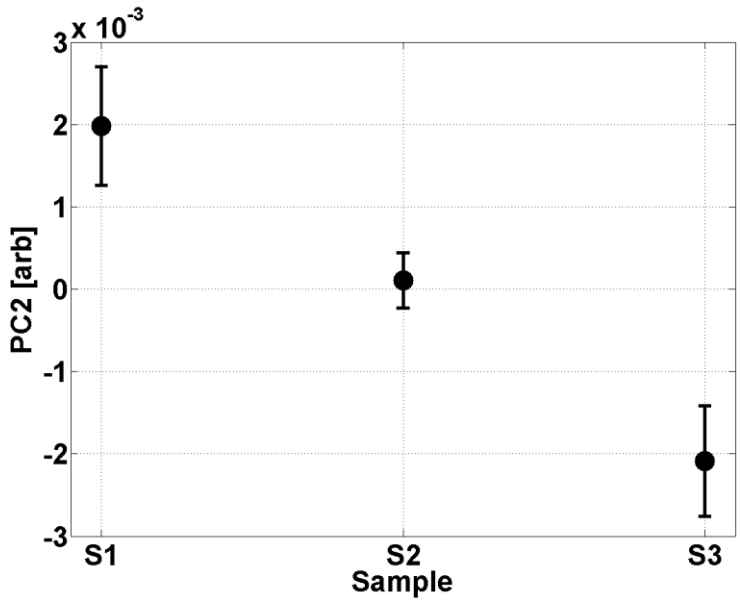

Figure 5.16: Plot of PC2 averaged over all the measurements per sample.

Best results were observed when the carrier signal data was scaled by 100 and both the carrier and tag data were rotated by 90º in opposite directions by multiply with the appropriate rotation matrix (Figure 5.17). The scale factor value was obtained by observing the behaviour of eigenvalue λ_2 as described in section 5.5.1. The 90º gradient angle was found by trial and error to give the largest mean-value separation between each sample.

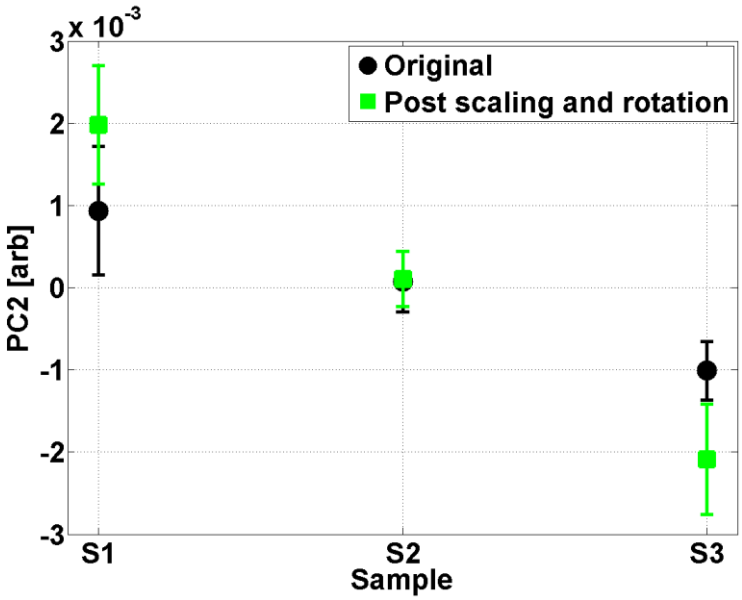

Figure 5.17: Plot showing PC2 of original data and PC2 of scaled and rotated data (linear gradient).

5.7 Free-Hand Measurements

For both the synthetic and experimental data, it was decided to have displacement only in the z direction for simplicity purposes. However, real measurements may include displacements in both x and z directions as well as angular (tilting) changes. To demonstrate the efficacy of the compensation method for both x and z direction displacements, free-hand measurements were performed. The samples and the experimental setup are the same as described in section 5.6. The only difference being that the position in both the x and z directions and the angular orientation of the reader coil with respect to the tag is completely free of any mechanical constraints.

Measurements were taken from each sample with the reader coil at unknown positions with respect to the tag. This was repeated 5 times for each sample with a total of 15 measurements. The measurement data are plotted in Figure 5.18 and Figure 5.19.

The plot of PC2 (Figure 5.20) averaged over the 5 measurements per sample shows good agreement with Figure 5.17 of the more controlled tests, demonstrating the ability of the method to compensate for x, z and angular position errors.

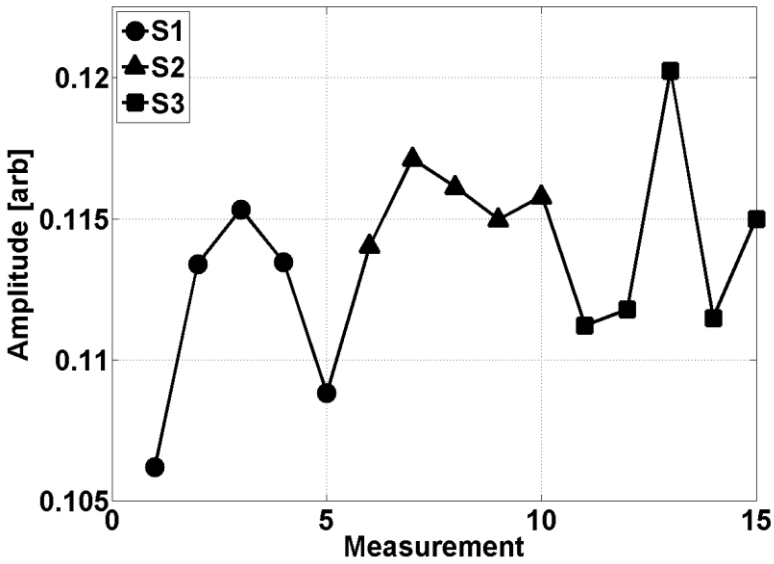

Figure 5.18: Plot of carrier signal amplitude for each sample measured at an unknown position.

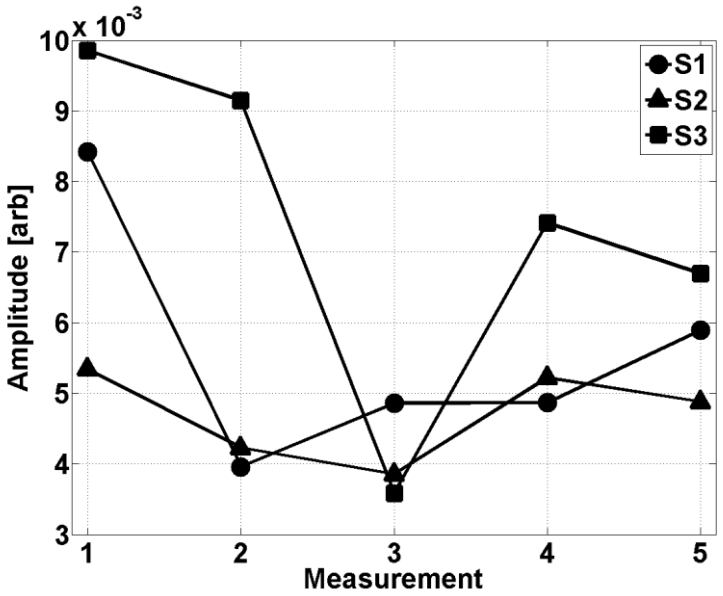

Figure 5.19: Tag signal amplitudes from free-hand measurements.

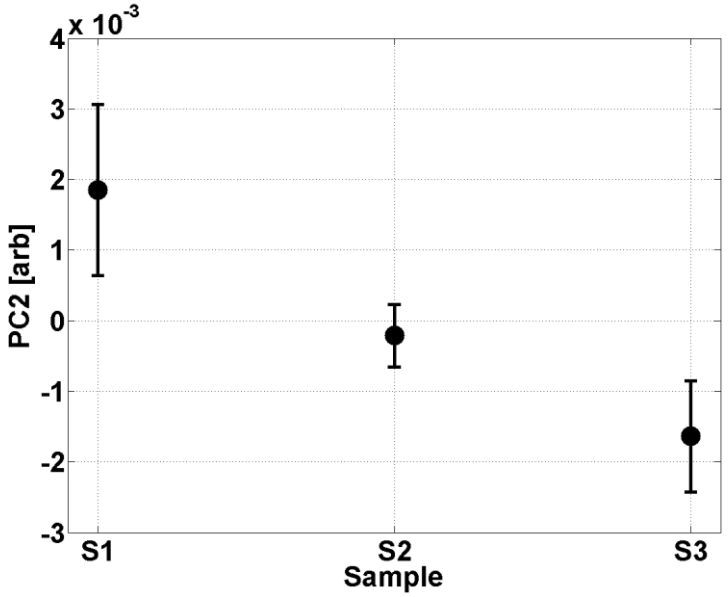

Figure 5.20: Plot of PC2 averaged over the 5 measurements per sample. The three samples are clearly distinguishable.

It is worth noting that in both the controlled and free-hand experiments, the carrier signal data is negatively correlated to the tag data. Though, it is also possible to show using the synthetic data that even if there was positive correlation between the two variables the position compensation works just as well. It is the strength of the correlation that determines how well the compensation will work. From the synthetic RFID data, it has been observed that the process works perfectly when $\boldsymbol{t}$ and $\boldsymbol{c}$ are only correlated with respect to position. However, by introducing corrosion information into $\boldsymbol{c}$ by adding a

linear gradient reduces the effectiveness of the method.

The reason why applying PCA to the chosen two variables results in position independence is due to the fact that the amplitude of the carrier signal ***c*** is predominantly a function of the height and angular displacement of the reader coil with respect to the metal surface. Whereas the amplitude of tag's signal ***t*** is dependent on both the tag-metal coupling (corrosion) and the reader coil position. In an ideal case we can say the following:

$\boldsymbol{c} = f$ (position)
$\boldsymbol{t} = f$ (position, corrosion)

The resultant principal components, **PC1** and **PC2**, are orthogonal to each other with **PC1** correlating with position information and **PC2** correlating with corrosion information.

In real RFID data, **c** is also a function of corrosion. However, the close proximity of the tag to the metal compared to the reader coil, means that change in conductivity and permeability due to corrosion will have a much bigger effect on the tag amplitude than the carrier amplitude. The smaller the effect of corrosion on the carrier signal, the better the position compensation will be. As demonstrated with the synthetic RFID data, in the ideal scenario where there is zero effect from change in corrosion on the carrier amplitude, there is complete position independence. Therefore, for best results ***t*** and ***c*** should both be functions of the reader position, while only ***t*** has corrosion information. In other words, the effect of PCA is to remove the collinearity between ***t*** and ***c***.

5.8 Temperature Independent Corrosion Measurement

An additional benefit of applying principal component analysis for position independence is that it can also be used for temperature independent measurements. An RFID tag placed on a pipe operating at high temperatures will have an output dependent on not only the corrosion condition but also the temperature. Therefore, it is essential to compensate for temperature variations in order to have accurate and reliable corrosion monitoring.

In general, an increase in temperature of a metal leads to an increase in resistivity and hence a decrease in conductivity. The Bloch–Grüneisen formula mathematically represents the relationship between temperature and resistivity for metals.

$$\rho(T) = \rho(0) + A\left(\frac{T}{\Theta_R}\right)^n \int_0^{\frac{\Theta_R}{T}} \frac{x^n}{(e^x - 1)(1 - e^{-x})} dx \tag{5.11}$$

Where $\rho(0)$ is the residual resistivity due to defect scattering. Θ_R is the Debye temperature. At high temperatures, the resistance of metals changes linearly with temperature.

Semiconductor components of an RFID tag, such as the microchip, also have a temperature dependence given by the Steinhart-Hart equation. The resistivity of semiconductors decreases with increasing temperature.

$$\frac{1}{T} = A + B\ln(\rho) + C(\ln(\rho))^3 \tag{5.12}$$

Where A, B and C are Steinhart-Hart coefficients.

Fortunately, the same technique applied for position independence can also be applied for temperature independence. All that is required are two variables that are collinear with respect to temperature. The first variable is obtained from the tag signal (*t*) since it also contains any corrosion information. The second variable is once again the carrier signal (c) since there is some thermal coupling between the hot plate/steel plate and the reader coil. Here, the frequency domain amplitude of the carrier signal is used.

5.8.1 Experimental setup

A TK5551 tag was placed on the centre of the corrosion patch on three (1 month, 3 months and 6 months exposure) samples from the corrosion progression sample set. Each plate was then placed on top of a hot plate (VWR VHP-C7) as shown in Figure 5.21 and measurements were taken with the reader coil at a fixed height 30mm above. The temperature of the hot plate was increased from 50 ^{o}C to 130 ^{o}C in steps of 10 ^{o}C. The output is sampled at 1 MHz.

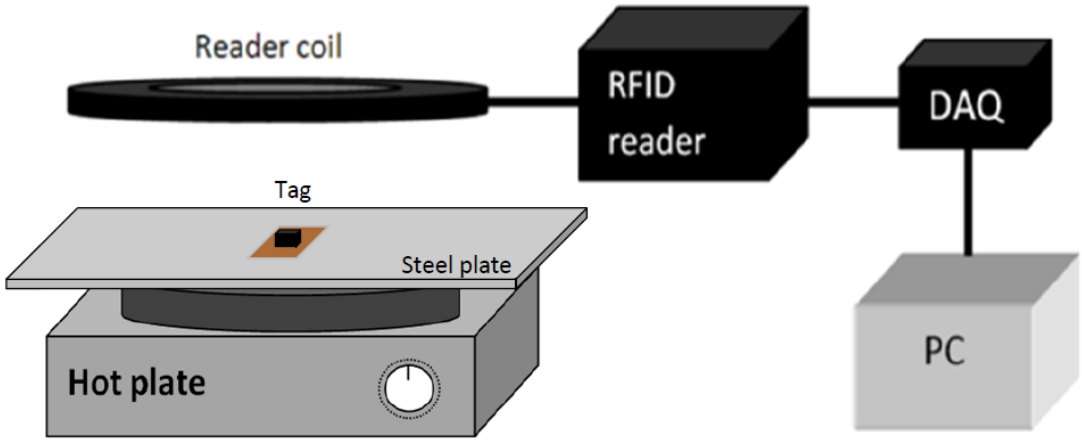

Figure 5.21: Experimental setup used to test corrosion measurements at varying temperatures.

5.8.2 Results and discussion

The peak amplitude from the frequency domain of the measured signals is plotted against temperature change in Figure 5.22. The results show that the peak amplitude decreasing with increasing temperature. This is due to increasing levels of resistivity leading to greater losses and less power being absorbed by the tag. The increases resistance dampens the resonant circuit. On the reader coil the signal amplitude is increasing with increasing temperature since the tag exerts less loading on the reader coil.

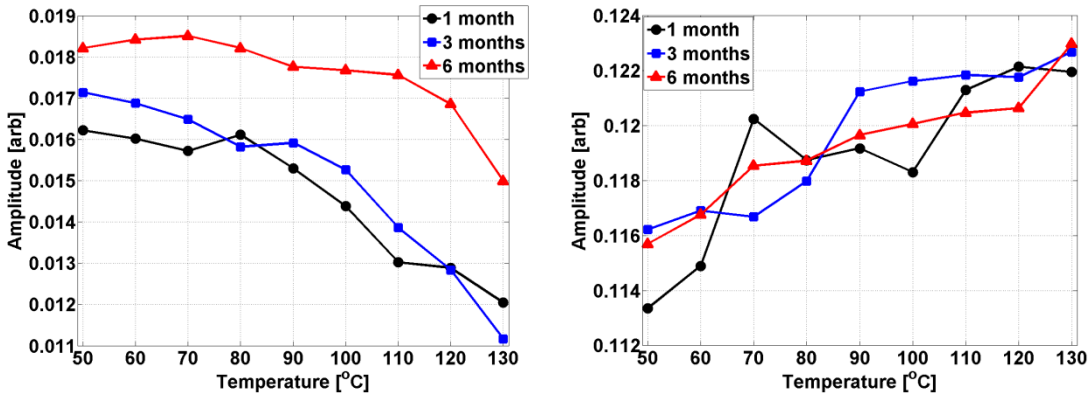

(a) (b)

Figure 5.22: Peak frequency domain amplitude against temperature increase for (a) tag signal and (b) carrier signal.

PCA is then applied to a 2×27 matrix; the results are shown in Figure 5.23. Averaging over the 9 measurements per sample, Figure 5.24, it can be seen that the mean values

are decreasing with increasing level of corrosion / exposure time as expected. However, there is significant overlap between the 1 month and 3 month exposure time samples. The trend is similar to that seen in section 5.6 and 5.7.

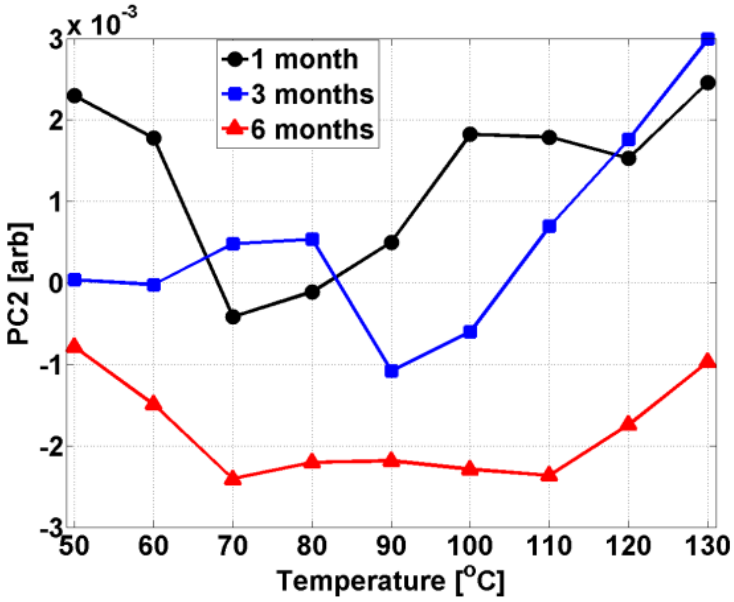

Figure 5.23: Results post PCA. Change in PC2 with increasing temperature.

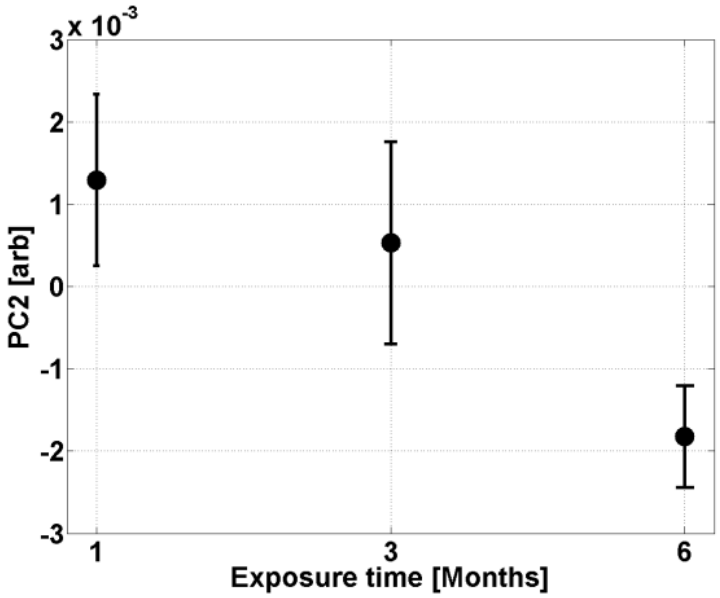

Figure 5.24: PC2 averaged over the 9 measurements per sample.

PCA for temperature independent corrosion measurement is not as effective as it is for position case because of the weak relationship between the variables *t* and *c* with respect to temperature. In the case of position independence, the two variables, *t* and *c*, are

strongly collinear with respect to the reader coil position. Whereas in this case the change in temperature at the sample surface may not be the same as the change that occurs at the reader coil. Although this is a tentative demonstration of the principal of using PCA to compensate for temperature variations, for it to be practical a better variable that is collinear with respect to temperature change is required.

5.9 Chapter Summary

In this chapter the problem of repositioning of the reader coil is discussed. It has been shown that even small changes in the position of the reader coil can mask changes in the tag's signal due to corrosion changes.

The solution to this problem comes about through the application of PCA to two features of the time/frequency domain RFID signals. The two features are the tag's signal amplitude and the carrier signal amplitude. The solution relies on the assumption that the tag's signal amplitude is a function of both corrosion change and position change. Whereas, the carrier signal amplitude is predominantly a function of reader coil position. The collinearity between the two features with respect to position is removed or reduced by PCA. The result is that the second principal component is corrosion or sample information independent of position change.

It has been demonstrated that position independence can be improved by increasing the scale of the carrier signal amplitude with respect to the tag's signal amplitude. This scaling improves the mean separation between different samples up to a certain scaling value, beyond which no further improvements are observed. This maximum scaling value can be found by observing the small eigenvalue. To a much lesser extent, it has been observed that by applying a negative gradient to the carrier signal amplitude measurements particularly, can also improve position independence. The application of a gradient or rotation is to minimise the effect of corrosion change on the carrier signal which has been shown to have a negative effect on position independence.

Using synthetic RFID data, carefully controlled experimental measurements and free-hand measurements the ability to obtain position independent corrosion measurements using PCA has been demonstrated.

The same PCA method has also shown potential in mitigating the effects of temperature on corrosion measurements. The plates were heated to a range of temperatures with the

tag on the surface. The results show that at temperatures above approximately 80^{o}C the tag amplitude decreases rapidly with increasing temperature. The reader coil, which is in a fixed position above the steel plate, also experiences the heat from the hot plate and thus its amplitude is also a function of temperature. Applying PCA to the measured data in a manner similar to the case of position independence, it is observed that there is potential for the PCA method to be extended for temperature independent measurements. The PCA method is not as effective in removing the effect of temperature in this case due to the weaker collinearity between the variables t and c with respect to temperature.

Chapter 6. Accelerated Corrosion under Insulation Testing

In previous experimental studies the samples were pre-prepared rectangular steel plates with a certain surface conditions or corrosion levels. In this chapter a more realistic experimental study has been conducted. Two insulated steel pipe sections have been subjected to accelerated corrosion testing. The factors that made this study more realistic are the salt water added to the insulation, high temperatures experienced by the tags and the curved surface of the pipes which restricts the types of tags that can be attached. Prior to the accelerated CUI testing, some preliminary tests were carried to investigate the factors such as water in insulation and paint.

6.1 Effect of Water in Insulation

It has been previously demonstrated that certain frequency ranges and particularly UHF RFID systems are strongly influenced by conductive materials such as water [120, 121]. LF RFID, however, is thought to have greater immunity to the presence of water near the tags. To put this to the test and considering the fact that thermal insulation surrounding pipes can store and hold large quantities of water, the following experiment has been conducted.

In Figure 6.1, 45 mm thick foam insulation is placed between the reader coil and an ATA5577 disk tag placed on a steel sample. Measurements were first taken with the insulation dry. The piece of insulation was then soaked in water. Measurements were then repeated with the fully saturated insulation layer. The measurements were repeated 5 times per dry and wet condition. The results are shown in Figure 6.2.

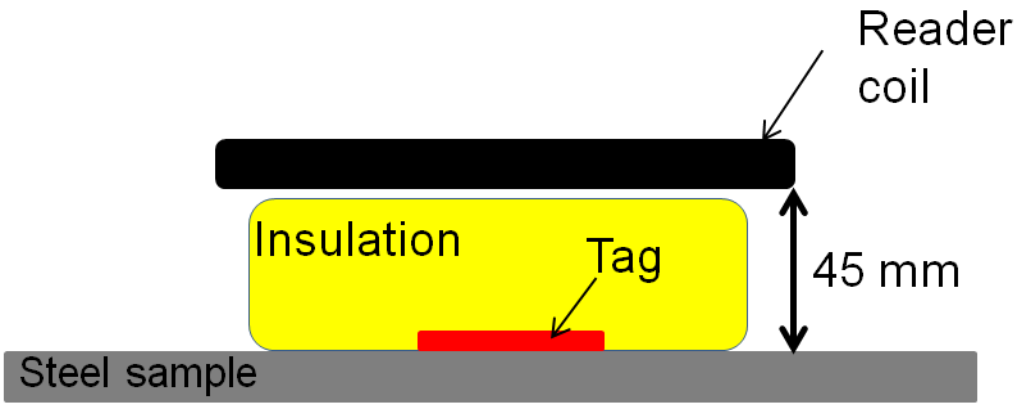

Figure 6.1: Experimental setup to test effect of water in the insulation layer on RFID tag signal.

The results show that the addition of water in the insulation layer makes no measurable effect on the RFID tag signal. This result is useful as it removes an important factor that may have influenced corrosion measurements.

	Amplitude [V]
Dry	0.7856 ± 0.006
Wet	0.7879± 0.0076

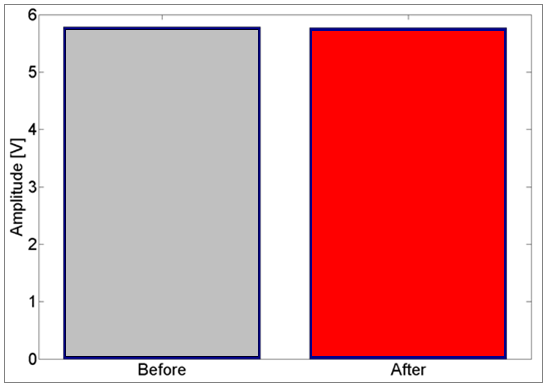

Figure 6.2: Results showing the negligible effect of water in insulation.

6.2 Effect of Paint Cure on RFID Signal

The paint used in this study is an ambient cured liquid paint. The issue with this type of coating is that film formation relies on reaction between component a (epoxy resin) and component b (amine curing agent) and full reaction does not occur under ambient conditions (this is due to a process called vitrification - as the reaction progresses the glass transition temperature Tg of the polymer gradually increases, when the Tg reaches ambient temperature the polymer vitrifies(changes from being in a rubbery to glassy phase) and the mobility of the reactive groups in the polymer greatly reduces therefore the rate of reaction drops by orders of magnitude. As a rule of thumb for a coating cured under ambient conditions (23^{o}C) the maximum achievable Tg will be ambient +30^{o}C, therefore this type of coating will never achieve full cure under ambient conditions (Tg of a fully cured version of the coating will be ~80^{o}C). However, if the coating is heated, as will be the case in the CUI scenario the ambient temperature will be 350^{o}C and under these conditions the vitrified coating passes back into the rubbery state and further reaction between the epoxy and amine groups rapidly occurs leading to a fully reacted coating..

A coated plate from the corrosion progression sample set was placed in a convection oven for 2 days at 100^{o}C to allow the coating to fully cure. Measurements were performed using the ATA5577 disk tag before and after being placed in the oven. The results are shown in Figure 6.3

	Amplitude [V]	
	Clean	Rust
Before	0.726 ± 0.004	0.796 ± 0.013
After	0.730± 0.005	0.788 ± 0.004

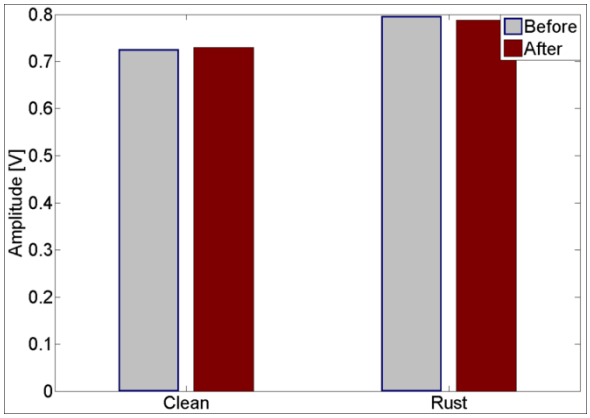

Figure 6.3: Measurements of the peak tag signal amplitude from a clean region and rust patch before and after the sample was placed in an oven to fully cure the coating.

The results show that, in this case there are no significant physical or electrical changes that result from the coating fully curing.

6.3 Accelerated Corrosion under Insulation Testing

The purpose of the accelerated CUI testing was to perform an experiment that was closer to an actual field-test. That is, to create and experiment which simulates some of the conditions found in actual operation such as high temperature and water/moisture.

The tests involved two coated 60 cm long sections of steel pipe with 6 cm diameter and 30 mm thickness. Each of the pipes had three TK5551 tags attached at three locations as shown in Figure 6.4. The tags were attached to the coated steel surface using a high temperature-resistant silicone based adhesive.

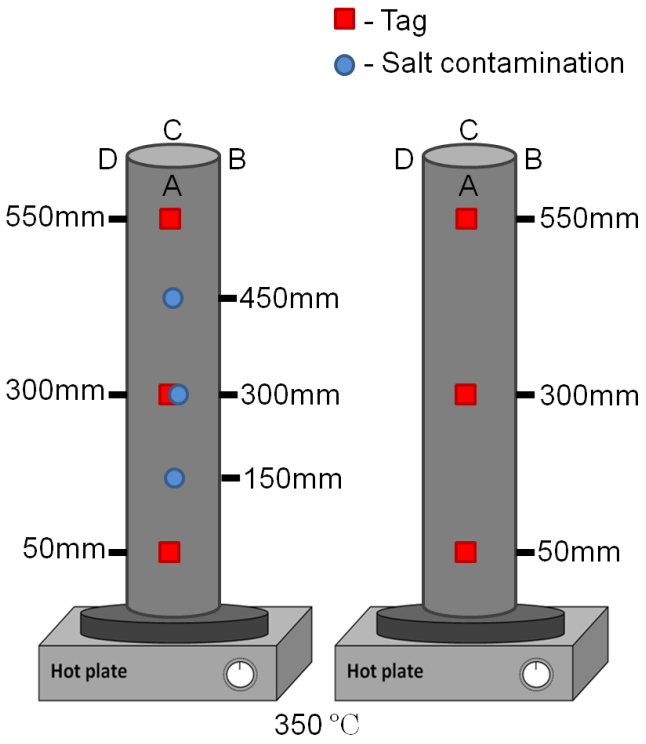

Figure 6.4: Accelerated CUI test setup showing location of tags and salt contaminations.

One of the pipes also had three salt contamination locations prior to coating. The purpose of the salt under the coating was to initiate and accelerate corrosion growth. Both pipes were then covered using 50 mm thick calcium silicate insulation. The pipe and insulation were then placed on top of two hot plates and heated to 350 ºC. The pipes were heated at that temperature for 8 hours per day and left to cool overnight. At the end of each heating cycle, 1 litre of water with 1% sodium chloride was poured into the insulation of each pipe. Measurements were performed at the beginning of the heating cycle with the pipes at room temperature. Before the saltwater was added, a one time temperature profile of each pipe was recorded using thermocouples. The highest temperature experienced by the tags placed 50 mm from the bottom of the pipe was approximately 240 ºC.

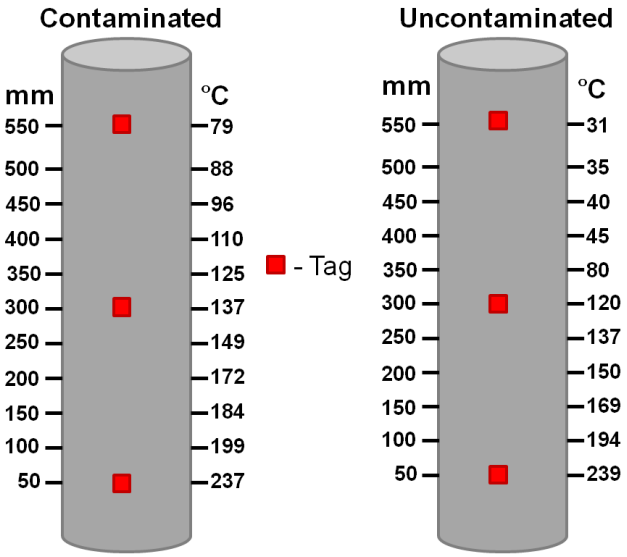

Figure: 6.5: Recorded temperature along each pipe

Before any measurements could be made a section of aluminium foil covering the insulation layer had to be removed as no response from the tag could be detected through it. Figure 6.6 shows the experimental setup and the removed section of aluminium. The challenges related to the aluminium layer will be discussed in the Further works sections.

Figure 6.6: picture o f experimental setup showing strip of aluminium foil removed.

The output of the RFID reader was sampled at 1 MHz. Initially, the tests were carried out for a period of 25 days. The results for the contaminated and uncontaminated pipes are shown in Figure 6.7and Figure 6.8 respectively.

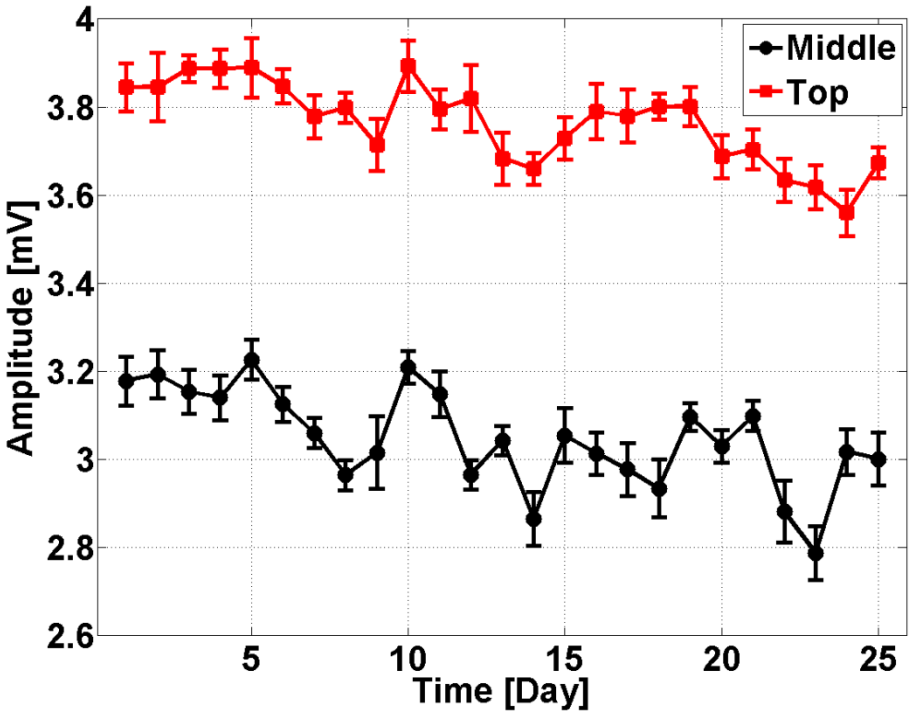

Figure 6.7: Peak amplitude measurements from the contaminated pipe over 25 days

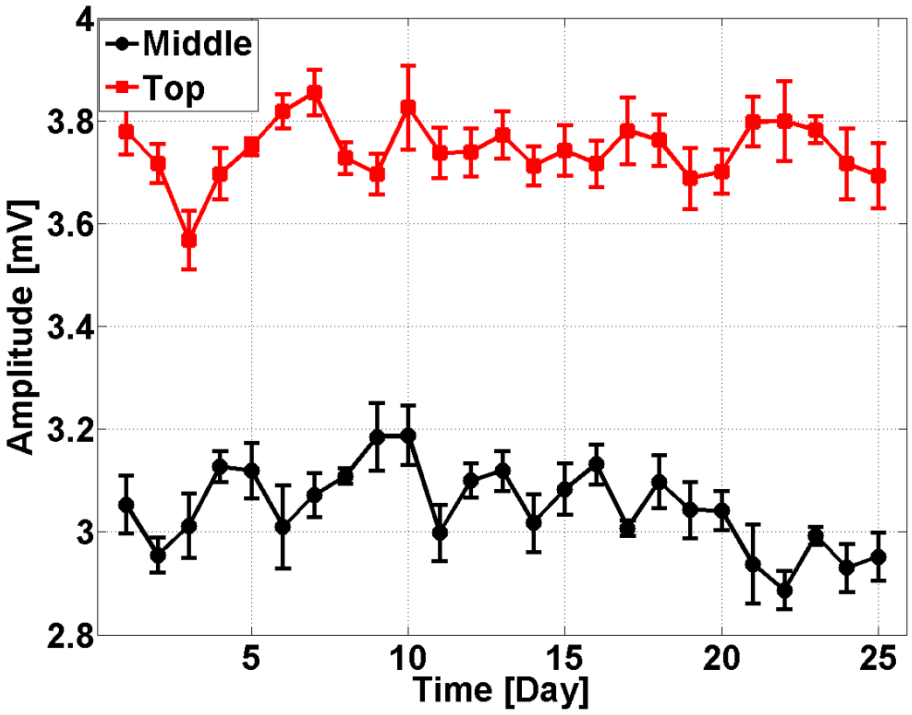

Figure 6.8: Peak amplitude measurements from the uncontaminated pipe over 25 days

Both tags at the bottom of the pipes became unresponsive after the first 8 hour heating period. It was later found that the tags were permanently damaged by the high temperature. The temperature experienced by the two bottom tags were far in excess of the maximum 125°C storage temperature. The two middle tags experienced temperatures close to the maximum storage temperature and thus survived for the entire duration of the experiment.

There are two notable observations that can be made of the results in Figure 6.7 and Figure 6.8. The first is that for both the pipes the tags located at the top have much higher amplitude than the tags located in the middle. This can be shown by the application of PCA to be a result of the reader coil position and not the difference metal electrical or physical properties. Figure 6.9 shows that the amplitude difference between top and middle tags disappears when looking at the second principal component, which has been demonstrated to be position independent in chapter 5.

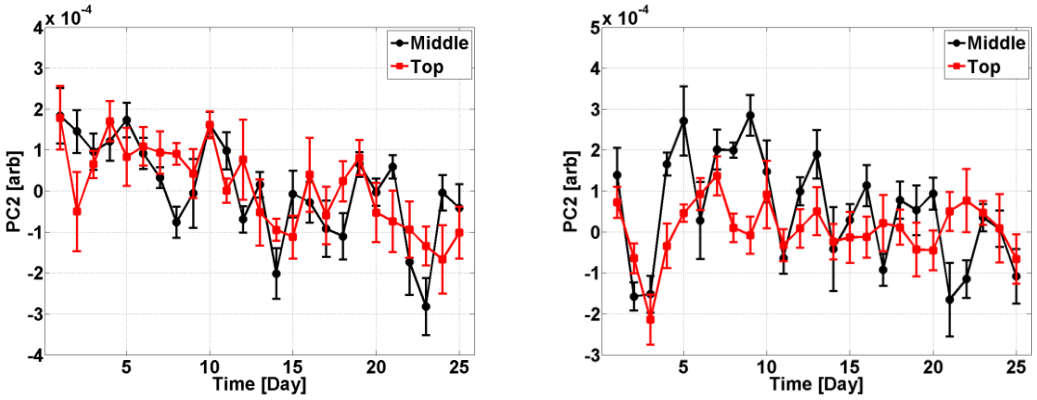

(a) (b)

Figure 6.9: Application of PCA removes amplitude difference between the top and middle located tags for both the (a) contaminated and (b) uncontaminated pipes.

The second notable result is that, other than a slight decrease in the amplitude over time for the contaminated pipe, there was no significant change in the tag's signal amplitude over the 25 days. This seemed to suggest that there was no significant corrosion activity under the coating. This was in stark contrast to the uncoated internal surface of the pipes which showed significant visible corrosion as seen in Figure 6.10. To check whether there was any corrosion developing on the surface it was decided to remove the contaminated pipe and inspect the surface beneath the coating.

Figure 6.10: Image of the top and internal surface of the one of the pipes showing significant corrosion development after 25 days.

The insulation from the contaminated pipe was removed and the paint from three locations was scraped off using a knife to see if there is any corrosion beneath. The positions correspond to two tag locations and two salt contamination locations. Figure 6.11 shows the images of these locations after the paint has been removed.

(a) (b)

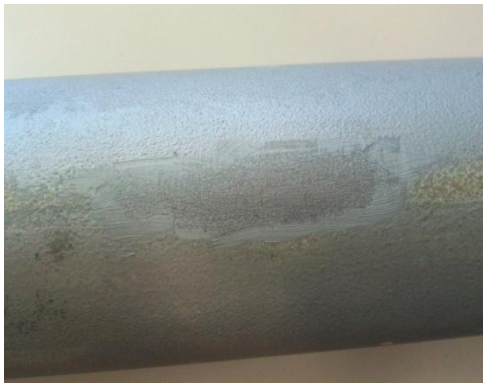

(c)

Figure 6.11: (a) Tag and salt contamination location 300mm from bottom, (b) salt contamination 450mm from bottom and (c) Tag location 550mm from bottom

As can be seen from Figure 6.11, the tag location 550 mm from the bottom of the pipe showed no visible signs of corrosion and the two salt contaminated locations showed a slight discoloration where the salt was added. However, despite the addition of salt there was no visible sign of corrosion development in those two locations. The anti-corrosive coating maintained its integrity and prevented any corrosion from developing beneath. This explains why there was very little change in the tag's signal amplitude.

The tags on the remaining uncontaminated pipe had cuts made in the coating layer near the edges around the tags in order to promote corrosion development and observe its effect on the tags response. The experiment was then continued a further 15 days. The results from the combined 40 days are displayed in Figure 6.12.

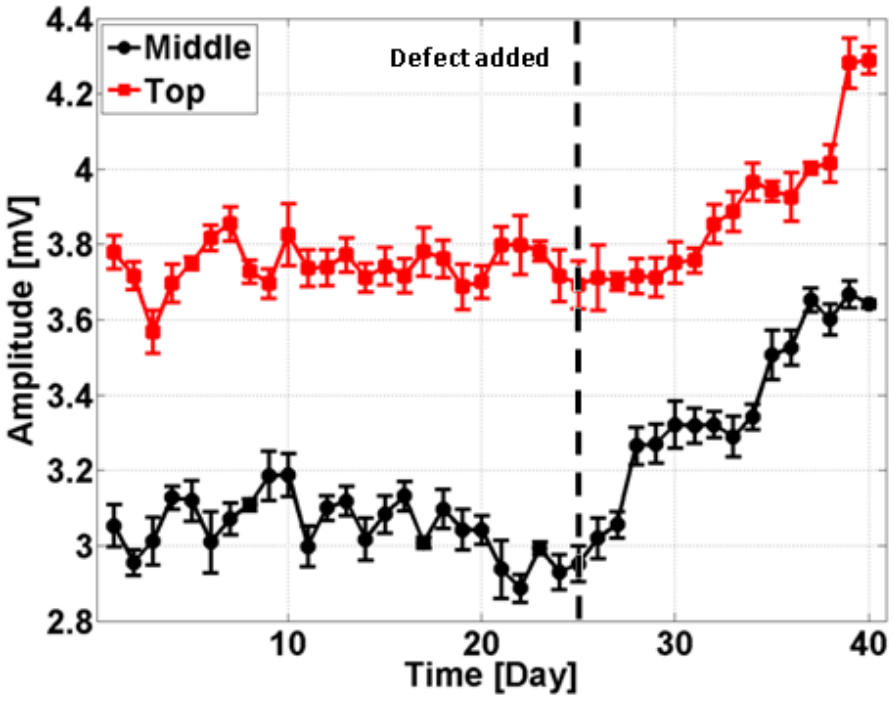

Figure 6.12: The results from the uncontaminated pipe after cuts were made in the coating on the 25th day.

As can be seen in Figure 6.12, almost immediately after the defects in the coating layer near the tags are added, the amplitude of the tag's signal starts increasing. There is a greater than 15% change in amplitude between the 25th day and the 40th day for the top tag and near 20% increase in amplitude for the middle tag. The accelerated CUI experiment was concluded after 40 days and the pipe was removed to inspect the areas under the tags for signs of corrosion. Figure 6.13 shows images of the metal beneath the two tags.

(a) (b)

Figure 6.13: A visible sign of corrosion under the (a) top and (b) bottom tags on the uncontaminated pipe.

In Figure 6.13 we can see clear signs of corrosion under the two tags which validates the results seen in Figure 6.12.

6.4 Chapter Summary

In this chapter accelerated CUI experimental study was carried out to test the RFID system in a more realistic environment. Two insulated steel pipes, each with three tags attached to the coated surface, were thermally cycled with salt water added to the insulation layer in order to promote and accelerate corrosion development.

After an initial 25 days of testing, no significant changes in the tag's signal amplitude was observed. Upon inspection of the metal beneath the coating layer it found that no corrosion was present beneath the tag locations. Even the locations which had salt contamination had no significant corrosion.

Cuts were then made to the coating layer near the tags on the remaining pipe to promote corrosion growth. After a further 15 days of testing, significant increases in amplitudes for both tags was observed. This indication of corrosion in the results was confirmed after coating under both tags was scraped off to reveal clear visible signs of corrosion.

In preliminary testing prior to the accelerated CUI experiment it was found that the RFID tag response was the same for dry and wet insulation as well as prior to and post fully cured coating. This eliminated factors which could have complicated the detection and monitoring of corrosion.

On the high temperature survivability of the tags, it was found that tags which experienced temperatures in excess of 200ºC did not survive the first 8 hour heating period.

The tags which experienced temperatures less than 140 ºC survived the entire duration of the experiment. The high temperature survivability of the tags is a particularly difficult challenge which will require novel solutions in order to expand the potential application environments that the RFID tags may be deployed in.

Chapter 7. Conclusions and Further Work

In this final chapter the project is summarised and conclusions are drawn about the performance and capabilities of the RFID system. Finally, potential directions for future research are outlined in terms of improving the system sensitivity and robustness.

7.1 Conclusions

Limitations of existing NDT&E techniques create opportunities for novel approaches to tackle the challenges posed by CUI. One such big challenge is inaccessibility of the pipe surface due to thick layer of insulation. From the literature it was found that methods to overcome the large standoff distance involved either high power PEC systems which have low sensitivity or through the use of guided waves. The latter methods require access to the surface of the pipe though small inspection holes. In this study, the potential of passive LF RFID tags for the monitoring of corrosion under insulation has been experimentally demonstrated.

Passive sensing is a dynamic and developing field of research. Many examples can be found in the literature exploring the uses of RFID tags to detect a variety of phenomena. The low cost and battery-free operation are two of the biggest factors enticing researchers to further explore this technology for sensing. Majority of the work in passive tag sensing involved modifications to the tags either through the use of special reactive thin films or sacrificial elements attached to the tags. These methods not only increase the costs but also limit the long term applicability of the tags. Furthermore, Changes in the thin films or the sacrificial elements may not accurately represent changes occurring in the structures the tags are attached to. The proposed method overcomes these problems by using the tag coil's interaction with the metal as the sensing mechanism. This requires no modifications to the tag, allowing commercial off-the-shelf tags to be used.

The fundamental operating principle, as described in Chapter 3, relies on the fact that reader and tag operate at resonance. In free space the tag's resonant frequency is the same as the reader operating frequency. When placed on metal, the inductive coupling between tag and metal causes the tag's resonant frequency to shift. This shift reduces the amount of power absorbed by the tag and hence the loading effect it has on the reader coil. As corrosion develops on the metal the decrease in electrical conductivity and magnetic permeability will result in the tag's resonant frequency shifting towards the free space value. On the hardware side, three commercially available tags were se-

lected as the sensors in this study. The tags are of a variety of sizes and shapes to cover different surfaces and applications. The reader unit is custom built with a 12 cm diameter reader coil. Tests have shown the reader capable of energising and reading a tag from a distance of up to 50mm, sufficient for the insulation type used in this study.

An initial experimental feasibility study, detailed in chapter 4, carried out using carefully designed samples demonstrated the systems detection capabilities. The studies were qualitative in nature, testing the systems capabilities to differentiate between different surface conditions and corrosion levels. The first sample set consisted of four mild steel plates with different levels of corrosion and surface preparation. The results showed that the RFID system was able not only to differentiate between the corroded and non-corroded samples but also to differentiate between samples with different surface roughness. The results also correlated well with laser profilometry measurements of the surface roughness. The second sample set used consisted of another set of rectangular mild steel plates with a 3×3 cm square corroded region in the centre of each plate. The plates were corroded by exposing them to the atmosphere for 1, 3, 6, 10 and12 months. The results demonstrated the RFID systems ability to differentiate between all the different levels of corrosion. As expected, the amplitude of the tags signal increased with increasing level of corrosion. Next, to test the tag's response to physical displacements between the tag and the steel surface, sheets of 100 micron thick paper was used. The results show that changes of at least 100 microns can be detected. Smaller increments weren't possible. This raises the prospect of employing the tags to detect coating related defects such as blisters and delaminations. Tests with the tags programmed with different data rates or switching frequencies showed that lower frequency tags have higher signal amplitudes. The final study in chapter 4 demonstrated the increased sensitivity of the RFID system over an equivalent eddy current system with no tag present. The test aimed to answer whether there is any benefit in terms of sensitivity of having a tag present. The resonant operation of the tag means that small changes in the surface condition of the steel is amplified by the tag resulting in almost 10 times greater amplitude change than the eddy current setup with no tag.

The dependence of the output signal amplitude on the position of the reader coil, first discussed in chapter 3, was experimentally explored in chapter 5. Since the tags are passive, obtaining all their energy from the electromagnetic field generated by the reader coil, the amplitude of the tag signal as measured at the reader coil is largely dependent on the reader coil position. It has been shown that even small changes in the position of

the reader coil can mask changes in the tag's signal due to corrosion changes. The solution to this problem comes about through the application of PCA to two features of the time/frequency domain RFID signals. The two features are the tag's signal amplitude and the carrier signal amplitude. The solution relies on the assumption that the tag's signal amplitude is a function of both corrosion change and position change. Whereas, the carrier signal amplitude is predominantly a function of reader coil position. The collinearity between the two features with respect to position is removed or reduced by PCA. The result is that the second principal component is corrosion or sample information independent of position change. Using synthetic RFID data, carefully controlled experimental measurements and free-hand measurements the ability to obtain position independent corrosion measurements using PCA has been demonstrated. Furthermore, a tentative demonstration of the extension of the PCA method to tackle the problem of temperature variation on corrosion measurement has also been performed. The results show that the method works in principal, however, a more robust feature that is collinear with the tag signal with respect to temperature is required if this is to be more practical.

In the final chapter accelerated CUI experimental study was carried out to test the RFID system in a more realistic environment. Two insulated steel pipes, each with three tags attached to the coated surface, were thermally cycled with salt water added to the insulation layer in order to promote and accelerate corrosion development. After an initial 25 days of testing, no significant changes in the tag's signal amplitude was observed. Upon inspection of the metal beneath the coating layer it found that no corrosion was present beneath the tag locations. Even the locations which had salt contamination had no significant corrosion. Cuts were then made to the coating layer near the tags on the remaining pipe to promote corrosion growth. After a further 15 days of testing significant increases in amplitudes for both tags was observed. This indication of corrosion in the results was confirmed after coating under both tags was scraped off to reveal clear visible signs of corrosion. In preliminary testing prior to the accelerated CUI experiment it was found that the RFID tag response was the same for dry and wet insulation as well as prior to and post fully cured coating. This eliminated factors which could have complicated the detection and monitoring of corrosion. On the high temperature survivability of the tags, it was found that tags which experienced temperatures in excess of 200ºC did not survive the first 8 hour heating period. The tags which experienced temperatures less than 140 ºC survived the entire duration of the experiment. The high temperature

survivability of the tags is a particularly difficult challenge which will require novel solutions in order to expand the potential application environments that the RFID tags may be deployed in.

7.2 Further Work

Future work with the RFID system will be geared towards improvements to the system to tackle other challenges related to CUI such as high temperature and metallic outer casing. These improvements will also be steps towards commercial feasibility.

The high temperature survivability of the tags is a significant problem limiting the wider applicability of RFID sensing. A large proportion of pipelines operate at temperatures far above the limits of current semiconductor technology. Radical, long term proposals may include looking at high temperature silicon carbide as a replacement for the silicon based microchips. Less radical, near term solution, is to replace the microchip inside the tags making the tags completely passive. The solder in the tags can also be replaced with higher temperature variants. Before this, a comprehensive investigation, involving computer modelling and experimental studies, into the high temperature failure of tags needs to be carried out to identify which components fail and when. This will then allow more targeted solutions to be proposed.

The inability of the system to operate through the aluminium outer layer presents another hurdle to potential field application of the system. Tackling this problem may require the design of much higher power reader unit. Additionally, investigations into whether carefully placed ferrite material near the tags can improve read range as well as operate through aluminium layer by concentrating flux towards the tag. Redesigning the tag coil to resonate at a lower frequency will help mitigate the problem of induced eddy currents on the outer conducting layer of the pipe.

Samples with coating related defects will be created to determine whether blisters, delaminations and other coating defects may be separated from corrosion change. The two different defects may look similar when analysed using current signal features. Therefore, new features may be required as well as looking into how the response from a defect changes over time as coating related defects such as blisters may appear as a sudden sharp change compared to corrosion.

Future work will also involve looking into methods to obtain quantitative information about the underlying steel such as conductivity and permeability change. This can be

achieved by correlating the output with samples with known conductivity and permeability and through simulation studies.

Although not address in this study, the design of the tag coil is another avenue of further research. Trade-offs may be made between increased cost and optimising tag coil geometry and frequency of operation. Furthermore, since RFID tags have a small area of coverage, the optimum placing of tags on a structure is another practical consideration that needs to be further explored.

References

[1] M. Alamin, T. Gui Yun, A. Andrews, and P. Jackson, "Principal Component Analysis of Pulsed Eddy Current Response From Corrosion in Mild Steel," *Sensors Journal, IEEE*, vol. 12, pp. 2548-2553, 2012.

[2] M. Alamin, G. Y. Tian, A. Andrews, and P. Jackson, "Corrosion detection using low-frequency RFID technology," *Insight - Non-Destructive Testing and Condition Monitoring*, vol. 54, pp. 72-75, 2012.

[3] M. Alamin, G. Y. Tian, A. Andrews, and P. Jackson, "Measurement and monitoring of corrosion under insulation using passive LF RFID," presented at the NDT 2013, Telford, UK, 2013.

[4] M. Lettich. "Is There A Cure For Corrosion Under Insulation?," Insulation.org. [Online]. Available: http://www.insulation.org/articles/article.cfm?id=IO051101 [Accessed: Mar. 2013].

[5] Y. P. Virmani and G. H. Koch. "Corrosion Costs and Preventive Strategies in the United State," nace.org. [Online]. Available: www.nace.org/uploadedFiles/Publications/ccsupp.pdf [Accessed: May. 2013].

[6] B. Goldie and K. Kapsams. (2009, Jul. 2009) Corrosion under Insulation: Basics and Resources for Understanding. *JPCL*. 34-37.

[7] R. Norsworthy and P. Dunn, "Corrosion under Thermal Insulation," *NACE Materials Performance*, 2002.

[8] K. Posteraro, "Thwart Corrosion under Industrial Insulation," *Chem. Eng. Progress*, vol. 95, pp. 43-47, 1999.

[9] M. Twomey, "Inspection Techniques for Detecting Corrosion under Insulation," *NDTnet*, vol. 3, 1998.

[10] M. Takemoto, "Extreme Stress Corrosion Cracking of Austenitic Stainless Steel Equipment," *NACE Corrosion 89*, 1989.

[11] F. De Vogelaere, "Corrosion under insulation," *Process Safety Progress*, vol. 28, pp. 30-35, 2009.

[12] V. M. Liss, "Preventing corrosion under insulation", Materials Engineering," *Materials Engineering*, pp. 97-100, 1987.

[13] J. W. Oldfield, "Electrochemical Theory of Galvanic Corrosion," in *Galvanic Corrosion*, ed Philadelphia: American Society for Testing and Materials, 1988, pp. 5-22.

[14] M. Halliday, "Preventing corrosion under insulation-new generation solutions for an age old problem," *Journal of protective coatings & linings*, vol. 24, pp. 24-36, 2007.

[15] J. F. Grubb, T. DeBold, and J. D. Fritz, "Corrosion of Stainless Steels," in *ASM Handbook Volume 13B, Corrosion: Materials*. vol. 13B, S. D. Cramer and B. S. Covino, Eds., ed Ohio: ASM International, 2005, pp. 63-63.

[16] M. Suresh Kumar, M. Sujata, M. A. Venkataswamy, and S. K. Bhaumik, "Failure analysis of a stainless steel pipeline," *Engineering Failure Analysis*, vol. 15, pp. 497-504, 7// 2008.

[17] B. J.-P. Rutherford, "Preventing corrosion under insulation in chemical manufacturing facilities," pp. 40-49, 1998.

[18] C. Lasarte, O. T. D. Rincon, and A. Montiel, "Predicting performance of coatings under thermal insulation at high temperatures," *Journal Name: Materials Performance; (United States); Journal Volume: 33:10*, pp. Medium: X; Size: Pages: 36-39, 1994.

[19] HSE. "Corrosion under insulation of plant and pipework," Health and Safety Executive. [Online]. Available:

http://www.hse.gov.uk/foi/internalops/hid_circs/technical_general/spc_tech_gen_18.htm [Accessed: May. 2013].
[20] G. W. Carriveau, "Detection of Corrosion Through Insulation," in *9th Ethylene Producers Conference*, 1997, pp. 672-687.
[21] Gamry. "Basics of Electrochemical Impedance Spectroscopy," Gamry.com. [Online]. Available: www.gamry.com/assets/Application-Notes/Basics-of-EIS.pdf [Accessed: May. 2013].
[22] A. Lasia, "Electrochemical Impedance Spectroscopy and its Applications," in *Modern Aspects of Electrochemistry*. vol. 32, B. E. Conway, J. O. M. Bockris, and R. White, Eds., ed: Springer US, 2002, pp. 143-248.
[23] A. Sophian, G. Y. Tian, and S. Zairi, "Pulsed magnetic flux leakage techniques for crack detection and characterisation," *Sensors and Actuators A: Physical*, vol. 125, pp. 186-191, 2006.
[24] M. Göktepe, "Non-destructive crack detection by capturing local flux leakage field," *Sensors and Actuators A: Physical*, vol. 91, pp. 70-72, 2001.
[25] Danamin. "Magnetic Flux Leakage Tank Floor Scanning," Danamin.com. [Online]. Available: http://www.danamin.com/magnetic-flux-inspection-services-48.aspx [Accessed: May. 2013].
[26] J. H. J. Stalenhoef and J. A. d. Raad, "MFL and PEC Tools for Plant Inspection," presented at the 7th ECNDT, 1998.
[27] D. L. Atherton, "Magnetic inspection is key to ensuring safe pipelines," *NDT and E International*, vol. 30, pp. 40-40, 1997.
[28] J. C. Drury. 05/2013). Magnetic Flux Leakage Technology. *2013(Apr 2013)*. Available: silverwinguk.com
[29] D. Kima, L. Udpa, and S. Udpa, "Remote field eddy current testing for detection of stress corrosion cracks in gas transmission pipelines," *Materials Letters*, vol. 58, pp. 2102-2104, 2004.
[30] N. R. Center. "Magnetic Field Orientation and Flaw Detectability," ndt-ed.org. [Online]. Available: http://www.ndt-ed.org/EducationResources/CommunityCollege/MagParticle/Physics/FieldOrientation.htm [Accessed: May. 2013].
[31] W. Yunjiang, W. Xiaofeng, and D. Keqin, "Width quantification of corrosion defect on pipeline based on pulsed magnetic flux leakage," *Journal of Test and Measurement Technology*, vol. 23, pp. 390-395, 2009.
[32] S. Kharkovsky and R. Zoughi, "Microwave and millimeter wave nondestructive testing and evaluation - Overview and recent advances," *Instrumentation & Measurement Magazine, IEEE*, vol. 10, pp. 26-38, 2007.
[33] N. N. Qaddoumi, W. M. Saleh, and M. Abou-Khousa, "Innovative Near-Field Microwave Nondestructive Testing of Corroded Metallic Structures Utilizing Open-Ended Rectangular Waveguide Probes," *Instrumentation and Measurement, IEEE Transactions on*, vol. 56, pp. 1961-1966, 2007.
[34] A. C. Ryley, M. T. Ghasr, S. Kharkovsky, R. Zoughi, and G. Steffes, "Application of Millimeter Wave, Eddy Current and Thermographic Methods for Detection of Corrosion in Aluminum Substrate," *AIP Conference Proceedings*, vol. 894, pp. 1258-1265, 2007.
[35] D. Hughes, N. Wang, T. Case, K. Donnell, R. Zoughi, R. Austin, and M. Novack, "Microwave Nondestructive Detection of Corrosion Under Thin Paint and Primer in Aluminum Panels," *Subsurface Sensing Technologies and Applications*, vol. 2, pp. 435-471, 2001/10/01 2001.
[36] W. Saleh and N. Qaddoumi, "Corrosion Detection and Thickness Evaluation Utilizing Active Near-Field Microwave Nondestructive Testing Techniques," in

Precision Electromagnetic Measurements Digest, 2004 Conference on, 2004, pp. 200-201.

[37] R. Jones, F. Simonetti, M. S. Lowe, and I. Bradley, "Use of Microwaves for the Detection of Water as a Cause of Corrosion Under Insulation," *Journal of Nondestructive Evaluation*, vol. 31, pp. 65-76, 2012/03/01 2012.

[38] H. S. Sousa, J. D. Sørensen, P. H. Kirkegaard, J. M. Branco, and P. B. Lourenço, "On the use of NDT data for reliability-based assessment of existing timber structures," *Engineering Structures*, vol. 56, pp. 298-311, 2013.

[39] D. W. Auckland, A. J. McGrail, C. D. Smith, B. R. Varlow, J. Zhao, and D. Zhu, "Application of ultrasound to the inspection of insulation," *Science, Measurement and Technology, IEE Proceedings* -, vol. 143, pp. 177-181, 1996.

[40] C. Dengfeng, J. Qichun, Z. Liang, and Z. Hongcai, "Application of pulsed eddy current and ultrasonic sensors in paint film thickness measuring," in *Control and Decision Conference, 2009. CCDC '09. Chinese*, 2009, pp. 4461-4464.

[41] M. G. Lozev, R. W. Smith, and B. B. Grimmett, "Evaluation of Methods for Detecting and Monitoring of Corrosion Damage in Risers," *Journal of Pressure Vessel Technology-transactions of The Asme*, vol. 127, 2005.

[42] L. Satyarnarayan, J. Chandrasekaran, B. Maxfield, and K. Balasubramaniam, "Circumferential higher order guided wave modes for the detection and sizing of cracks and pinholes in pipe support regions," *NDT & E International*, vol. 41, pp. 32-43, 2008.

[43] M. G. Lozev, R. W. Smith, and B. B. Grimmett, "Evaluation of Methods for Detecting and Monitoring of Corrosion Damage in Risers," *ASME*, vol. 127, pp. 244-254, 2005.

[44] D. Tuzzeo and F. Lanza di Scalea, "Noncontact Air-Coupled Guided Wave Ultrasonics for Detection of Thinning Defects in Aluminum Plates," *Research in Nondestructive Evaluation*, vol. 13, pp. 61-78, 2001/06/01 2001.

[45] Y. Sohn and S. Krishnaswamy, "Interaction of a scanning laser-generated ultrasonic line source with a surface-breaking flaw," *The Journal of the Acoustical Society of America*, vol. 115, pp. 172-181, 2004.

[46] W. Gao, C. Glorieux, and J. Thoen, "Laser ultrasonic study of Lamb waves: determination of the thickness and velocities of a thin plate," *International Journal of Engineering Science*, vol. 41, pp. 219-228, 2003.

[47] Wikipedia. "Electromagnetic acoustic transducer," wikipedia.org. [Online]. Available: http://en.wikipedia.org/wiki/File:EMATDIA.JPG [Accessed: May. 2013].

[48] K. Mirkhani, C. Chaggares, C. Masterson, M. Jastrzebski, T. Dusatko, A. Sinclair, R. J. Shapoorabadi, A. Konrad, and M. Papini, "Optimal design of EMAT transmitters," *NDT & E International*, vol. 37, pp. 181-193, 2004.

[49] F. Huang, Z. Zhou, and J. Lin, "A new testing method combining EMAT with eddy current," presented at the 17th World Conference on Nondestructive Testing, Shanghai, 2008.

[50] R. S. Edwards, A. Sophian, S. Dixon, G. Y. Tian, and X. Jian, "Dual EMAT and PEC non-contact probe: applications to defect testing," *NDT & E International*, vol. 39, pp. 45-52, 2006.

[51] J. M. D. E. Bardal, "Corrosion Detection and Diagnosis," *Materials Science and Engineering*, vol. 3, 2004.

[52] R. Johnson and B. E. Bjornsen, "Weld Root Corrosion Monitoring with a new Electrical Field Signature Mapping Inspection Tool," presented at the NACE International Corrosion, Orlando, 2000.

[53] M.W. Joosten, K.P. Fischer, R. Strommen, and K. C. Lunden, "Internal Corrosion Monitoring of Subsea Oil and Gas Production Equipment," *NACE Materials Performance*, pp. 44-48, 1995.
[54] B. D. Howard, "Corrosion Detection Devices," presented at the Army Corrosion Summit, Florida, 2003.
[55] A. Sophian, G. Y. Tian, D. Taylor, and J. Rudlin, "Design of a pulsed eddy current sensor for detection of defects in aircraft lap-joints," *Sensors and Actuators A: Physical*, vol. 101, pp. 92-98, 2002.
[56] S. Giguère, B. A. Lepine, and J. M. S. Dubois, "Pulsed Eddy Current Technology: Characterizing Material Loss with Gap and Lift-off Variations," *Research in Nondestructive Evaluation*, vol. 13, pp. 119-129, 2001/01/01 2001.
[57] J. Skramstad, R. A. Smith, and D. Edgar, "Enhanced Detection of Deep Corrosion Using Transient Eddy Currents," presented at the 7th Joint DoD/FAA/NASA conference on Aging Aircraft, New Orleans, 2003.
[58] D. L. Atherton, "Remote field eddy current inspection," *Magnetics, IEEE Transactions on*, vol. 31, pp. 4142-4147, 1995.
[59] C. Murner and J. P. Hansen, "Buried corrosion detection in multi-layer airframe structures using pulsed eddy current," presented at the 17th World Conference on NDT, Shanghai,, 2008.
[60] P. Crouzen and I. Munns, "Pulsed Eddy Current Corrosion Monitoring in Refineries and Oil Production Facilities – Experience at Shell," presented at the ECNDT, 2006.
[61] R. Scottini and H. J. Quakkelsteijn, "Monitoring Average Wall Thickness of Insulated or Difficult to Access Objects with Pulsed Eddy Current," *J. Pressure Vessel Technology*, vol. 127, pp. 244-255, 2005.
[62] G. Y. Tian and A. Sophian, "Reduction of lift-off effects for pulsed eddy current NDT," *NDT & E International*, vol. 38, pp. 319-324, 2005.
[63] M. Cacciola, A. Gasparics, F. C. Morabito, M. Versaci, and V. Barrile, "Advances in Signal Processing to Reduce Lift-off Noise in Eddy Current Tests," *Piers Online*, vol. 3, pp. 517-521, 2007.
[64] H. Hoshikawa, K. Koyama, and H. Karasawa, "A new ECT surface probe without lift-off noise and with phase information on flaw depth," *AIP Conference Proceedings*, vol. 557, pp. 969-976, 2001.
[65] G. G. Diamond and D. A. Hutchins, "A New Capacitive imaging Technique for NDT," presented at the ECNDT, Berlin, 2006.
[66] X. Yin, D. A. Hutchins, G. Chen, and W. Li, "Detecting surface features on conducting specimens through an insulation layer using a capacitive imaging technique," *NDT & E International*, vol. 52, pp. 157-166, 11// 2012.
[67] T. Chen and N. Bowler, "A capacitive probe for quantitative nondestructive evaluation of wiring insulation," *NDT & E International*, vol. 52, pp. 9-15, 11// 2012.
[68] D. Sharma, R. Khanna, S. SGoyal, and A. Mukherjee, "Non-destructive Testing of Materials using Capacitive Sensing Technique," *MIT International Journal of Electronics and Communications Engineering*, vol. 1, pp. 73-77, 2011.
[69] X. Dérobert, J. Iaquinta, G. Klysz, and J.-P. Balayssac, "Use of capacitive and GPR techniques for the non-destructive evaluation of cover concrete," *NDT & E International*, vol. 41, pp. 44-52, 1// 2008.
[70] Z. Zhiling, F. Shangchun, and Z. Dezhi, "Non-destructive testing of solid wood plate using variable permittivity plate capacitor," in *Instrumentation and Control Technology (ISICT), 2012 8th IEEE International Symposium on*, 2012, pp. 153-156.

[71] X. Li, A. S. Zyuzin, and A. V. Mamishev, "Measuring moisture content in cookies using dielectric spectroscopy," in *Electrical Insulation and Dielectric Phenomena, 2003. Annual Report. Conference on*, 2003, pp. 459-462.
[72] K. Sundara-Rajan, L. Byrd, II, and A. V. Mamishev, "Moisture content estimation in paper pulp using fringing field impedance spectroscopy," *Sensors Journal, IEEE,* vol. 4, pp. 378-383, 2004.
[73] C. Namjun, S. Seong-Jun, K. Sunyoung, K. Shiho, and Y. Hoi-Jun, "A 5.1uW UHF RFID tag chip integrated with sensors for wireless environmental monitoring," in *Solid-State Circuits Conference, 2005. ESSCIRC 2005. Proceedings of the 31st European*, 2005, pp. 279-282.
[74] G. Marrocco and D. Scarana, "Permittivity passive RFID sensor for non-cooperating objects," *IET Seminar Digests*, vol. 2007, pp. 420-420, 2007.
[75] R. Bhattacharyya, C. Floerkemeier, and S. Sarma, "Towards tag antenna based sensing - An RFID displacement sensor," in *RFID, 2009 IEEE International Conference on*, 2009, pp. 95-102.
[76] A. Mitrokotsa and C. Douligeris, *Integrated RFID and Sensor Networks: Architectures and Applications*: CRC Press, 2009.
[77] R. S. Mackay and B. Jacobson, "Endoradiosonde," *Nature*, vol. 179, pp. 1239-1240, 1957.
[78] K. J. Loh, J. P. Lynch, and N. A. Kotov, "Passive wireless sensing using SWNT-based multifunctional thin film patches," *International Journal of Applied Electromagnetics and Mechanics,* vol. 28, pp. 87-95, 2008.
[79] J. Yi, M. Heiss, F. Qiuyun, and N. A. Gay, "A Prototype RFID Humidity Sensor for Built Environment Monitoring," in *Education Technology and Training, 2008. and 2008 International Workshop on Geoscience and Remote Sensing. ETT and GRS 2008. International Workshop on*, 2008, pp. 496-499.
[80] R. A. Potyrailo and W. G. Morris, "Multianalyte Chemical Identification and Quantitation Using a Single Radio Frequency Identification Sensor," *Analytical Chemistry*, vol. 79, pp. 45-51, 2007/01/01 2006.
[81] R. A. Potyrailo, H. Mouquin, and W. G. Morris, "Position-independent chemical quantitation with passive 13.56-MHz radio frequency identification (RFID) sensors," *Talanta,* vol. 75, pp. 624-8, 2008.
[82] R. A. Potyrailo and C. Surman, "A passive radio-frequency identification (RFID) gas sensor with self-correction against fluctuations of ambient temperature," *Sensors and Actuators B: Chemical*, vol. 185, pp. 587-593, 8// 2013.
[83] W. Leon-Salas, S. Kanneganti, and C. Halmen, "Development of a smart RFID-based corrosion sensor," in *Sensors, 2011 IEEE*, 2011, pp. 534-537.
[84] M. M. Andringa, D. P. Neikirk, N. P. Dickerson, and S. L. Wood, "Unpowered wireless corrosion sensor for steel reinforced concrete," in *Sensors, 2005 IEEE*, 2005, p. 4 pp.
[85] F. J. Friedersdorf and T. A. Wavering. "Corrosion Sensor Development for Military Applications," ntscenter.biz. [Online]. Available: http://www.nstcenter.biz/docs/PDFs/MR2007/MR2007-Thurs-SessionII-MR2007-16-FFriedersdoff.pdf [Accessed: May. 2013].
[86] S. X. Liu, W. Xin, and K. Q. Ding, "Simulation of corrosion on detection for pulsed eddy current," 2010, pp. 1839-1842.
[87] R. A. Smith and G. R. Hugo, "Transient eddy current NDE for ageing aircraft - capabilities and limitations," *Insight: Non-Destructive Testing and Condition Monitoring*, vol. 43, pp. 14-25, 2001.
[88] Y. He, F. Luo, and M. Pan, "Defect characterisation based on pulsed eddy current imaging technique," *Sensors and Actuators A: Physical,* vol. 164, pp. 1-7.

[89] B. Yang and F. Luo, "The Detection of Corrosion in Airplane Using Pulsed Eddy Current Nondestructive Testing Technology," *Journal of Test and Measurement Technology*, vol. 19, pp. 27-29, 2005.
[90] Y. Gotoh, H. Hirano, M. Nakano, K. Fujiwara, and N. Takahashi, "Electromagnetic non-destructive testing of rust region in steel," in *Magnetics Conference, 2005. INTERMAG Asia 2005. Digests of the IEEE International*, 2005, pp. 423-424.
[91] K. Kalyanasundaram and P. B. Nagy, "A simple numerical model of the apparent loss of eddy current conductivity due to surface roughness," *NDT & E International*, vol. 37, pp. 47-56, 2004.
[92] F. Yu and P. B. Nagy, "Numerical method for calculating the apparent eddy current conductivity loss on randomly rough surfaces," *Journal of Applied Physics*, vol. 95, pp. 8340-8351, 2004.
[93] J. C. Moulder, E. Uzal, and J. H. Rose, "Thickness and conductivity of metallic layers from eddy current measurements," *Review of Scientific Instruments*, vol. 63, pp. 3455-3465, June 1992.
[94] S. J. Norton and J. R. Bowler, "Theory of eddy current inversion," *Journal of Applied Physics*, vol. 73, pp. 501-512, 1993.
[95] K. Arora, H. Mallinson, A. Kulkarni, J. Brusey, and D. McFarlane, "The Practical Feasibility of Using RFID in a Metal Environment," in *Wireless Communications and Networking Conference, 2007.WCNC 2007. IEEE*, 2007, pp. 1679-1683.
[96] D. M. Dobkin and S. M. Weigand, "Environmental effects on RFID tag antennas," in *Microwave Symposium Digest, 2005 IEEE MTT-S International*, 2005, p. 4 pp.
[97] D. D. Deavours, "Improving the near-metal performance of UHF RFID tags," in *RFID, 2010 IEEE International Conference on*, 2010, pp. 187-194.
[98] J. Xin, Z. Xiaoping, and Z. Li, "An Innovative Semicircular Spiral Antenna for On-Metal Passive RFID Applications," *Antennas and Propagation, IEEE Transactions on*, vol. 61, pp. 1026-1031, 2013.
[99] D. Ciudad, P. Cobos Arribas, P. Sanchez, and C. Aroca, "RFID in Metal Environments: An Overview on Low (LF) and Ultra-Low (ULF) Frequency Systems," in *Radio Frequency Identification Fundamentals and Applications Design Methods and Solutions*, C. Turcu, Ed., ed: InTech, 2010.
[100] K. Finkenzeller, *RFID Handbook: Fundamentals and Applications in Contactless Smart Cards and Identification*, 3 ed.: John Wiley & Sons LTD, 2003.
[101] D. H. S. Cheng, "The Reflected Impedance of a Circular Coil in the Proximity of a Semi-Infinite Medium," *Instrumentation and Measurement, IEEE Transactions on*, vol. 14, pp. 107-116, 1965.
[102] C. V. Dodd and W. E. Deeds, "Analytical Solutions to Eddy-Current Probe-Coil Problems," *Journal of Applied Physics*, vol. 39, pp. 2829-2838, 1968.
[103] J. H. Rose, C.-C. Tai, and J. C. Moulder, "Scaling relation for the inductance of a coil on a ferromagnetic half-space," *Journal of Applied Physics*, vol. 82, pp. 4604-4610, 1997.
[104] J. C. Moulder, T. Cheng-Chi, B. F. Larson, and J. H. Rose, "Inductance of a coil on a thick ferromagnetic metal plate," *Magnetics, IEEE Transactions on*, vol. 34, pp. 505-514, 1998.
[105] C. A. Balanis, *Antenna Theory - Analysis and Design (3rd Edition)*: Wiley-Interscience, 2004.

[106] L. O. Hoeft and J. S. Hofstra, "Experimental and theoretical analysis of the magnetic field attenuation of enclosures," *Electromagnetic Compatibility, IEEE Transactions on,* vol. 30, pp. 326-340, 1988.
[107] N. Bowler and Y. Huang, "Electrical conductivity measurement of metal plates using broadband eddy-current and four-point methods," *Measurement Science & Technology,* vol. 16, pp. 2193–2200, 2005.
[108] Q. Xianming and C. Zhi Ning, "Proximity Effects of Metallic Environments on High Frequency RFID Reader Antenna: Study and Applications," *Antennas and Propagation, IEEE Transactions on,* vol. 55, pp. 3105-3111, 2007.
[109] N. R. Center. "Conductivity Measurements," ndt-ed.org. [Online]. Available: http://www.ndt-ed.org/EducationResources/CommunityCollege/EddyCurrents/Applications/conductivitymeasurements.htm [Accessed: Nov. 2013].
[110] Microchip. "125 kHz RFID System Design Guide," Microchip.com. [Online]. Available: ww1.microchip.com/downloads/en/devicedoc/51115f.pdf [Accessed: May. 2013].
[111] Atmel. "Tk5551 Data sheet," Atmel.com. [Online]. Available: www.atmel.com/Images/doc4709.pdf [Accessed: May. 2013].
[112] Atmel. "ATA5567 Data sheet," [Online]. Available: www.atmel.com [Accessed: May. 2013].
[113] Atmel. "Application Note: Atmel LF-RFID Kit," Atmel.com. [Online]. Available: www.atmel.com/Images/doc4980.pdf [Accessed: May. 2013].
[114] F. Yu and P. Nagy, "Dynamic Piezoresistivity Calibration for Eddy Current Nondestructive Residual Stress Measurements," *Journal of Nondestructive Evaluation,* vol. 24, pp. 143-143-143, 2005.
[115] R. A. Potyrailo, H. Mouquin, and W. G. Morris, "Position-independent chemical quantitation with passive 13.56-MHz radio frequency identification (RFID) sensors," *Talanta,* vol. 75, pp. 624-628, 2008.
[116] R. A. Potyrailo and W. G. Morris, "Multianalyte chemical identification and quantitation using a single radio frequency identification sensor," *Analytical chemistry,* vol. 79, pp. 45-51, 2007.
[117] A. A. Afifi and V. Clark, *Computer-aided multivariate analysis*. London: Chapman & Hall, 1996.
[118] T. Chen, G. Y. Tian, A. Sophian, and P. W. Que, "Feature extraction and selection for defect classification of pulsed eddy current NDT," *NDT & E International,* vol. 41, pp. 467-476, 2008.
[119] A. Sophian, G. Y. Tian, D. Taylor, and J. Rudlin, "A feature extraction technique based on principal component analysis for pulsed Eddy current NDT," *NDT & E International,* vol. 36, pp. 37-41, 2003.
[120] A. J. Mercer, R. K. James, G. Bennett, P. Patel, C. Johnston, and J. Cai, "Performance testing of RFID systems with RF-harsh materials," in *RFID-Technologies and Applications (RFID-TA), 2011 IEEE International Conference on,* 2011, pp. 537-543.
[121] J. D. Griffin, G. D. Durgin, A. Haldi, and B. Kippelen, "RF Tag Antenna Performance on Various Materials Using Radio Link Budgets," *Antennas and Wireless Propagation Letters, IEEE,* vol. 5, pp. 247-250, 2006.

Appendix 1: Signal Processing Algorithms

1.1 Peak Detection

```
function [maxtab, mintab]=peakdet(v, delta, x)
%PEAKDET Detect peaks in a vector
%        [MAXTAB, MINTAB] = PEAKDET(V, DELTA) finds the local
%        maxima and minima ("peaks") in the vector V.
%        MAXTAB and MINTAB consists of two columns. Column 1
%        contains indices in V, and column 2 the found values.
%
%        With [MAXTAB, MINTAB] = PEAKDET(V, DELTA, X) the indices
%        in MAXTAB and MINTAB are replaced with the corresponding
%        X-values.
%
%        A point is considered a maximum peak if it has the maximal
%        value, and was preceded (to the left) by a value lower by
%        DELTA.

% Eli Billauer, 3.4.05 (Explicitly not copyrighted).
% This function is released to the public domain; Any use is allowed.

maxtab = [];
mintab = [];

v = v(:); % Just in case this wasn't a proper vector

if nargin < 3
x = (1:length(v))';
else
x = x(:);
if length(v)~= length(x)
error('Input vectors v and x must have same length');
end
end

if (length(delta(:)))>1
error('Input argument DELTA must be a scalar');
end

if delta <= 0
error('Input argument DELTA must be positive');
end

mn = Inf; mx = -Inf;
mnpos = NaN; mxpos = NaN;

lookformax = 1;

for i=1:length(v)
this = v(i);
if this > mx, mx = this; mxpos = x(i); end
if this < mn, mn = this; mnpos = x(i); end

if lookformax
if this < mx-delta
maxtab = [maxtab ; mxpos mx];
mn = this; mnpos = x(i);
lookformax = 0;
```

```
end
else
if this > mn+delta
mintab = [mintab ; mnpos mn];
mx = this; mxpos = x(i);
lookformax = 1;
end
end
end
```

1.2 Principal Component Analysis

```
% PCA (Covariance)=====================================================================


% PCA input matrix
PCA_var = fm;

% remove the mean variable-wise (row-wise)
PCA_var=PCA_var-repmat(mean(PCA_var,2),1,size(PCA_var,2));

% calculate eigenvectors (loadings) W, and eigenvalues of the covariance matrix

% covariance matix
cov_mat = cov(PCA_var');
% eigen decomposition
[W, EigValMat] = eig(cov_mat');
EigVals = diag(EigValMat);

% Principal components
pc = W * PCA_var;
pc = pc';
pc1 = pc(:,2);
pc2 = pc(:,1);
```

1.3 FFT Bandpass Filter

```
function [filtOut] = FFTbpf(BPFin,N,Fs,LCF,HCF)

% FFT bandpass filter ==================================================================

% Fs = sampling frequency
% LCF = low cut-off frequency Hz
% HCF = high cut-off frequency Hz

% calculate the frequency corresponding to each FFT bin.
% this includes negative frequencies!
freqbase=Fs*(mod(((0:N-1)+floor(N/2)), N)-floor(N/2))/N;

% build a mask [... 0 0 0 1 1 ... 1 1 0 0 0 ...]
% with one entry per frequency
% set low and high cut-off frequencies
mask=(abs(freqbase) > LCF) .* (abs(freqbase) < HCF);
mask = mask';
```

```
% to frequency domain
BPFFT= fft(BPFin);

% apply filter
BPFFT = BPFFT .* mask;

% back to time domain
filtOut = ifft(BPFFT);

% overwrite original data
% real() is needed to remove imaginary part caused by finite numerical precision
filtOut = real(filtOut);
end
```

1.4 FFT using Zero Padding

```
% Function for creating smooth FFT using padding

%=========================================================================
function [sspectrum, psd_peak_freq, psd_peak_amplitude, freq] =
smoothFFT(inputsig,Fs)
%% Input signal
Ts = 1/Fs; %sampling time interval
t = 0:Ts:2-Ts; %sampling period
%inputsig = samples_mat(:,3);
%% FFT
L = length(inputsig);
k1=0:L-1;     %create a vector from 0 to N-1
T1=L/Fs;      %get the frequency interval
freq1=k1/T1;    %create the frequency range
y_FFT = fft(inputsig,L)/L;

%only want the first half of the FFT, since it is redundant
cutOff1 = ceil(L/2);

%take only the first half of the spectrum
y_FFT = y_FFT(1:cutOff1);
freq1 = freq1(1:cutOff1);

%% Smooth FFT (zero padded)
zeroPadFactor = nextpow2(length(inputsig)) + 5;
N = 2^zeroPadFactor;
k=0:N-1;     %create a vector from 0 to N-1
T=N/Fs;      %get the frequency interval
freq=k/T;    %create the frequency range
X=fft(inputsig,N)/length(inputsig); % normalize the data

%only want the first half of the FFT, since it is redundant
cutOff = ceil(N/2);

%take only the first half of the spectrum
X = X(1:cutOff);
X = abs(X).^2;
psd_peak_freq = freq(X == max(X));
```

```
psd_peak_amplitude = max(X);
freq = freq(1:cutOff);

sspectrum = abs(X);
end
```

1.5 Synthetic RFID Data

```
clear all; close all;clc;


%% Create synthetic RFID data=============================================
% Tag data
mtf = [0.3;0.2;0.1;0.35;0.25;0.15;0.4;0.3;0.2;];
% Reader/ carrier data
mrf = [2;3;4;2;3;4;2;3;4;];

cf = [mtf , mrf]; % Combined features tag and reader

%% Vector rotation (adding linear gradient)=====================================
x = 1:1:length(mrf);
tdeg = 30; % angle in degrees;
theta = tdeg * (pi / 180); % rotation angle in degrees > radians
rot_mat = [cos(theta),-sin(theta);sin(theta),cos(theta);]; % anti-clockwise
mrf_mat = [x', mrf];
mtf_mat = [x', mtf];

mrf_rot = rot_mat * mrf_mat';
mrf_rot = mrf_rot';
mrf_rot = mrf_rot(:,2);

mtf_rot = rot_mat * mtf_mat';
mtf_rot = mtf_rot';
mtf_rot = mtf_rot(:,2);

cf2 = [mtf, mrf_rot];


%% Plot synthetic data ===================================================
MARKER = {'-o','-o','-o','-^','-^','-^','-s','-s','-s'};
COLOUR = {'g','r'};

figure(11)
mc=1;
for count = 1:1:length(mrf)
    plot(count,mrf(count),MARKER{count},'MarkerSize',25, 'MarkerFaceColor','k')
    hold on
end
set(gca,'FontSize',32, 'FontWeight','Bold')
xlabel('Z Position [mm]','FontSize',32,'FontWeight','Bold')
ylabel('Amplitude [arb]','FontSize',32,'FontWeight','Bold')
grid on;


figure
plot(mtf,'-sk','MarkerSize',20,'LineWidth',4, 'MarkerFaceColor','k')
set(gca,'FontSize',32, 'FontWeight','Bold')
xlabel('Measurement','FontSize',32,'FontWeight','Bold')
```

```
ylabel('Amplitude [arb]','FontSize',32,'FontWeight','Bold')


%% PCA (covariance)=====================================================================

% PCA input matrix
PCA_var = cf;

% remove the mean variable-wise (row-wise)
PCA_var=PCA_var-repmat(mean(PCA_var,2),1,size(PCA_var,2));

% calculate eigenvectors (loadings) W, and eigenvalues of the covariance matrix

% covariance matix
cov_mat = cov(PCA_var');
% eigen decomposition
[W, EigValMat] = eig(cov_mat');
EigVals = diag(EigValMat);

% Principal components
pc = W * PCA_var;
pc = pc';
pc1 = pc(:,2);
pc2 = pc(:,1);

% Plot pc1 and pc2=====================================================================

figure
plot(pc1'ok','MarkerSize',15,'LineWidth',6, 'MarkerFaceColor','k')
set(gca,'FontSize',32, 'FontWeight','Bold')
xlabel('Measurements','FontSize',32,'FontWeight','Bold')
ylabel('PC1 [arb]','FontSize',32,'FontWeight','Bold')
grid on;

figure
plot(pc2'ok','MarkerSize',15,'LineWidth',6, 'MarkerFaceColor','k')
set(gca,'FontSize',32, 'FontWeight','Bold')
xlabel('Measurements','FontSize',32,'FontWeight','Bold')
ylabel('PC1 [arb]','FontSize',32,'FontWeight','Bold')
grid on;
```

1.6 Temperature Independent Corrosion Measurements

```
clear all; clc; close all;

%% Load data
cd('F:\Temperature_28_01_13');
% Load data files
load('S20')
load('S20_C')
load('S16')
load('S16_C')
load('S2')
load('S2_C')

%% Combine tag data and carrier data into one array
```

```
t = [S20,S16,S2]; % tag signal features
c = [S20_C,S16_C,S2_C]; % carrier signal features

%% PCA (Cvarance)============================================================

% PCA input matrix
PCA_var = [t;c*100000];

% remove the mean variable-wise (row-wise)
PCA_var=PCA_var-repmat(mean(PCA_var,2),1,size(PCA_var,2));

% calculate eigenvectors (loadings) W, and eigenvalues of the covariance
% matrix
% covariance matix
cov_mat = cov(PCA_var');
% eigen decomposition
[W, EigValMat] = eig(cov_mat');
EigVals = diag(EigValMat);

% Principal components
pc = W * PCA_var;
pc = pc';
pc1 = pc(:,2);  % principal component 2
pc2 = pc(:,1);  % principal component 1

%% Plot
figure
plot(pc2(1:9),'-ok','MarkerSize',15,'LineWidth',4, 'MarkerFaceColor','k')
hold on
plot(pc2(10:18),'-sb','MarkerSize',15,'LineWidth',4, 'MarkerFaceColor','b')
hold on
plot(pc2(19:end),'-^r','MarkerSize',15,'LineWidth',4, 'MarkerFaceColor','r')
set(gca,'FontSize',32, 'FontWeight','Bold')
xlabel('Temperature [^oC]','FontSize',32,'FontWeight','Bold')
ylabel('PC2 [arb]','FontSize',32,'FontWeight','Bold')
set(gca, 'XTick',[1:1:9],'XLim',[0.9
9.1],'XTickLabel',{'50','60','70','80','90','100','110','120','130'})
grid on;
hold off
% plot average values
figure
errorbar(1,mean(pc2(1:9)),  std(pc2(1:9))*2,'ok','MarkerSize',20,'LineWidth',4,
'MarkerFaceColor','k')
hold on
errorbar(2,mean(pc2(10:18)),
std(pc2(10:18))*2,'ok','MarkerSize',20,'LineWidth',4, 'MarkerFaceColor','k')
hold on
errorbar(3,mean(pc2(19:end)),
std(pc2(19:end))*2,'ko','MarkerSize',20,'LineWidth',4, 'MarkerFaceColor','k')
set(gca,'FontSize',32, 'FontWeight','Bold')
xlabel('Exposure time [Months]','FontSize',32,'FontWeight','Bold')
ylabel('PC2 [arb]','FontSize',32,'FontWeight','Bold')
set(gca, 'XTick',[1:1:3],'XLim',[0.9 3.1],'XTickLabel',{'1','3','6'})
grid on;
hold off
```